REPORT DOCUMENTATION PAGE

AFRL-SR-BL-TR-99-

0170

d reviewing
Information

1. AGENCY USE ONLY *(Leave blank)*	2. REPORT DATE	3. REPL
	June 1999	FINAL REPORT 1 Apr 95 - 31 Mar 98

4. TITLE AND SUBTITLE
A BASIC RESEARCH PROGRAM FOR THE CHARACTERIZATION OF THE MECHANICAL BEHAVIOR OF TEXTILE-TYPE COMPOSITES

5. FUNDING NUMBERS
F49620-95-1-0269

61102F
2302/BS

6. AUTHOR(S)
ADNAN H. NAYFEH

7. PERFORMING ORGANIZATION NAME(S) AND ADDRESS(ES)
UNIVERSITY OF CINCINNATI
DEPARTMENT FO AEROSPACE ENGINEERING AND \
ENGINEERING MECHANICS
CINCINNATI, OH 45221

8. PERFORMING ORGANIZATION REPORT NUMBER

9. SPONSORING/MONITORING AGENCY NAME(S) AND ADDRESS(ES)
AIR FORCE OFFICE OF SCIENTIFIC RESEARCH (AFOSR)
801 N. RANDOLPH STREET, ROOM 732
ARLINGTON, VA 22203-1977

10. SPONSORING/MONITORING AGENCY REPORT NUMBER

11. SUPPLEMENTARY NOTES

12a. DISTRIBUTION AVAILABILITY STATEMENT
APPROVED FOR PUBLIC RELEASE, DISTRIBUTION UNLIMITED

12b. DISTRIBUTION CODE

13. ABSTRACT *(Maximum 200 words)*

A micromechanical model is advanced in order to study the stress transfer and associated damage and failure in classes of conventional and textile type fibrous composites. Unidirectionally reinforced matrix with straight and undulated fibers define the repeating constructing cell for conventional and textile composites, respectively. Starting with the case of straight reinforcement, we approximate and model the actual discrete composite as a concentric cylindrical system. For axisymmetric loading, and upon adopting some appropriate restrictions on the radial behavior of some field quantities, an elasticity-based procedure reduces the two-dimensional field equations, which hold in both fiber and matrix components together with the appropriate interface, symmetry and boundary conditions, to a quasi-one-dimensional system. This analysis is further extended to cases involving undulated fibers. Based upon local directions (slopes) of the undulated fibers, the linear transformation is used to obtain local stress distributions along the undulated fibers. The total stress field is found to be combinations of these local stresses and the inherent contributions obtained from the transformations of the normal loads along the undulated directions in the absence of reinforcement. This simple system retains total account of the system's physics and presents itself in the form of coupled partial differential equations in the longitudinal displacements and stresses of both the fiber and matrix components. According to this model, damage is simulated in the form of stress free boundary conditions. Perpetuation of damage is based upon the maximum normal stress criterion.

14. SUBJECT TERMS

15. NUMBER OF PAGES
98

16. PRICE CODE

17. SECURITY CLASSIFICATION OF REPORT	18. SECURITY CLASSIFICATION OF THIS PAGE	19. SECURITY CLASSIFICATION OF ABSTRACT	20. LIMITATION OF ABSTRACT
UNCLASSIFIED	UNCLASSIFIED	UNCLASSIFIED	

A Final Report Submitted to the
Air Force Office of Scientific Research

by

University of Cincinnati
Cincinnati, Ohio 45221

entitled

A BASIC RESEARCH PROGRAM FOR THE CHARACTERIZATION OF THE MECHANICAL BEHAVIOR OF TEXTILE-TYPE COMPOSITES

Grant No. F49620-95-1-0269

Principal Investigator:
Adnan H. Nayfeh
Professor of Engineering Mechanics
Department of Aerospace Engineering
and Engineering Mechanics
(513) 556-3557

June 14, 1999

Personnel supported or associated with the research efforts:

1. **A. H. Nayfeh**, Professor, Principal Investigator.

2. **Wael Abdelrahman,** Recently Graduated with a PhD degree on modeling the stress distribution in the fiber and matrix components of textile composites with damage when subjected to either static or dynamic loading.

Publications:

1. Abdelrahman, W. G. and Nayfeh, A. H., "Stress Transfer and Stiffness Reduction in Orthogonally Cracked Laminates," *Mechanics of Materials*, Vol. 31, pp. 303-316, 1999.

2. Nayfeh, A. H. and Abdelrahman, W. G., "Dynamic Stress Transfer in Fibrous Composites with Damage," *Composites, Part B: Engineering*, Vol. 30, pp. 233-243, 1999.

3. Nayfeh, A. H., Faidi, W. and Abdelrahman, W. G., "An Approximate Model for Wave Propagation in Piezoelectric Materials: I. Laminated Composites," *Journal of Applied Physics*, 85, 4, pp. 2237-2346, 1999.

4. Nayfeh, A. H. and Abdelrahman, W. G., "Micromechanical Modeling for Load Transfer in Fibrous Composites," *Mechanics of Materials*, Vol. 30, pp. 307-324, 1998.

5. Abdelrahman, W. G. and Nayfeh, A. H., "Micromechanical Modeling of Stress Distribution in Undulated Composites under Axial Loading," *Mechanics of Materials*, Vol. 30, pp. 83-90, 1998.

6. Nayfeh A. H. and Abdelrahman, W. G., "An Improved Continuum Mixture Model forWave Propagation in Fibrous Composites," *Journal of the Acoustical Society of America*, Vol. 104, 2, pp. 867-873, 1998.

Papers accepted for publication:

1. Nayfeh A. H., Abdelrahman, W. G. and Nagy P. B., "Analyses of Axisymmetric Waves in Layered Piezoelectric Rods and Their Composites," accepted for publication in *Journal of the Acoustical Society of America*, Nov. 1998.

2. Nayfeh, A. H. and Abdelrahman, W. G., "An Improved Mixture Model for Wave Propagation in Laminated Orthotropic Media", accepted for publication in *Journal of the Acoustical Society of America*, Oct., 1998.

3. Nayfeh, A. H. and Abdelrahman, W. G., "Vibration Characteristics of Fibrous Composites with Damage," accepted for publication in *Journal of Vibration and Control.*

Proceeding Publications:

1. N. Alhuniti and A. Nayfeh, "Constitutive Relation Modeling of Woven and Textile Composites" ICCE/4, Hawaii, July 6-14,1997, D. Hui, editor.

2. W. Abdelrahman and A. Nayfeh, "Micromechanical Modeling of Stress Distribution in Textile Composites", ICCE/4, Hawaii, July 6-14, 1997, D. Hui, editor.

3. A. Nayfeh and W. Abdelrahman , "Dynamically Induced Stress Distribution in Undulated Fibrous Composites", Review of Progress in Quantitative NDE, San Diego, Calif. July 27-August 1, 1997, D.O.Thompson, editor.

ABSTRACT

A micromechanical model is advanced in order to study the stress transfer and associated damage and failure in classes of conventional and textile type fibrous composites. Unidirectionally reinforced matrix with straight and undulated fibers define the repeating constructing cell for conventional and textile composites, respectively. Starting with the case of straight reinforcement, we approximate and model the actual discrete composite as a concentric cylindrical system. For axisymmetric loading, and upon adopting some appropriate restrictions on the radial behavior of some field quantities, an elasticity-based procedure reduces the two-dimensional field equations, which hold in both fiber and matrix components together with the appropriate interface, symmetry and boundary conditions, to a quasi-one-dimensional system. This analysis is further extended to cases involving undulated fibers. Based upon local directions (slopes) of the undulated fibers, the linear transformation is used to obtain local stress distributions along the undulated fibers. The total stress field is found to be combinations of these local stresses and the inherent contributions obtained from the transformations of the normal loads along the undulated directions in the absence of reinforcement. This simple system retains total account of the system's physics and presents itself in the form of coupled partial differential equations in the longitudinal displacements and stresses of both the fiber and matrix components.

According to this model, damage is simulated in the form of stress free boundary conditions. Perpetuation of damage is based upon the maximum normal stress criterion. The adverse effect of such damage on the stiffness properties of the composite is

predicted. Results show the favorable effect of undulation in decreasing the rate of property degradation with increasing damage. The model is quite general and has been applied to several situations. These include response to static loading, and other vibration and wave propagation applications. Confidence in our modeling procedure has been confirmed by comparisons with whatever available analytical models, experimental data and finite element calculations.

TABLE OF CONTENTS

LIST OF TABLES

LIST OF FIGURES

LIST OF SYMBOLS

A	approximation function for the shear stress
B	approximation function for the radial displacement for both cases of lateral constraint
C	approximation function for the radial displacement for laterally free case
E	Young's modulus of the composite
f_{ij}	elements of the stiffness matrix for the fiber material
L	length of the composite representative unit cell
m_{ij}	elements of the stiffness matrix for the matrix material
P	external composite axial stress
r_1	radius of the fiber cross-section
r_2	radius of the unit cell cross-section
S	coupling term of the constituents stress-strain relations
u	axial displacement
v	radial displacement
X_f, X_m	maximum allowable stress for the fiber and matrix, respectively
x-r-θ	global coordinate system for the representative unit cell
z-r-θ	local coordinate system for undulated segment
α	coefficient of thermal expansion
ϕ	undulated fiber azimuthal angle
λ_f, λ_m	Lame' elastic constant for isotropic fiber and matrix, respectively
μ_f, μ_m	shear modulus for isotropic fiber and matrix, respectively
ν_f, ν_m	Poisson's ratio for isotropic fiber and matrix, respectively

θ	undulation angle
ρ_f, ρ_m	density of the fiber and the matrix constituents
σ_{rf}, σ_{rm}	radial normal stress for the fiber and the matrix constituents, respectively
σ_{rzf}, σ_{rzm}	shear stress for the fiber and the matrix constituents, respectively
σ_{zf}, σ_{zm}	axial normal stress for the fiber and the matrix constituents, respectively
$\sigma_{\theta f}$, $\sigma_{\theta m}$	transverse normal stress for the fiber and the matrix constituents, respectively.
ω	dynamic loading angular frequency

CHAPTER 1

INTRODUCTION

Textile composites are emerging as a new generation of advanced complex materials with the potential of enhancing shortcomings of conventional unidirectional fibrous composites. Advanced structural applications have recently required significant improvements of the damage tolerance and reliability of composites. To achieve such improvements, a high level of through thickness and interlaminar strengths is required. Such requirements can be easily tailored by undulated (textile) fibrous composites. For these classes of complex materials, only limited and mostly recent attempts have been carried out on their modeling and analysis. In micromechanical modeling, as a minimum, models are needed to characterize their effective properties. Even here, very little work is available. For more sophisticated and advanced applications, especially those concerned with damage tolerance, information about the local distributions of stresses in the fiber and matrix constituents individually are practically absent although of prime importance. To put future discussion into perspective, it is instructive at this stage to digress and give a short account of the various classes of composite materials. Composite materials have gone several classification processes, both on the micro- and on the macro-scales. One classification in particular is based on the shape and distribution of one phase, namely a fiber, into another phase, the matrix. In this context, fibrous composites are divided into straight fibrous composites and undulated fibrous composites. This latter class can exist in several shapes, including 2-D and 3-D braids, plain weave and 3-D woven composites, all define classes of textile materials.

Textile structural composites in particular are defined as textile-containing materials designed for structural or load bearing applications. Like conventional composites, because of their higher strength-to-weight ratio and stiffness-to-weight ratio, textiles are also considered superior to ordinary metal alloys. The idea of using an assembly of yarns woven together to produce a structural composite came from the clothing industry. Even the technologies used in producing such composites have their origins in clothing factories. As textiles continue to be more and more important in many structural applications, there is a growing need for accurate prediction of their mechanical performance under various loading conditions.

It is usually the case that analysis of textile composites is based on analyses of straight fibrous composites. Comparatively speaking, for composites reinforced by straight fibers, the literature is almost saturated by the number of studies that are devoted to deriving their effective properties. It is beyond this work, however, to review this vast literature. For updated review see, for example, Nayfeh [1] and Al-Huniti [2]. Studies concerning the distribution of local stresses and the degree of load transfer between the straight fiber and matrix components have also received reasonable attention. The importance of the problem is attributed to the fact that accurate prediction of the resulting stress distribution in both constituents has a strong bearing upon the predicted mechanical integrity of the loaded composite.

The majority of existing models of straight fibrous composites included various restrictions on the material properties, field equations and interface and boundary conditions. According to some theoretical models, these resulted in a second order differential equation that describes the behavior of either interfacial shear stress or normal

stress in the fiber or the matrix; examples include the work of Smith and Spencer [3], Nayfeh [4,5], Steif [6], Gao et al. [7], Carapella et al. [8], and Kishore et al. [9].

More recently, McCartney [10] presented a micromechanically-based analysis that can predict the stress transfer between the fiber and matrix in a uniaxially straight fiber reinforced composite. The system was modeled as a concentric cylindrical system with stress free outer boundary. Broadly speaking, this situation corresponds to the case of plane stress loading. Thermomechanical loads in which the mechanical ones are applied as tension along the fiber direction are applied. The approach uses an elasticity based analysis and starts with approximating some of the field variables and proceeds to satisfy the appropriate field equations of equilibrium, constitutive relations and the associated interface and boundary conditions. In contrast to above mentioned older models, McCartney's analysis lead to a fourth order differential equation that has more versatility leading to better prediction of the actual stress distribution in the composite. In particular, McCartney was able to simulate localized damage by stress free boundary conditions.

An even fewer number of attempts are available which model the micromechanical distribution of stresses in other than straight fiber reinforced composites; namely in classes textile materials. Due to the complexity of the system, some finite element and boundary element based studies have been applied to the problem at hand to obtain approximate numerical solutions. Nedele and Winsom [11], in a finite element parametric study, showed that geometrical variations in unidirectional composites have a higher influence on the stresses than the changes in the constituent

properties. Goldberg and Hopkins [12] developed a new boundary element formulation for the micromechanical analysis of composites and applied it to some textile composites.

Based upon the above various models, several authors have constructed similar models for laminated composites and then proceeded to estimate the strength of the overall composite. This greater body of research has been devoted to laminated composites since they were the first to be used in industry and because of their relative simplicity of modeling. Failure criteria that are based on the maximum stress, the maximum strain or the more general Tsai-Wu theory [13] have been employed. Among the earliest models stands the work of Reifsnider and Talug [14] in which they derived a simple shear lag model to predict failure in composite laminates. Later on Highsmith and Reifsnider [15] verified these results experimentally. More thorough analyses followed, including the work of Hashin [16] and Talreja [17,18]. Hashin took the analysis a step further by dealing with the three dimensional problem of orthogonally cracked laminates [19], while the modeling of McCartney [20] enabled him to study the stress transfer process in repetitively damaged composites on the micro-level. Damage accumulation studies in laminated composites was discussed by Akshantala and Talreja [21].

A very limited number of publications combine the geometric and analytic complexity of straight or undulated fibers in attempts to model damage accumulation. Among these stands the work of Allen and Harris [22] who developed a model to predict the degradation in the material properties of damaged textile composites subject to thermomechanical loading. Later on, Pochiraju et al. [23] used the concept of parameterized Macro-cells to represent the woven fiber architecture and then adopted an averaging technique to estimate the textile composite strength under in-plane loading. To

our knowledge, there exist no further studies of the damage accumulation or property degradation in these classes composites.

1.1 Building Block Approach

The main objective of this work is to develop a unified approach to model the micromechanical stress distribution in straight and undulated fibrous composites subjected to thermal and mechanical loading. This will be sought in the absence or presence of damage mechanisms. Damage perpetuation and accumulation leading to failure is also among our prime objectives. To accomplish these objectives, an elasticity based procedure, that involves use of the interface quantities and averaging technique, is used to reduce the two-dimensional dynamic field equations together with the interface, symmetry and boundary conditions to a quasi-one-dimensional system. Following a building block approach, we specifically consider the following steps towards our understanding of the undulated system's behavior:

1. construct and verify a model for the micromechanical stress distribution in straight fibrous composites with or without local damage,
2. construct and verify a model for the micromechanical stress distribution in undulated fibrous composites with or without local damage,
3. use the above results to study the failure behavior of these classes of composites under static and dynamic loading.

In chapters 2 and 3, we lay the foundation of the work by starting with the most commonly used fiber-matrix arrangement, namely the straight fibrous composites. The composite repeating unit cell is modeled as a concentric cylindrical system. To maintain

material generality, the fiber and the matrix will be allowed to have anisotropic or isotropic properties. Two structural situations can be dealt with using the composite cylinder model. These relate to different constraining boundary conditions. On a macro-scale, a composite panel can be either thick or thin. Both situations correspond to a certain lateral constraint condition on the corresponding unit cell. In both situations, the composite might be damage free or has a single or multiple fiber breaks or matrix transverse cracks, or even a delamination region between the fiber and the matrix constituents. Furthermore, any of the above mentioned arrangements might be subjected to either a static or a dynamic (harmonic) type of loading. These different possibilities are arranged below in figure 1.1.

Chapter 2 is devoted to the general composite described by the bold line in the figure, namely, the laterally constrained damage-free composite under dynamic loading. In chapter 3, we exploit the generality of the above model and show how solutions for many other cases can be obtained from this analysis. We then present comparisons of these solutions with published results.

In chapter 4, the additional geometric complexity of undulation is added to the model obtained in chapter 2. This will be done as follows: for a given geometric undulation, we identify and analytically describe the local tangent to the fiber. Subsequently, we transform the global coordinates and applied loads to the local systems consisting of the tangent directions and their normal in the planes of undulation. We then adapt the results obtained for straight fibers to "straight" segmented fibers along the

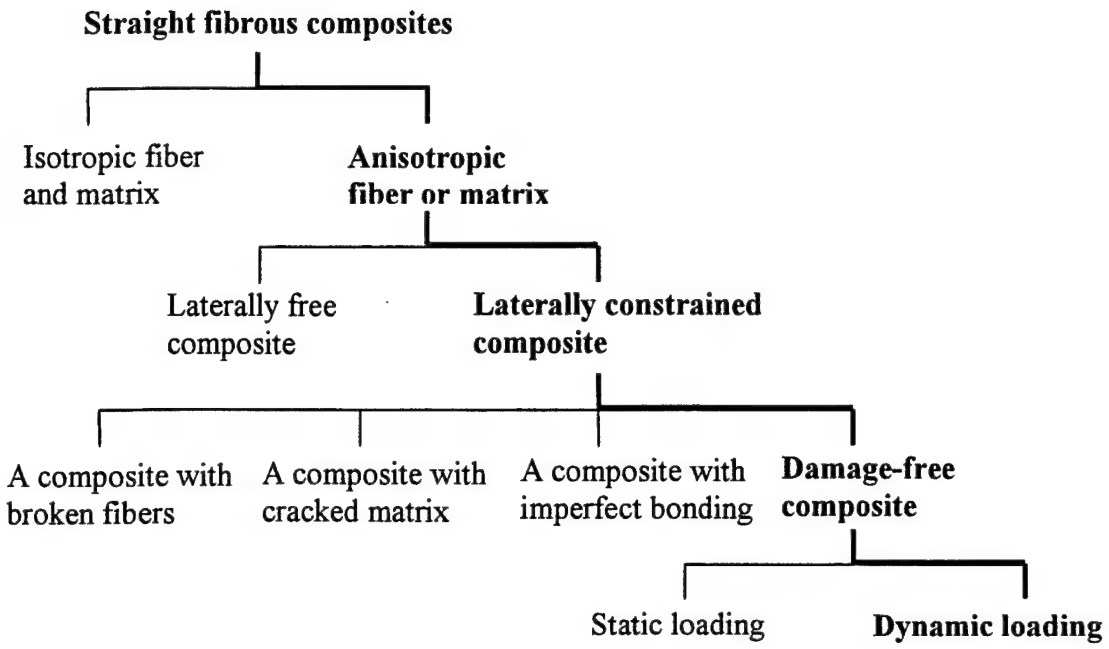

Figure 1.1: Classification of possible straight fibrous composite arrangements.

Bold case indicates model of chapter 2

tangents. The local stresses obtained using this procedure are then supplemented with the stress contributions that inherently rise in any oriented direction with respect to the loading direction. As in chapter 2, the analysis of the undulated fibrous case will be carried out for a damage free composite under dynamic loading. In chapter 5, this analysis will then be utilized to solve different problems involving different types of damage, see fig 1.1, under both types of loading. Comparisons of the results with finite element solutions will also be established.

In chapter 6, we carry the modeling further and use the stress tensor components, as predicted in chapters 2 and 4 in order to investigate the failure behavior of straight and

undulated fibrous reinforced panel. In particular, the degradation of the composite's in-plane properties, represented by Young's modulus of elasticity, is investigated. Load-damage dependence is investigated to determine the strength reduction of the composite. Attention is also given to the problem of delamination progression between the fiber and the matrix and its effect on the overall composite stiffness.

Finally, in Chapter 7, we show the versatility of the suggested formulation by applying it to investigate the vibration characteristics of damaged fibrous composites. The effects of damage location and the fiber volume fraction on the composite system natural frequencies are studied, and several interesting observations are drawn. We then conclude by presenting conclusions and recommendations for further studies.

CHAPTER 2

DEVELOPMENT OF THE MODEL FOR STRAIGHT FIBROUS COMPOSITES

2.1 Introduction

It was established in Chapter 1 that the basic building block for the modeling of textile fibrous composites starts with straight fiber reinforcement. Now, we start by developing a unified generic but improved analytical model for the mechanically induced stress and displacement fields in a unidirectional straight fibrous composite under inplane dynamic loading. In chapter 3, we then discuss applications of this model and verify its validity by comparisons to published analytical results and finite element calculations.

Several existing models have been used to describe the behavior of a fiber-matrix composite mixture under inplane static loading, see for example references [5] and [6]. The major improvement in the present modeling over existing ones is the retaining of the term representing the rate of change of the radial displacement with the axial coordinate in the shear constitutive relation. Furthermore, since in practical situations, the fiber may be multi-layered, the continuum mixture treatment has to be applicable to anisotropic media. For this reason, we shall treat both the fiber and matrix constituents as transversely isotropic. Situations involving isotropic material fibers or matrix can be easily obtained as special cases by merely imposing the appropriate restrictions on their anisotropic properties. The analysis will proceed first assuming perfectly bonded constituents with no damage. Later on, different types of composite damage will be addressed. These will include breakage of the fibers in planes perpendicular to the

composite principal direction, transverse cracking in the matrix and frictional slip on the fiber-matrix interfaces.

2.2 Formulation of the Problem

Consider the general unidirectionally reinforced periodic composite shown in figure 2.1a. The fiber can consist of several concentric layers, and an additional outer layer works as an interphase. It is due to failure in this layer that fiber-matrix debonding occurs and frictional slip takes place. The composite has a hexagonal symmetry with a representative unit cell as shown in figure 2.1b. The specific geometry shown corresponds to a widely common sample. For our present analysis, the fiber layers are assumed to be perfectly bonded together and, in turn, to the matrix. Since the continuum mixture solutions are most appropriate for two homogenous phase media, namely for media consisting of single material fiber and matrix, we need to model the multilayered fiber as an effective homogenized one. Due to the biased geometry of the fiber layers, the effective fiber will have anisotropic properties or more precisely, will exhibit transverse isotropy. The effective anisotropic properties of the three-component fiber are constructed by a repetitive use of the procedure developed by Nayfeh [1] for deriving effective properties for two component fibrous composites. To facilitate our analysis, we further approximate the unit cell with a concentric cylinder as shown in figure 2.1c. The unit cell has an outer radius r_2 with the effective fiber having a radius r_1.

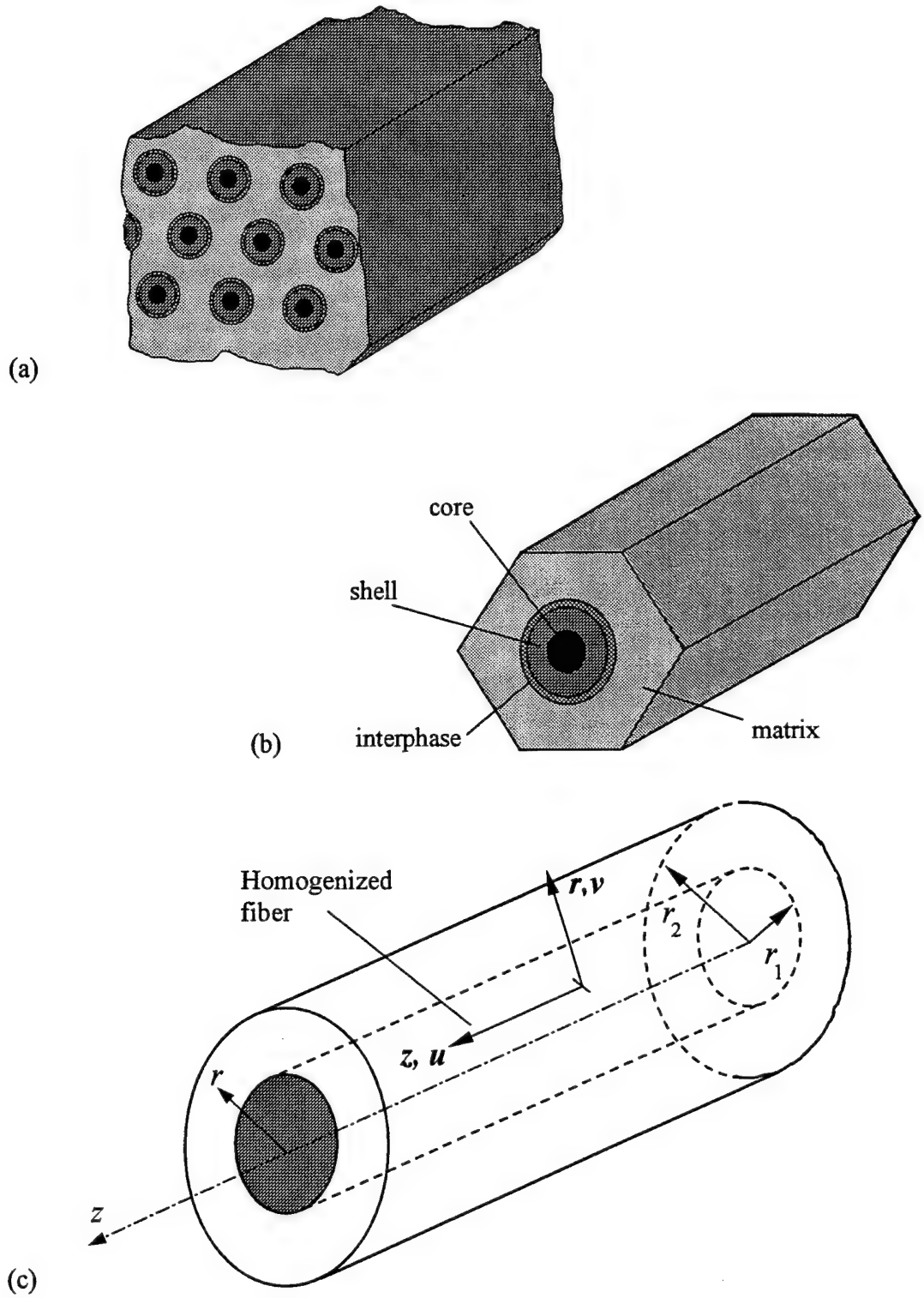

Fig. 2.1: The composite panel model: (a) the composite panel,

(b) the representative unit cell, (c) the effective fiber concentric cylinder model.

For the present modeling, the behavior of the composite under dynamic loading is described by the following two-dimensional momentum equations:

$$\frac{\partial \sigma_z}{\partial z}+\frac{1}{r}\frac{\partial}{\partial r}(r\sigma_{rz})=\rho\frac{\partial^2 u}{\partial t^2} \tag{2.1}$$

$$\frac{\partial \sigma_r}{\partial r}+\frac{\partial \sigma_{rz}}{\partial z}+\frac{1}{r}(\sigma_r-\sigma_\theta)=\rho\frac{\partial^2 v}{\partial t^2} \tag{2.2}$$

Here σ_r, σ_z, σ_θ and σ_{rz} are the non-vanishing components of the stress tensor; u and v are the displacement components in the longitudinal and radial directions, respectively. Identifying the fiber and matrix materials with the subscripts f and m, respectively, the fiber and matrix have the transversely isotropic materials constitutive relations take the form:

$$\begin{Bmatrix}\sigma_z\\ \sigma_\theta\\ \sigma_r\\ \sigma_{r\theta}\\ \sigma_{rz}\\ \sigma_{\theta z}\end{Bmatrix}_f=\begin{bmatrix}f_{11} & f_{12} & f_{12} & 0 & 0 & 0\\ f_{12} & f_{22} & f_{23} & 0 & 0 & 0\\ f_{12} & f_{23} & f_{22} & 0 & 0 & 0\\ 0 & 0 & 0 & f_{44} & 0 & 0\\ 0 & 0 & 0 & 0 & f_{55} & 0\\ 0 & 0 & 0 & 0 & 0 & f_{55}\end{bmatrix}\begin{Bmatrix}\varepsilon_z\\ \varepsilon_\theta\\ \varepsilon_r\\ \gamma_{r\theta}\\ \gamma_{rz}\\ \gamma_{\theta z}\end{Bmatrix}_f, \tag{2.3}$$

$$\begin{Bmatrix}\sigma_z\\ \sigma_\theta\\ \sigma_r\\ \sigma_{r\theta}\\ \sigma_{rz}\\ \sigma_{\theta z}\end{Bmatrix}_m=\begin{bmatrix}m_{11} & m_{12} & m_{12} & 0 & 0 & 0\\ m_{12} & m_{22} & m_{23} & 0 & 0 & 0\\ m_{12} & m_{23} & m_{22} & 0 & 0 & 0\\ 0 & 0 & 0 & m_{44} & 0 & 0\\ 0 & 0 & 0 & 0 & m_{55} & 0\\ 0 & 0 & 0 & 0 & 0 & m_{55}\end{bmatrix}\begin{Bmatrix}\varepsilon_z\\ \varepsilon_\theta\\ \varepsilon_r\\ \gamma_{r\theta}\\ \gamma_{rz}\\ \gamma_{\theta z}\end{Bmatrix}_m, \tag{2.4}$$

where

$$\varepsilon_z=\frac{\partial u}{\partial z},\ \varepsilon_r=\frac{\partial v}{\partial r},\ \varepsilon_\theta=\frac{v}{r},\ \gamma_{rz}=\frac{\partial v}{\partial z}+\frac{\partial u}{\partial r}, \tag{2.5}$$

are the axisymmetric strain displacement relations. We chose to expand the above equations for further use. For axisymmetric dynamic behavior, the applicable constitutive relations are

$$\sigma_z = C_{11}\frac{\partial u}{\partial z} + \frac{C_{12}}{r}\frac{\partial}{\partial r}(r v), \tag{2.6}$$

$$\sigma_r = C_{33}\frac{\partial v}{\partial r} + \frac{C_{23}}{r} v + C_{12}\frac{\partial u}{\partial z}, \tag{2.7}$$

$$\sigma_\theta = C_{22}\frac{v}{r} + C_{23}\frac{\partial v}{\partial r} + C_{12}\frac{\partial u}{\partial z}, \tag{2.8}$$

$$\sigma_{rz} = C_{55}(\frac{\partial v}{\partial z} + \frac{\partial u}{\partial r}), \tag{2.9}$$

which hold for the fiber if $C_{ij} = f_{ij}$ and for the matrix if $C_{ij} = m_{ij}$. The use of the stress-strain relations is more convenient in the following analysis than the commonly used choice of strain-stress relations.

Several symmetry and continuity conditions have to be satisfied in the model. The composite symmetry requires the vanishing of the shear stresses at the center and outer surface of the unit cell. Also, the lateral constraint assumption implies the vanishing of the radial displacement at its outer surface. Finally, axial and radial stresses and displacements have to be continuous across the fiber-matrix interface. The above field equations are, therefore, supplemented with the following conditions (see figure 2.2):

Symmetry:

$$v_f(z,0,t) = 0 \ , \qquad \sigma_{rzf}(z,0,t) = 0 \qquad , \qquad \sigma_{rzm}(z,r_2,t) = 0 \tag{2.10a}$$

lateral constraint:

$$v_m(z,r_2,t) = 0 \tag{2.10b}$$

Continuity (on $r = r_1$):

$$\sigma_{rzf}(z,r_1,t) = \sigma_{rzm}(z,r_1,t) \quad , \quad v_f(z,r_1,t) = v_m(z,r_1,t), \tag{2.10c}$$

$$\sigma_{rf}(z,r_1,t) = \sigma_{rm}(z,r_1,t) \quad , \quad u_f(z,r_1,t) = u_m(z,r_1,t). \tag{2.10d}$$

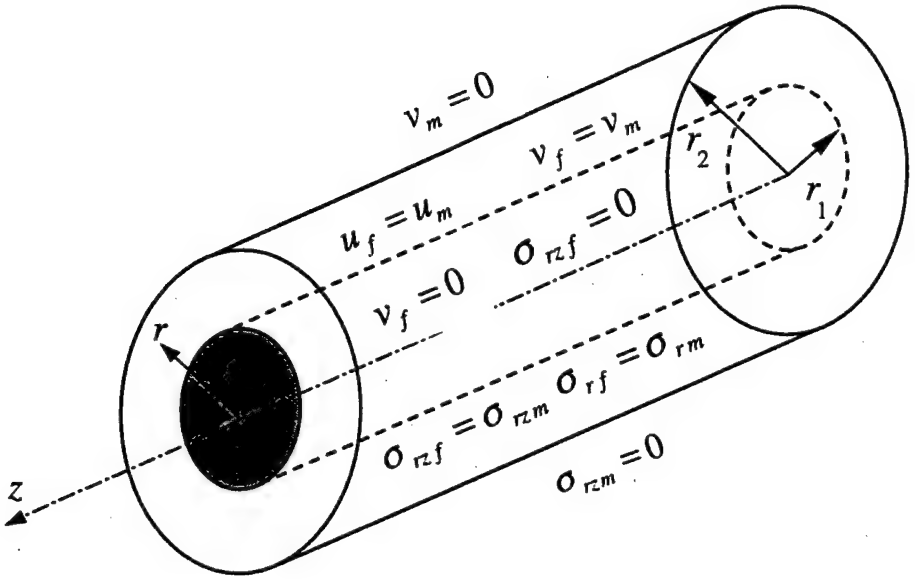

Fig 2.2: Symmetry and continuity condition in the representative unit cell.

2.3 Method of Solution

Following the procedure outlined in [4], if equations (2.1) and (2.6) are averaged according to

$$\overline{(\ )}_f = \frac{1}{\pi r_1^2}\int_0^{r_1} 2\pi r(\ )_f\, dr, \tag{2.11a}$$

$$\overline{(\ )}_m = \frac{1}{\pi (r_2^2 - r_1^2)}\int_{r_1}^{r_2} 2\pi r(\ )_m\, dr, \tag{2.11b}$$

and if the symmetry and continuity conditions (2.10a, b, c) are used, one obtains the quasi-one-dimensional momentum equations

$$n_f \frac{\partial \overline{\sigma}_{zf}}{\partial z} = -\tau + n_f \rho_f \frac{\partial^2 \overline{u}_f}{\partial t^2}, \tag{2.12}$$

$$n_m \frac{\partial \overline{\sigma}_{zm}}{\partial z} = \tau + n_m \rho_m \frac{\partial^2 \overline{u}_m}{\partial t^2}, \tag{2.13}$$

and the constitutive relations

$$n_f \overline{\sigma}_{zf} = f_{12} S + n_f f_{11} \frac{\partial \overline{u}_f}{\partial z}, \tag{2.14}$$

$$n_m \overline{\sigma}_{zm} = -m_{12} S + n_m m_{11} \frac{\partial \overline{u}_m}{\partial z}. \tag{2.15}$$

Here n_f and n_m stand for the volume fractions of the fiber and matrix materials, respectively and τ and S denote the momentum and the constitutive relations interaction terms, respectively; these quantities are defined as:

$$n_f = r_1^2 / r_2^2 \quad , \qquad n_m = (r_2^2 - r_1^2) / r_2^2 \, , \tag{2.16a, b}$$

$$\tau = 2 n_f \sigma^* / r_1 \, , \qquad S = 2 n_f v^* / r_1 \, , \tag{2.17a, b}$$

where σ^* and v^* are the interface shear stress and radial displacement; namely:

$$\sigma^* = \sigma_{rzf}(z, r_1, t) = \sigma_{rzm}(z, r_1, t), \tag{2.18}$$

$$v^* = v_f(z, r_1, t) = v_m(z, r_1, t). \tag{2.19}$$

The remaining constitutive relations (Eqs. 2.7-2.9) will now be utilized to derive the relevant partial differential equations describing the system in terms of the interaction terms τ and S and the axial displacements $\overline{u}_f$ and $\overline{u}_m$. Once this is done, the problem described by Eqs. (2.12-2.15) reduces to a quasi-one-dimensional one, which retains the

integrity of the propagation in the individual fiber and matrix components subject to the interaction terms τ and S. This cannot, however, be done without adopting appropriate approximations. These concern the radial dependence of the radial displacement and the shear stress, which can be adopted from known elasticity solutions (see for example [4]) as:

$$v_f(z,r,t) = B(z,t)r, \tag{2.20a}$$

$$\sigma_{rzf}(z,r,t) = A(z,t)r, \tag{2.20b}$$

$$v_m(z,r,t) = B(z,t)\frac{n_f}{n_m}(\frac{r_2^2}{r^2}-1)r, \tag{2.21a}$$

$$\sigma_{rzm}(z,r,t) = A(z,t)\frac{n_f}{n_m}(\frac{r_2^2}{r^2}-1)r, \tag{2.21b}$$

chosen to automatically satisfy the symmetry conditions (2.10a, b) and the interface continuity conditions (2.10c).

Introducing these approximations into the functions defined in Eq. (2.17) yields

$$\tau = 2n_f A, \tag{2.22}$$

$$S = 2n_f B. \tag{2.23}$$

Using these expressions in equations (2.12-2.15) leads to

$$n_f \frac{\partial \overline{\sigma}_{zf}}{\partial z} = -2n_f A + n_f \rho_f \frac{\partial^2 \overline{u}_f}{\partial t^2}, \tag{2.24}$$

$$n_m \frac{\partial \overline{\sigma}_{zm}}{\partial z} = 2n_f A + n_m \rho_m \frac{\partial^2 \overline{u}_m}{\partial t^2}, \tag{2.25}$$

$$n_f \overline{\sigma}_{zf} = 2n_f f_{12} B + n_f f_{11} \frac{\partial \overline{u}_f}{\partial z}, \tag{2.26}$$

$$n_m \overline{\sigma}_{zm} = -2m_{12} n_f B + n_m m_{11} \frac{\partial \overline{u}_m}{\partial z}. \tag{2.27}$$

At once, we notice that two coupled equations can be obtained by substituting $\overline{\sigma}_{zf}$ and $\overline{\sigma}_{zm}$ from Eqs. (2.26) and (2.27) into Eqs. (2.24) and (2.25), respectively. This yields

$$n_f f_{11} \frac{\partial^2 \overline{u}_f}{\partial z^2} + 2n_f f_{12} \frac{\partial B}{\partial z} = -2n_f A + n_f \rho_f \frac{\partial^2 \overline{u}_f}{\partial t^2}, \tag{2.28}$$

$$n_m m_{11} \frac{\partial^2 \overline{u}_m}{\partial z^2} - 2n_f m_{12} \frac{\partial B}{\partial z} = 2n_f A + n_m \rho_m \frac{\partial^2 \overline{u}_m}{\partial t^2}. \tag{2.29}$$

Next, we start by satisfying the shear constitutive relation (2.9). Multiplying it with r^2 and integrating by parts in accordance with Eq. (2.11a), we directly obtain

$$u^* - \overline{u}_f = \frac{r_1^2}{4}\left(\frac{A}{f_{55}} - \frac{\partial B}{\partial z}\right), \tag{2.30a}$$

where u^* is the interface value of u_f.

Similarly, for the matrix material, if we multiply Eq. (2.9) by $(r^2 - r_2^2)$, substitute from Eq. (2.21b) and integrate by parts according to Eq. (2.11b) we get

$$u^* - \overline{u}_m = \frac{r_1^2 Q}{4}\left(\frac{A}{m_{55}} - \frac{\partial B}{\partial z}\right), \tag{2.30b}$$

where we have used the continuity relation required by Eq. (2.10d), namely

$$u^*(z,t) = u_f(z, r_1, t) = u_m(z, r_1, t). \tag{2.31}$$

Here $Q = \frac{1}{n_m^2}\left(n_f^2 - 4n_f + 3 + 2\ln n_f\right)$, is a function of the volume fractions only. By eliminating u^* from Eqs. (2.30a) and (2.30b) we get the important relation:

$$\overline{u}_m - \overline{u}_f = \eta_2 A - \eta_1 \frac{\partial B}{\partial z}, \tag{2.32a}$$

where

$$\eta_1 = \frac{r_1^2}{4}(1-Q) \qquad \text{and} \qquad \eta_2 = \frac{r_1^2}{4}(\frac{1}{f_{55}} - \frac{Q}{m_{55}}). \tag{2.32b}$$

Next, we turn our attention to the radial and tangential stresses. Subtracting Eq. (2.8) from Eq. (2.7) we get

$$\sigma_r - \sigma_\theta = 2C_{44}(\frac{\partial v}{\partial r} - \frac{v}{r}). \tag{2.33}$$

Specializing this equation to the fiber using the approximation of Eq. (2.20a) yields

$$\sigma_{rf} = \sigma_{\theta f}, \tag{2.34a}$$

as one expects in the static limit. Specializing the same equation to the matrix, using Eq. (2.21a), gives

$$\sigma_{rm} - \sigma_{\theta m} = -\frac{4m_{44}}{n_m}\frac{r_1^2}{r^2}B. \tag{2.34b}$$

Following the above procedure, if we substitute from Eqs. (2.20b) and (2.34a) into Eq. (2.2), multiply the resulting equation by r^2 and integrate according to Eq. (2.11a), we get

$$\sigma_r^* - \overline{\sigma}_{rf} + \frac{r_1^2}{4}(\frac{\partial A}{\partial z} - \rho_f \frac{\partial^2 B}{\partial t^2}) = 0. \tag{2.35a}$$

Similarly, substituting from Eqs. (2.21b) and (2.34b) into Eq. (2.2), multiplying the resulting equation by $(r^2 - r_2^2)$ and integrating as per Eq. (2.11b) we obtain

$$\sigma_r^* - \overline{\sigma}_{rm} + \frac{2m_{55}}{n_m^2}(n_m + n_f \ln n_f)B + \frac{r_1^2 Q}{4}(\frac{\partial A}{\partial z} - \rho_m \frac{\partial^2 B}{\partial t^2}) = 0, \tag{2.35b}$$

where

$$\sigma_r^*(z,t) = \sigma_{rf}(z,r_1,t) = \sigma_{rm}(z,r_1,t), \tag{2.36}$$

is the common interfacial radial stress.

Eliminating σ_r^* from Eqs. (2.35a) and (2.35b) yields

$$\overline{\sigma}_{rf} - \overline{\sigma}_{rm} = \frac{r_1^2}{4}\left(\frac{\partial A}{\partial z} - \rho_f \frac{\partial^2 B}{\partial t^2}\right) - \frac{r_1^2 Q}{4}\left(\frac{\partial A}{\partial z} - \rho_m \frac{\partial^2 B}{\partial t^2}\right) - \frac{2m_{44}}{n_m^2}(n_m + n_f \ln n_f)B. \tag{2.37}$$

So far all required interface conditions have been identically satisfied. We now need to eliminate $\overline{\sigma}_{rf}$ and $\overline{\sigma}_{rm}$ from the above equations. In order to do this, we specialize the constitutive equation (2.7) for the fiber and matrix by substituting into it from Eqs. (2.20a) and (2.21a), respectively to get

$$\sigma_{rf} = (f_{22} + f_{23})B + f_{12}\frac{\partial u_f}{\partial z}, \tag{2.38a}$$

$$\sigma_{rm} = -\frac{n_f}{n_m}(m_{22} + m_{23} + 2m_{544}\frac{r_2^2}{r^2})B + m_{12}\frac{\partial u_m}{\partial z}. \tag{2.38b}$$

Averaging Eqs. (2.38) according to Eq. (2.11) yields, for the fiber and the matrix, respectively

$$\overline{\sigma}_{rf} = (f_{22} + f_{23})B + f_{12}\frac{\partial \overline{u}_f}{\partial z}, \tag{2.39a}$$

$$\overline{\sigma}_{rm} = -\frac{n_f}{n_m}(m_{22} + m_{23} - \frac{2m_{44}}{n_m}\ln n_f)B + m_{12}\frac{\partial \overline{u}_m}{\partial z}. \tag{2.39b}$$

Eliminating $\overline{\sigma}_{rf}$ and $\overline{\sigma}_{rm}$ between Eqs. (2.37) and (2.39a, b) we finally get the following important equation

$$\xi_1 B + \xi_2 \frac{\partial^2 B}{\partial^2 t} = m_{12}\frac{\partial \overline{u}_m}{\partial z} - f_{12}\frac{\partial \overline{u}_f}{\partial z} + \eta_1 \frac{\partial A}{\partial z}, \tag{2.40a}$$

where

$$\xi_1 = \frac{1}{n_m}\left[n_m(f_{22}+f_{23})+n_f(m_{22}+m_{23})+2m_{44}\right] \qquad \text{and} \qquad \xi_2 = \frac{r_1^2}{4}(\rho_f - Q\rho_m)\,.$$

(2.40b)

The behavior of the composite system is completely described by Eqs. (2.28), (2.29), (2.32) and (2.40). As seen, this system consists of four partial differential equations that couple the two longitudinal averaged displacements, interfacial shear stress and interfacial radial displacement. In the next chapter these equations will be utilized and manipulated to facilitate the analysis of several important problems involving both static and dynamic loading, in the presence or absence of three types of damage; fiber breaks, matrix cracks and fiber-matrix debonding.

CHAPTER 3

APPLICATIONS OF THE STRAIGHT FIBROUS MODEL

3.1 Introduction

As mentioned in chapter 1, it is the theme in this work to use straight fibrous composites analysis as the first building block unit for the more complex analysis of undulated fibrous composites. It is important, therefore, to have a deeper understanding of the active stress transfer mechanisms that takes place upon loading this class of composites. These mechanisms change according to the type of loading and whether the composite has some sort of internal damage in one of its constituents. The systems of equations derived in the previous chapter for both the laterally constrained and laterally free cases can be successfully used to study these different situations involving straight fibrous composites. The simplest of which is the problem involving only static loading with or without damage. They can also be used to solve the more general problem of harmonic dynamic loading of the straight fibrous composite.

3.2 Cases of Static Loading

The system of equations (2.28), (2.29), (2.32) and (2.40) for the case of laterally constrained composite segment derived in the previous chapter can be applied to cases of static loading, by simply setting time-dependent terms equal to zero. Upon doing so, this system of differential equations can be simplified and combined, after some algebraic

manipulations, into a single fourth order differential equation. This equation takes the form:

$$a_1\bar{\sigma}_{zf}'''+a_2\bar{\sigma}_{zf}''+a_3\bar{\sigma}_{zf}+a_4=0 \tag{3.1}$$

where the prime indicates $\partial/\partial z$ and a_i, i=1, 2, 3, are functions of the fiber and matrix material properties and volume fractions, defined as:

$$a_1=-\frac{\eta_1^{\,2}}{2D}, \tag{3.2a}$$

$$a_2=\frac{\eta_2}{2}-\frac{2\eta_1}{n_m D}\left(n_f\frac{m_{12}}{m_{11}}+n_m\frac{f_{12}}{f_{11}}\right), \tag{3.2b}$$

$$a_3=-\frac{2}{n_m^{\,2}D}\left(n_f\frac{m_{12}}{m_{11}}+n_m\frac{f_{12}}{f_{11}}\right)^2, \tag{3.2c}$$

with a_4 depending on the external axial loading as

$$a_4=\frac{P}{n_m m_{11}}\left[1+\frac{2m_{12}}{n_m D}\left(n_f\frac{m_{12}}{m_{11}}+n_m\frac{f_{12}}{f_{11}}\right)\right]. \tag{3.2d}$$

In the above definitions, D is given by

$$D=\frac{1}{n_m}\left[n_f(m_{22}+m_{23})+n_m(f_{22}+f_{23})+2m_{44}-2\left(n_f\frac{m_{12}^{\,2}}{m_{11}}+n_m\frac{f_{12}^{\,2}}{f_{11}}\right)\right].$$

It is our intent to drop the overscore on the axial stresses and displacements from now on, since no more averaging is going to take place in the following chapters.

3.2.1 Laterally Free System

Laterally free systems are important since they represent a widely common class of composites, namely thin fibrous composites. Due to the similarity in the field equations, associated interface conditions and most of the symmetry conditions between

the laterally free and the laterally constrained systems, we shall not attempt to repeat the procedure described above for this case. It is sufficient to mention that for the laterally free situation, the symmetry condition in Eq. (2.10 b) is no longer valid and should be replaced with the appropriate stress free boundary condition, namely

$$\sigma_{rm}(z, r_2, t) = 0. \tag{3.3}$$

With this restriction, the analysis identically parallels that of the laterally constrained case, and the resulting system of equations can be reduced into a single fourth order differential equation identical to equation (3.1). In this case, however, the coefficients a_i take different forms.

The fourth order differential equation (3.1), together with the set of coefficients (3.2) or their alternative form for the laterally free case, are general and can be applied to a variety of situations. These include situations pertaining to the loading conditions and also to the presence or absence of damage in the system. Also these equations can be applied to finite as well as to infinitely extended, along the fiber direction, composites. Loading conditions consisting of uniform heating, mechanical loading or combinations of both are possible. Damage in the system includes the possibility of matrix cracking or fiber break. A complete study of these situations was published in a recent paper [24].

3.2.2 Damage Free case

For the case of perfectly bonded damage-free fibrous composite under axisymmetric loading, the solution for the fiber normal stress is obtained by solving equation (3.1) subject to the boundary conditions

$$\sigma_{zf}(0) = P_{0f} \quad , \sigma_{zf}(L) = P_{Lf} \quad , \sigma'_{zf}(0) = 0 \quad , \sigma'_{zf}(L) = 0 \tag{3.4}$$

where P_{0f} and P_{Lf} are the fiber end stresses calculated from the composite total stress and the fiber volume fraction. The appropriate equations of the analysis of chapter 2 can then be used to obtain the distributions of the remaining stress components, namely the matrix normal stress, the shear stress and the radial normal stress.

This procedure is applied for the case shown in figure 3.1. The length of the composite segment is chosen as $L = 8r_1$ and the fiber has a volume fraction of 0.444. The stresses at both ends are taken to be the same in the isotropic fiber and matrix. The silica fiber and the aluminum alloy matrix have the following values for Young's modulus and Poisson's ratio:

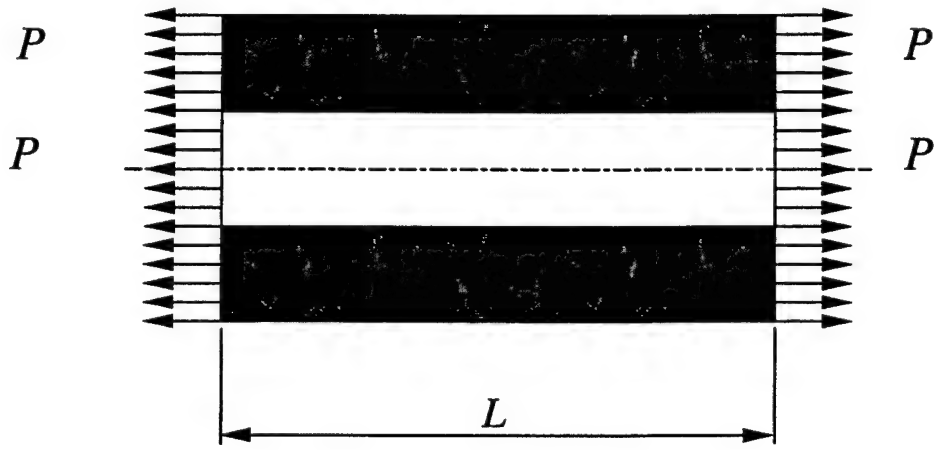

Figure 3.1: Geometry and loading of the case of a finite length undamaged composite.

$E_f = 73$ GPa , $\nu_f = 0.177$,

$E_m = 70.5$ GPa , $\nu_m = 0.345$.

Figures 3.2, 3.3 and 3.4 show the resulting distributions of the fiber normal stress, interfacial shear stress and interfacial radial stress, normalized with respect to the composite total stress P. Symmetry of the solutions are evident in both cases of laterally

free and laterally constrained segments. In the absence of damage, a general symmetric loading along the fiber direction, namely at $z = 0$ and $z = L$ will insure, as a minimum, the vanishing of shear stress and normal displacements u_f and u_m at the center of the system i.e., at $z = L/2$. The effect of the lateral constraint is seen to increase the value of the interfacial radial stress.

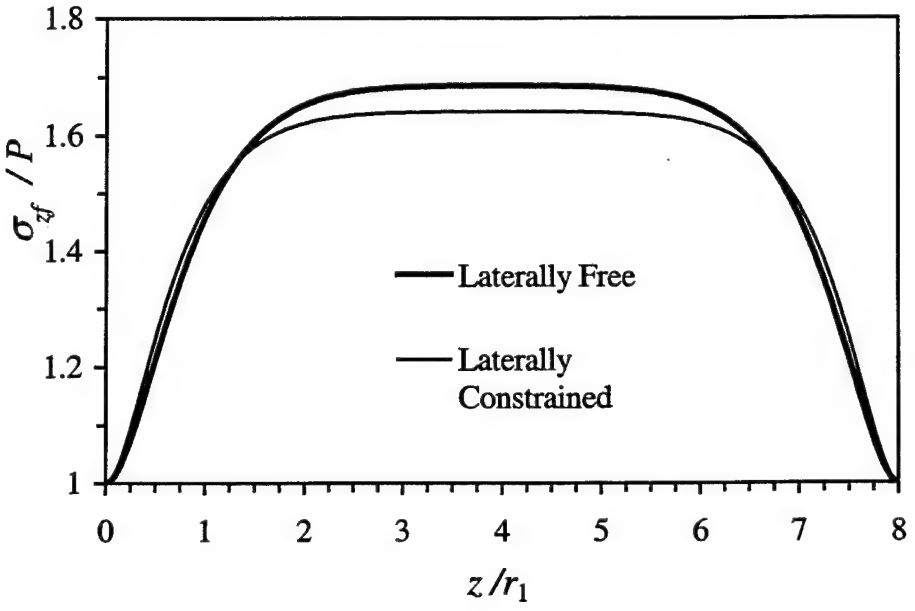

Figure 3.2: Comparison of the fiber normal stress distribution in both laterally free and laterally constrained systems for the case of finite undamaged fiber-matrix composite

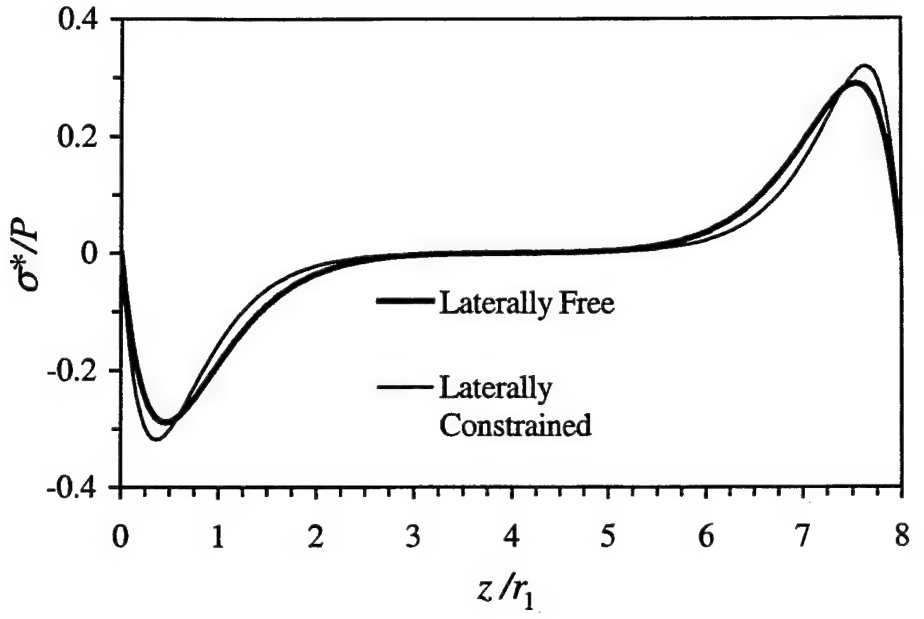

Figure 3.3: Comparison of the interfacial shear stress distribution in both laterally free and laterally constrained systems for the case of finite undamaged fiber-matrix composite

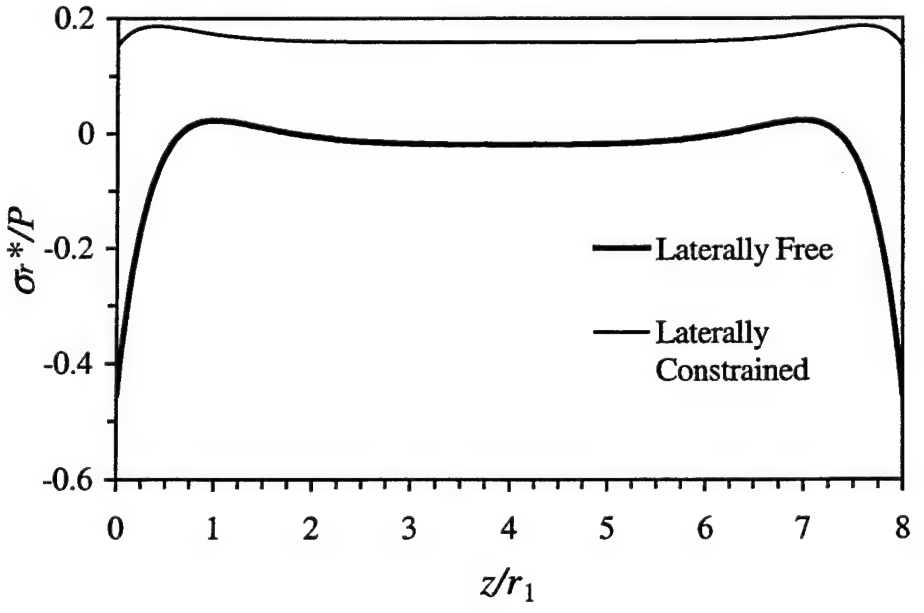

Figure 3.4: Comparison of the interfacial radial stress distribution in both laterally free and laterally constrained systems for the case of finite undamaged fiber-matrix composite

It is important to emphasize the fact that despite the integration operations during the analysis in chapter 2, we can still recover the distribution of stress components as functions of z and r. For example the shear stress distribution in both the fiber and matrix for the present undamaged fiber-matrix composite is shown in figure 3.5. Positive and negative values of the stress are given in shades of white and black, respectively.

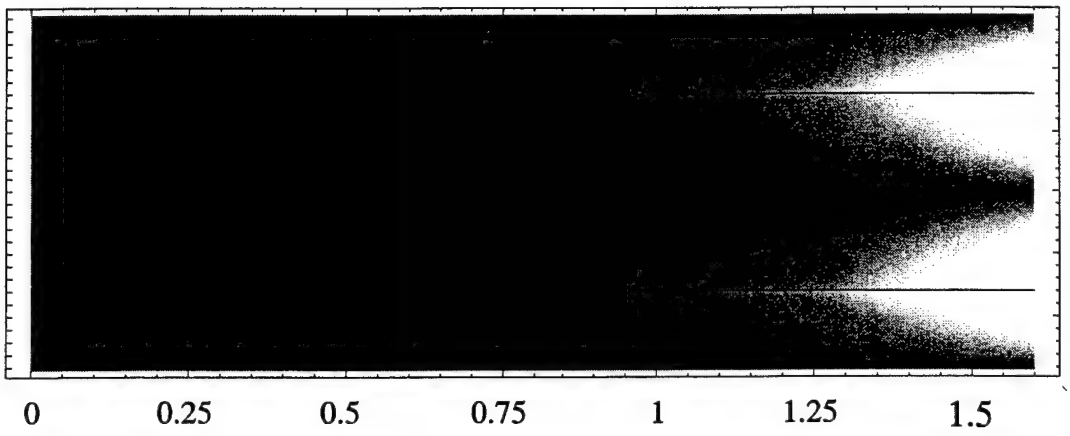

Figure 3.5: Distribution of the shear stress in an undamaged fiber-matrix composite under axial loading.

3.2.3 Broken fiber case

For cases involving a fiber break, say at $z = 0$ the shear stresses σ_{rzf} and σ_{rzm} and the matrix normal displacement $\overline{u}_m$ vanish at that location. The applicable boundary conditions are:

$$\sigma_{zf}(0) = 0 \ , \ \sigma_{zf}(L) = P_{Lf} \ , \ \sigma'_{zf}(0) = 0 \ , \ \sigma'_{zf}(L) = 0 \qquad (3.5)$$

In all the numerical illustrations involving damaged composites, arrangements studied by McCartney [10] have been used. However, these arrangements have been studied for both types of lateral constraint. Curves belonging to the laterally free system can be directly compared with those presented in McCartney's paper.

As a numerical example, we treat the situation of a broken fiber in a perfectly bonded fiber-matrix infinite system in the absence of thermal loading as shown in fig. 3.6. This system, which was described in [10], section 8.1, is assumed to be infinitely long, so that the fiber end stress P_{Lf} is equal to its remote value based on an equi-strain assumption, namely σ_{zf}^{∞}. The silica fiber and the aluminum alloy matrix have the same properties of the illustration in the previous sub-section 3.2.2. For the arbitrarily selected value of strain, $\varepsilon = 0.1$, the remote normal stresses have the following values

$\sigma_{zf}^{\infty} = 7.3484\,\text{GPa}$, $\sigma_{zm}^{\infty} = 7.0969\,\text{GPa}$ for the laterally free system, and

$\sigma_{zf}^{\infty} = 8.3331\,\text{GPa}$, $\sigma_{zm}^{\infty} = 12.260\,\text{GPa}$ for the laterally constrained system.

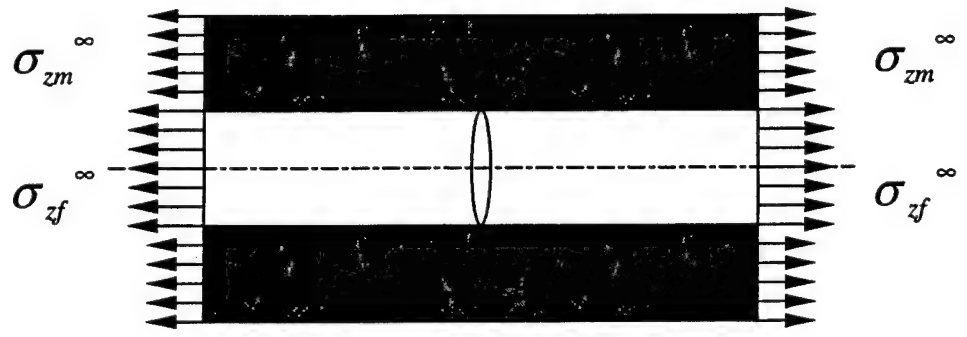

Figure 3.6: Geometry and loading of the case of broken fiber.

Solutions for this case are obtained from Eqs. (3.1) with coefficients obtained from (3.2), subject to the boundary conditions (3.5). Results of the fiber normal stress σ_{zf} and the matrix normal stress σ_{zm} are plotted and compared in Fig. 3.7 for both the laterally free system and the laterally constrained system. In the absence of the break, the normal stresses in both the fiber and matrix are constant and equal to their asymptotic values σ_{zf}^{∞} and σ_{zm}^{∞} as predicted by the Lame' solutions. In the presence of the fiber break, however, this figure clearly shows the normal stress transfer between the fiber and the matrix. From this figure it is evident that the matrix-fiber load transfer takes place in the vicinity of the fiber break and is almost complete within a distance of $2r_1$.

The interfacial shear stress σ^* and the interfacial radial stress σ_r^* for the above case are normalized with respect to the remote normal matrix stress σ_{zm}^{∞} and are plotted and compared in Figs. 3.8 and 3.9 for both lateral constraint cases. Once again, both figures clearly show that most of the activities take place in the vicinity of the break and that the respective stresses asymptotically approach those pertaining to the damage free systems as predicted by the Lame' solutions. Figure 3.8 also shows that the condition of zero interfacial shear stress at the fiber breakage location is exactly satisfied and that the location of the maximum value of σ^* is closer to the location of the broken fiber surface in the laterally constrained case than that in the laterally free case. The maximum value of σ^* itself is considerably higher in the former. σ_r^* is seen in Fig. 3.9 to be dramatically affected by the lateral constraint. This is perhaps due to the fact that the laterally constrained system, in which the lateral strain vanishes, creates large radial stresses at the outer boundary and at inner locations in the system.

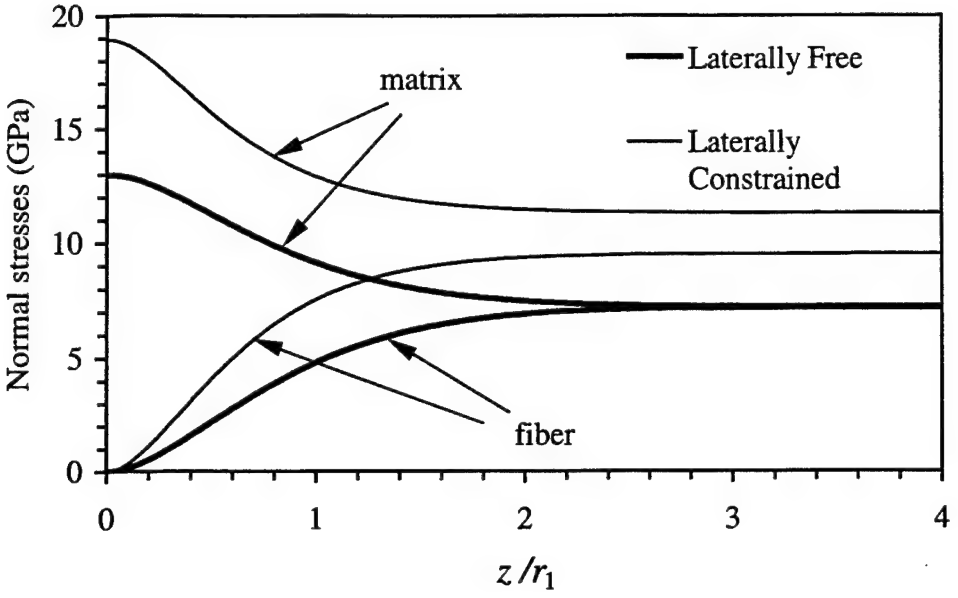

Figure 3.7: Comparison of the normal stress distributions in the fiber and the matrix for both laterally free and laterally constrained systems in the presence of broken fiber at z=0.

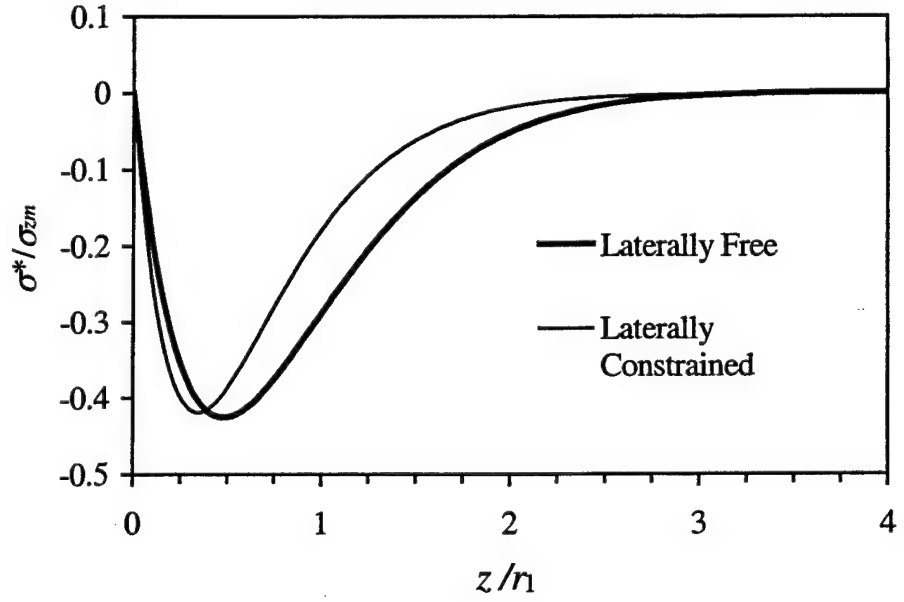

Figure 3.8: Comparison of the interfacial shear stress in both laterally free and laterally constrained systems in the presence of broken fiber at $z = 0$.

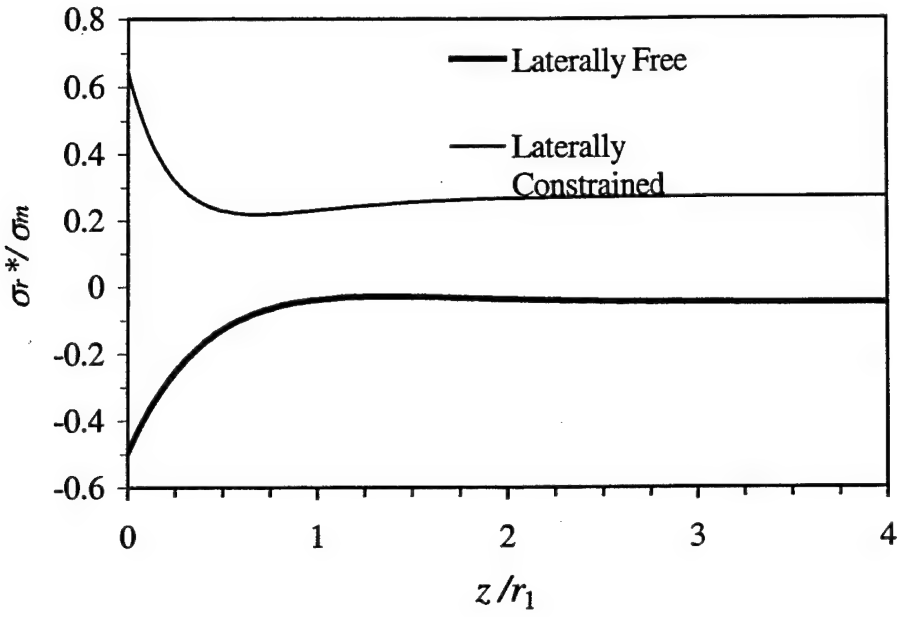

Figure 3.9: Comparison of the interfacial radial stress in both laterally free and laterally constrained systems in the presence of broken fiber at $z = 0$.

Finally, the effect of a single mid-span fiber break on the shear stress redistribution in the initially undamaged composite of section 3.2.2 is shown in figure 3.10. The complete antisymmetry indicates that the condition of zero shear stress at the break surface is completely satisfied.

3.2.4 Cracked matrix case

Opposite to the case of the broken fiber, cases involving matrix cracking transverse to the fiber direction, say at $z = 0$, will exhibit the vanishing of the fiber normal displacement $\bar{u}_f$ at that location. Here the applicable boundary conditions then become

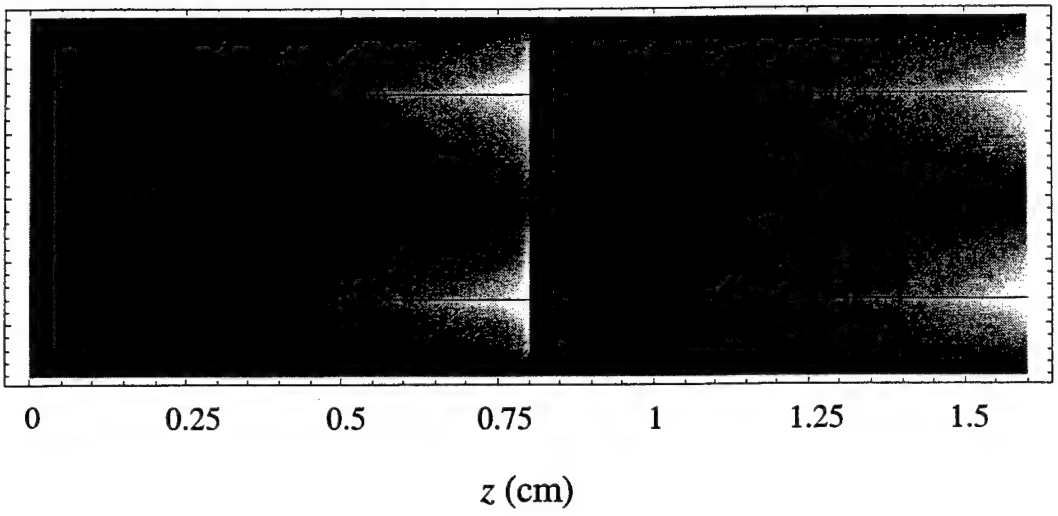

Figure 3.10: Distribution of the shear stress in a fiber-matrix composite under axial loading with a single fiber break.

$$\sigma_{zf}(0) = P_0 / n_f \quad , \sigma_{zf}(L) = P_{Lf} \quad , \sigma'_{zf}(0) = 0 \quad , \sigma'_{zf}(L) = 0 \tag{3.6}$$

As an illustration we treat the problem of a cracked matrix in a perfectly bonded fiber-matrix infinite system with thermal loading, as shown in figure 3.11. Again, this system, which was described in [10], section 8.2, is assumed to be infinitely long. The fiber volume fraction is 0.4, and the applied strain ε_z is 0.8%. The overall system is subjected to a temperature T = -550°C below the stress free temperature. Thermal loading provides no more difficulty in the analysis, since its effect follows that of the external mechanical loading P, and thus adds to its term in equation 3.1. The fiber and matrix material properties are isotropic and have the following values for Young's modulus, Poisson's ratio and the coefficient of thermal expansion

$E_f = 220$ GPa , $\nu_f = 0.1$, $\alpha_f = 5.5\times10^{-6}/^\circ\mathrm{C}$

$E_m = 70$ GPa , $\nu_m = 0.2$, $\alpha_m = 10^{-5}/^\circ\mathrm{C}$

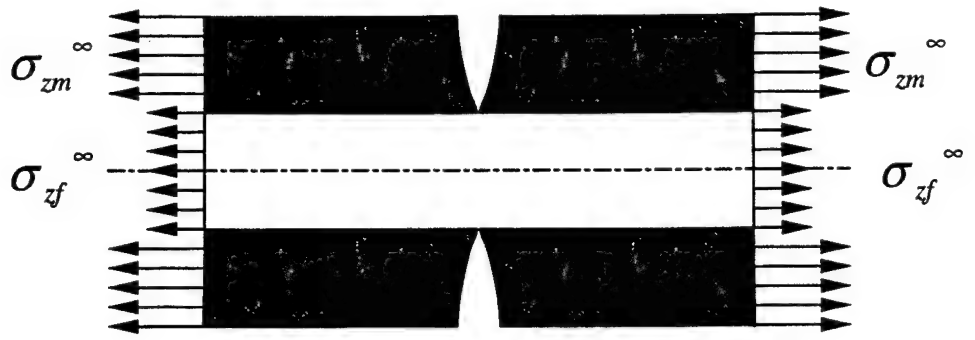

Figure 3.11: Geometry and loading of the case of a cracked matrix with heating.

Solutions for this case are obtained from Eq. (3.1) subject to the boundary conditions (3.2). The remote normal stress values for this case are calculated as

$\sigma_{zf}^{\infty} = 1.5866$ GPa, $\sigma_{zm}^{\infty} = 0.6781$ GPa for the laterally free system, and

$\sigma_{zf}^{\infty} = 1.7361$ GPa, $\sigma_{zm}^{\infty} = 0.9498$ GPa for the laterally constrained system.

The fiber normal stress, the interfacial shear stress and the interfacial radial stress are presented and compared in Fig. 3.12, 3.13 and 3.14. These figures exhibit, to a large degree, the overall features of the corresponding figures 3.7, 3.8 and 3.9 in both regions of maximum activities and asymptotic values. It is worth noting that the lateral constraint changed the nature of the distribution of the interfacial radial stress. Instead of being totally compressive except near the matrix crack, it is tensile all over in the case of laterally constrained system.

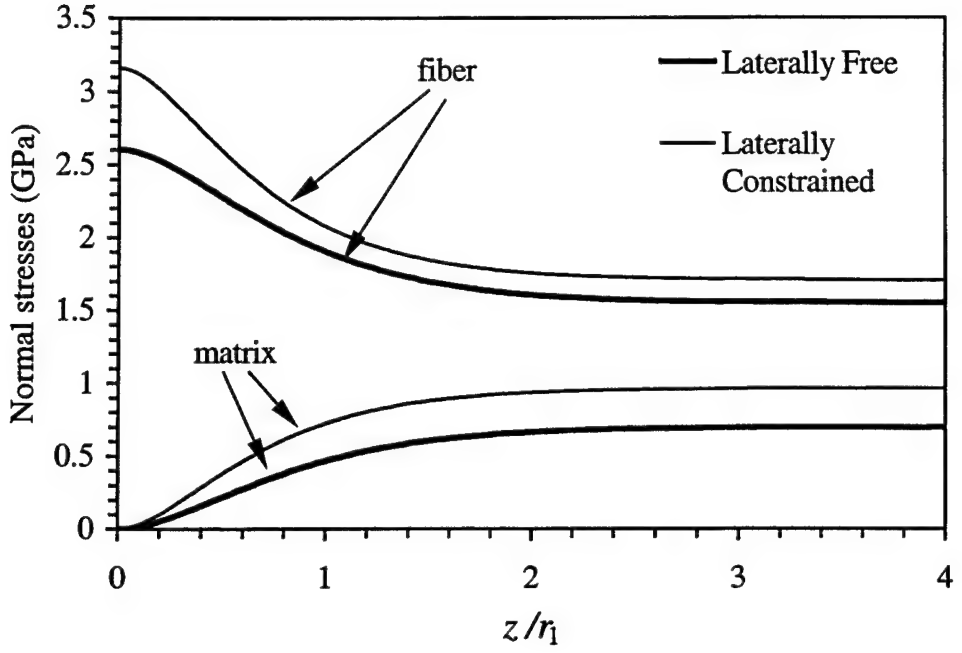

Figure 3.12: Comparison of the fiber and matrix normal stress in both laterally free and laterally constrained systems for the case of a cracked matrix at $z = 0$ with $\varepsilon = 0.8\%$.

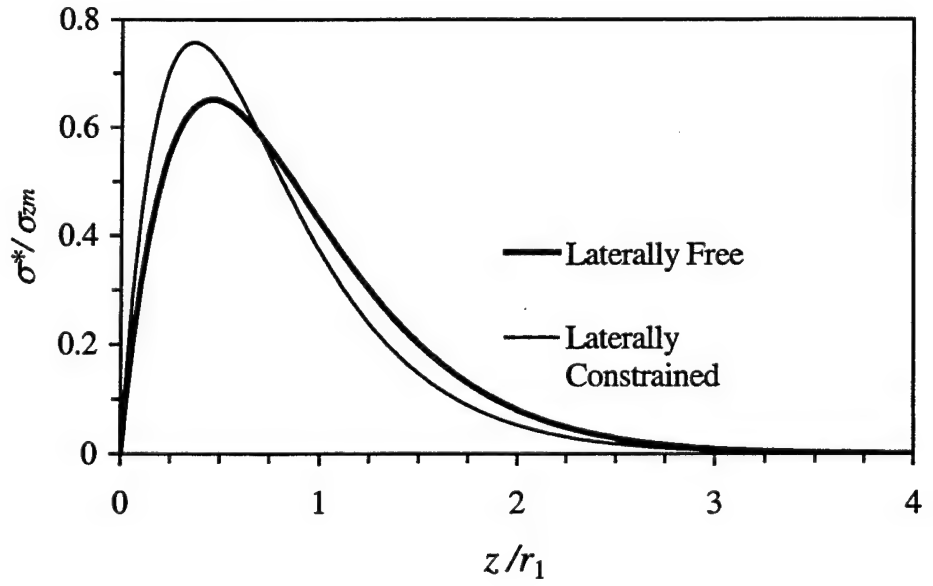

Figure 3.13: Comparison of the interfacial shear stress in both laterally free and laterally constrained systems for the case of a cracked matrix at $z = 0$ with $\varepsilon = 0.8\%$.

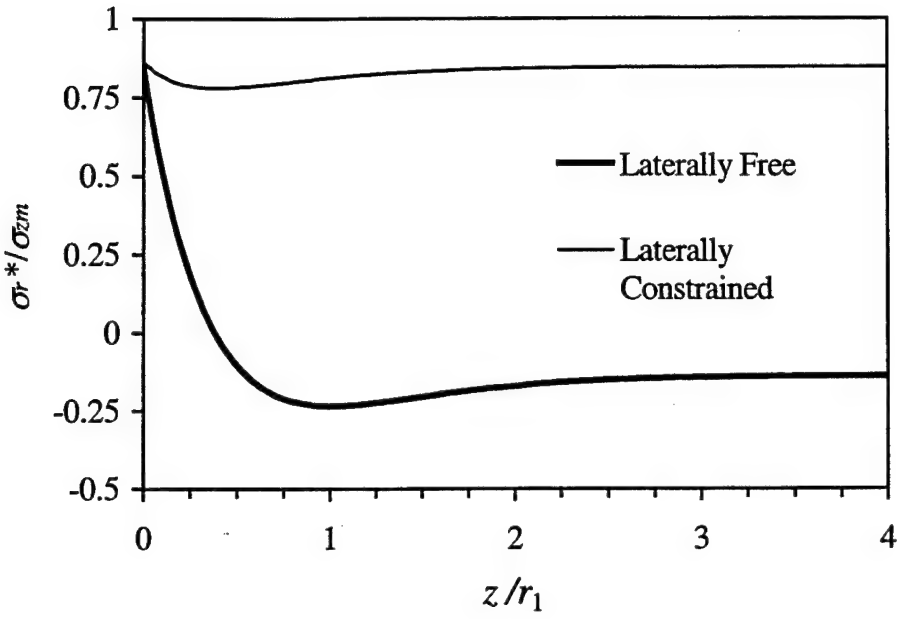

Figure 3.14: Comparison of the interfacial radial stress in both laterally free and laterally constrained systems for the case of a cracked matrix at $z = 0$ with $\varepsilon = 0.8\%$.

3.3 Cases of Dynamic Loading

We already established in the previous sections of this chapter that the analyses of the laterally free case and the laterally constrained case are parallel. We will choose only one of them for any single application, with the understanding that similar argument can be established for the other. As far as dynamic loading is concerned, we will deal only with the laterally constrained case, discussed in Chapter 2. The behavior of a laterally constrained composite system is therefore described by the four coupled equations (2.28), (2.29), (2.32) and (2.40). Unlike the case of static loading, these equations, in their full form can not be reduced to a single equation similar to equation (3.1), and have to be dealt with as is. In order to do so, we assume a steady state harmonic solution for the system as

$$u_f = X_1 e^{\alpha z + i\omega t} \tag{3.7a}$$

$$u_m = X_2 e^{\alpha z + i\omega t} \tag{3.7b}$$

$$A = X_3 e^{\alpha z + i\omega t} \tag{3.7c}$$

$$B = X_4 e^{\alpha z + i\omega t} \tag{3.7d}$$

where X_i, i =1..4 are amplitudes yet to be determined as part of the solution, ω is the circular frequency and α is an unknown parameter.

Substituting these expressions into the system of equations (2.28, 2.29, 2.32, 2.40) and rearranging in matrix form, we get for the case of isotropic fiber

$$\begin{bmatrix} n_f(\lambda_f + 2\mu_f)\alpha^2 + n_f\rho_f\omega^2 & 0 & 2n_f & 2n_f\lambda_f\alpha \\ 0 & n_m(\lambda_m + 2\mu_m)\alpha^2 + n_m\rho_m\omega^2 & -2n_f & -2n_f\lambda_m\alpha \\ -1 & 1 & -\eta_2 & \eta_1\alpha \\ -\lambda_f\alpha & \lambda_m\alpha & \eta_1\alpha & \xi_2\omega^2 - \xi_1 \end{bmatrix} \begin{Bmatrix} X_1 \\ X_2 \\ X_3 \\ X_4 \end{Bmatrix} = \underline{0} \tag{3.8}$$

For nontrivial solutions, the determinant of the left hand side must be zero. Upon doing this we get six values for the exponent α. We have a complete set of coefficients X_i, i=1..4 corresponding to each value of α. At this point of the solution only their ratios can be determined and therefore, we chose to solve for X_2, X_3 and X_4 in terms of X_1.

Using the method of superposition, the formal solutions for the displacement

$$(u_f, u_m, A, B) = \sum_{q=1}^{6} (1, V_{2q}, V_{3q}, V_{4q}) X_{1q} e^{\alpha_q z + i\omega t}, \tag{3.9}$$

$$(\sigma_{zf}, \sigma_{zm}, \sigma^*) = \sum_{q=1}^{6} (D_{1q}, D_{2q}, D_{3q}) X_{1q} e^{\alpha_q z + i\omega t}, \tag{3.10}$$

where

$$D_{1q} = (\lambda_f + 2\mu_f)\alpha_q + 2\lambda_f V_{4q},$$

$$D_{2q} = (\lambda_m + 2\mu_m)\alpha_m V_{mq} - 2\frac{n_f}{n_m}\lambda_m V_{4q},$$

$$D_{3q} = r_1 V_{3q}.$$

The external loading, as well as the two damage types are now imposed as boundary conditions to the problem.

3.3.1 Undamaged fiber matrix Composite

In the absence of damage, the applicable boundary conditions at both ends of the composite can be summarized as

$$\sigma_{zf}(-L/2) = Pe^{i\omega t} \quad , \sigma_{zm}(-L/2) = Pe^{i\omega t} \quad , \sigma^*(-L/2) = 0 \tag{3.11a}$$

$$\sigma_{zf}(L/2) = Pe^{i\omega t} \quad , \sigma_{zm}(L/2) = Pe^{i\omega t} \quad , \sigma^*(L/2) = 0 \tag{3.11b}$$

Where P_{i0}, P_{iL}, i = 1,2 are the fiber and matrix normal stresses at both ends. Since all load amplitudes are chosen equal, the deformation of the system is symmetric about its center z=0 and an equivalent set of boundary conditions will then be $\overline{u}_f(0) = \overline{u}_m(0) = \sigma^*(0) = 0$ and also either of equations (3.11a) or (3.11b) is to be satisfied. Solutions for this case are obtained from Eqs. (3.9) and (3.10), where X_{1q} values are obtained from satisfying the boundary conditions (3.11).

The effect of the loading frequency ω, in krad/s, on the distributions of the amplitudes of the fiber average normal stress σ_{zf}, the matrix average normal stress σ_{zm} and the interfacial shear stress σ^* is displayed in Figs. 3.15, 3.16 and 3.17, respectively.

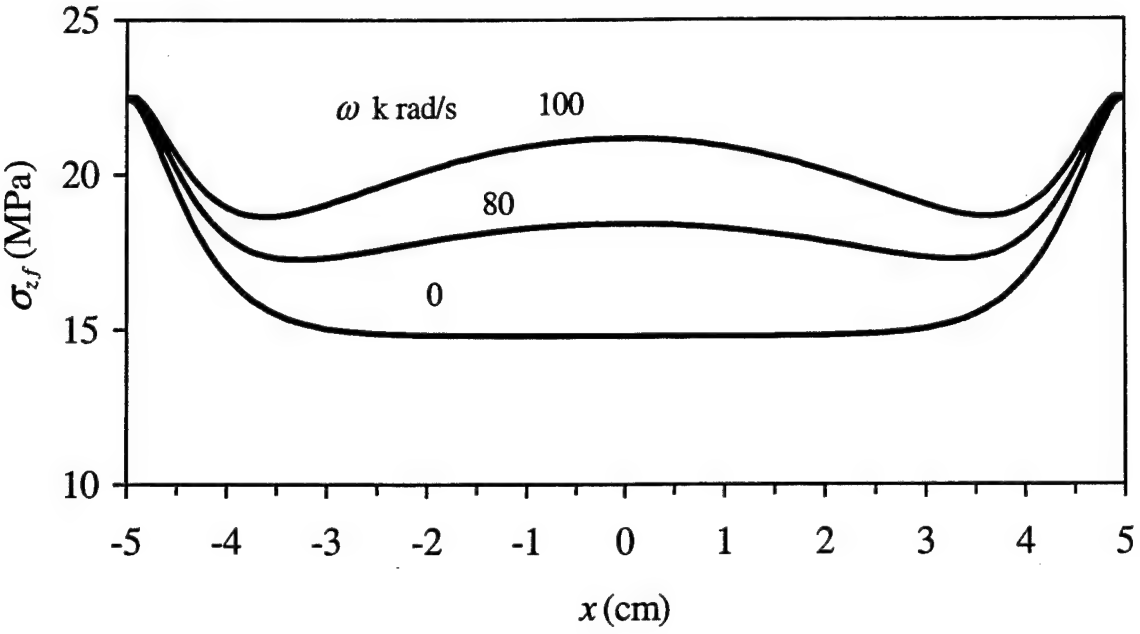

Figure 3.15: Variation of the amplitude of the fiber normal stress distribution with the loading frequency for the case of fiber pull-out.

In these figures the fiber and matrix properties are the same as those used in the cases of static loading, and only the fiber is loaded, to simulate the important case of fiber pull-out. In all figures we notice that most stress variations take place in the vicinity of the outer edges near the applied loads. For each frequency, moving from the loaded end inward, we see that the fiber normal stress decreases to its minimum value at the center and that of the matrix increases to the limiting value at the same location. The interfacial shear stress starts and ends with zero values at the outer and center locations but has a sharp variation close to the loaded ends. For normal stresses, it is seen that an increase in frequency leads to a pronounced stiffening of the material and hence to an increase in the values of these stresses. This is in contrast with the interfacial shear stress, which seem to be rather insensitive to frequency variations.

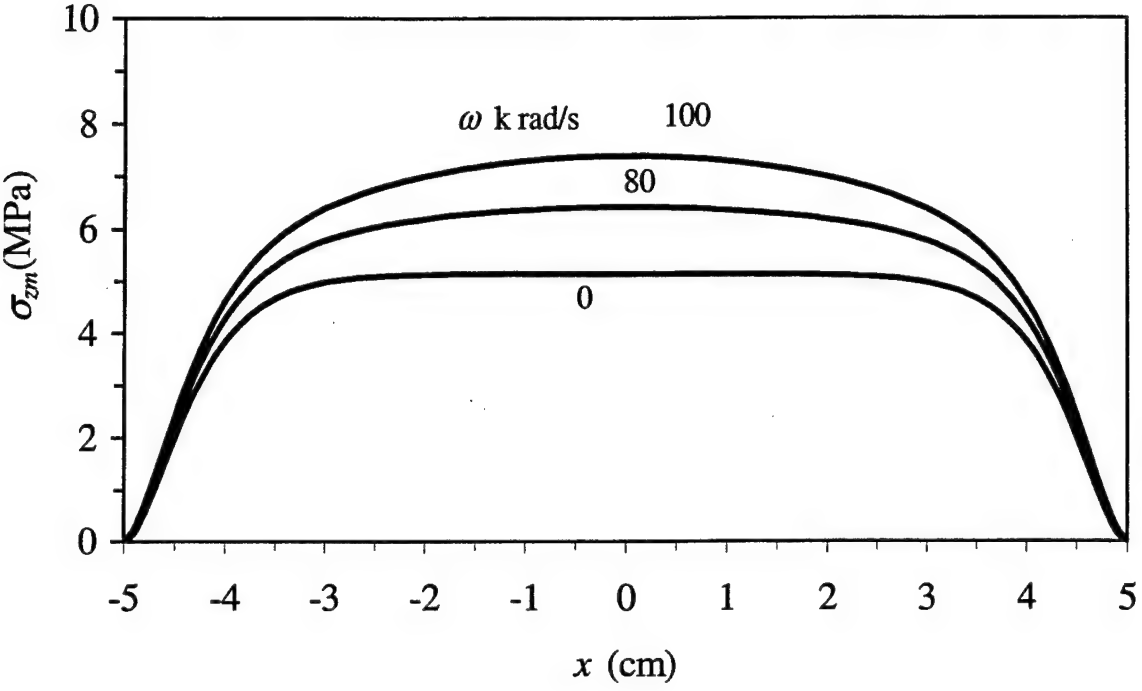

Figure 3.16: Variation of the amplitude of the matrix normal stress distribution with the loading frequency for the case of fiber pull-out.

The above observations suggest, at least for the fiber, that fiber breaks, if occur, will most probably take place at the center of the slab. For this reason, in the next two subsections we discuss the possibilities of a matrix crack or a fiber break at the center of the slab separately.

3.3.2 Broken Fiber Case

For the case of a broken fiber at $z = 0$, the shear stress in both media, the normal stress in the fiber and the displacement $\bar{u}_2$ in the matrix all vanish at the break location. Here, the applicable boundary conditions then become

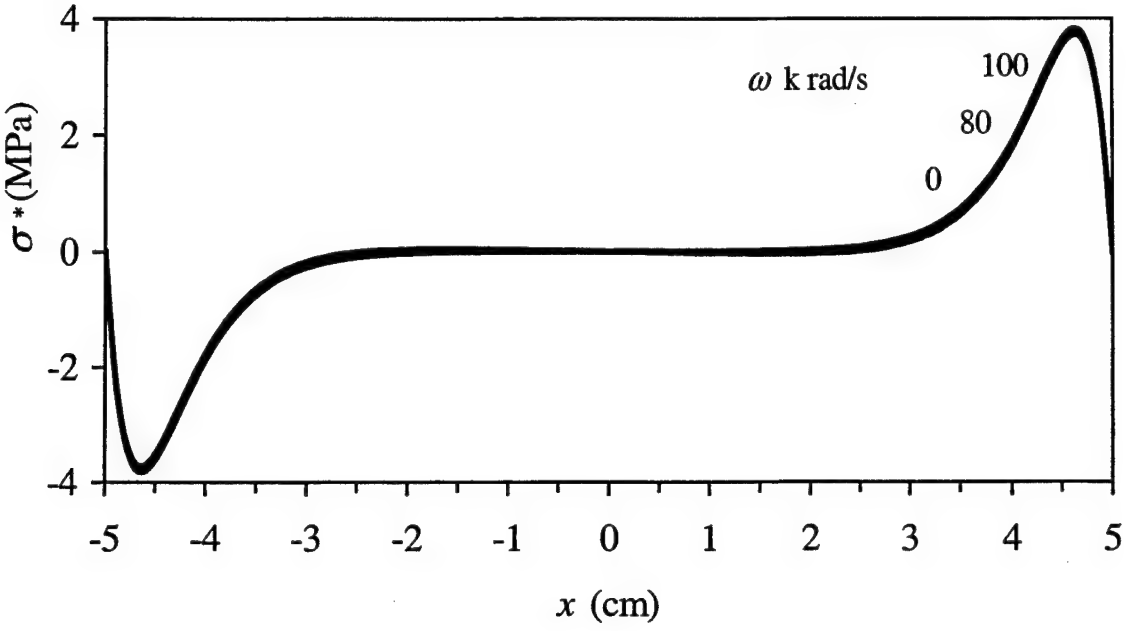

Figure 3.17: Variation of the amplitude of the interfacial shear stress distribution with the loading frequency for the case of fiber pull-out.

$$\sigma_{zf}(0)=0\ , \qquad u_m(0)=0\ , \qquad \sigma^*(0)=0 \tag{3.12a}$$

$$\sigma_{zf}(L/2)=Pe^{i\omega t}\ , \quad \sigma_{zm}(L/2)=Pe^{i\omega t}\ , \quad \sigma^*(L/2)=0 \tag{3.12b}$$

Under these boundary conditions, we solve for the appropriate amplitudes X_{1q} from Eqs. (3.9) and (3.10). The effect of the load frequency on the distributions of the amplitudes of the fiber average normal stress σ_{zf}, the matrix average normal stress $\overline{\sigma}_{z2}$ and the interfacial shear stress σ^* is displayed in Figs. 3.18, 3.19 and 3.20, respectively.

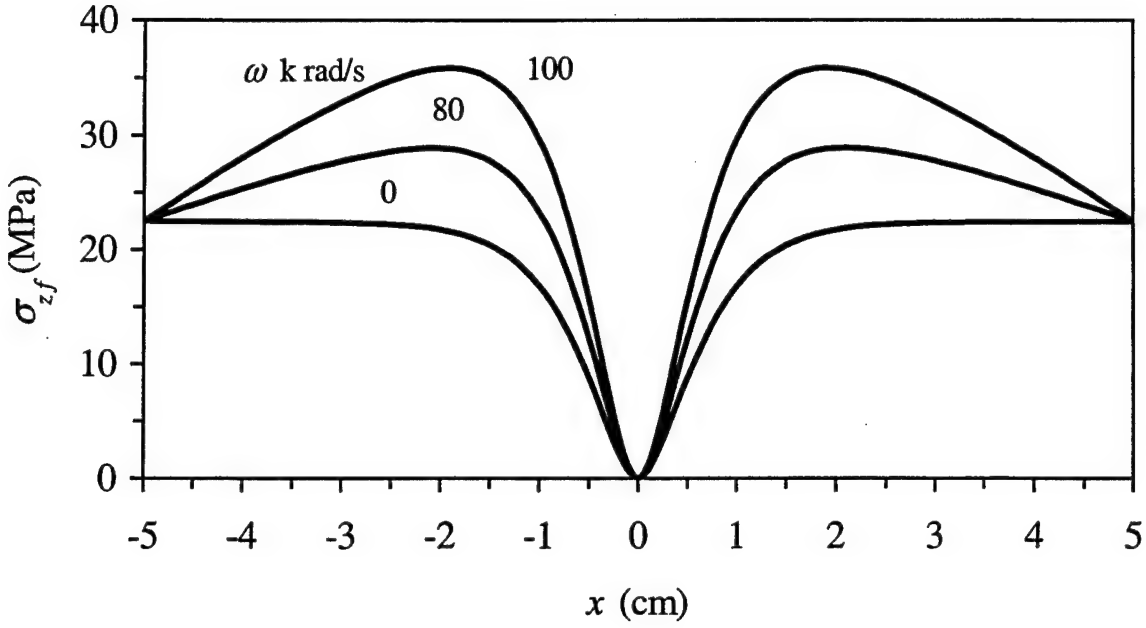

Figure 3.18: Variation of the amplitude of the average fiber normal stress distribution with the loading frequency for the case of a broken fiber at $z = 0$.

In these figures, once again, the results are presented for the same frequencies used in the previous situation. All figures clearly show comparative increase in the stresses for increasing frequency. All stresses are seen to be more or less similar to those corresponding to the undamaged case in the vicinity of the edge loads. Pronounced changes in the stress pattern take place in the vicinity of the break. This is due to the large transfer of the load between the matrix and the fiber. Beside such a transfer between the normal stress components, a pronounced variation of the interfacial shear stress takes place close to the break. It should be noted that the crack opening can be obtained from Eq. (2.32) by setting $u_2 = 0$ and $A = 0$, resulting in

$$u_1(0) = \eta_1 \left. \frac{\partial B}{\partial z} \right|_{z=0} . \tag{3.13}$$

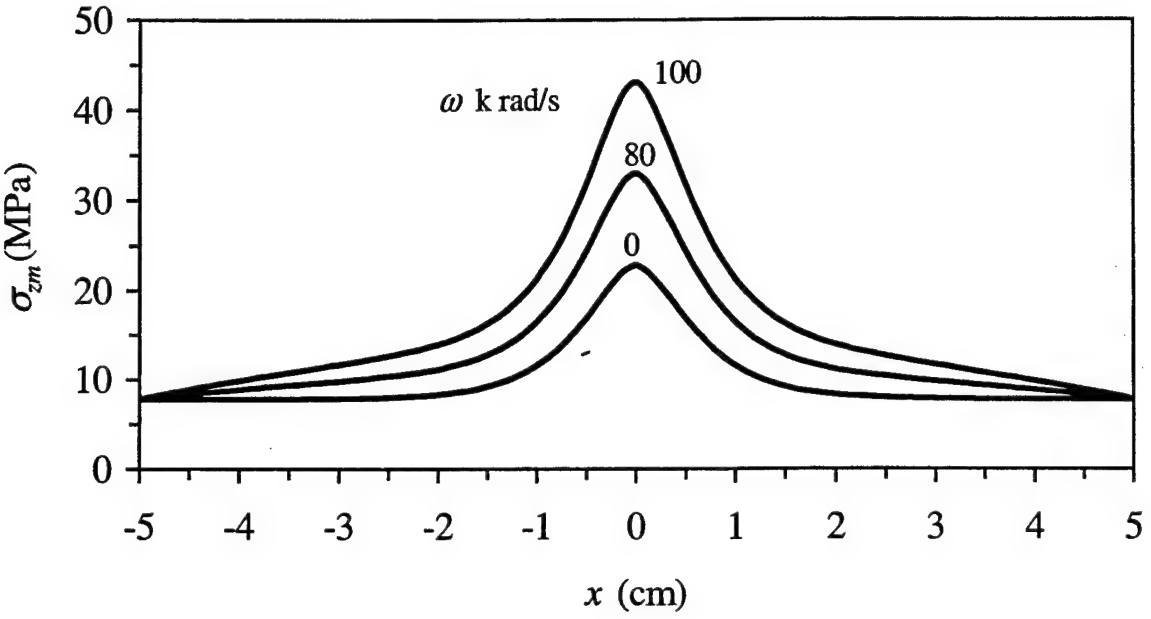

Figure 3.19: Variation of the amplitude of the matrix normal stress distribution with the loading frequency for the case of a broken fiber at $z = 0$.

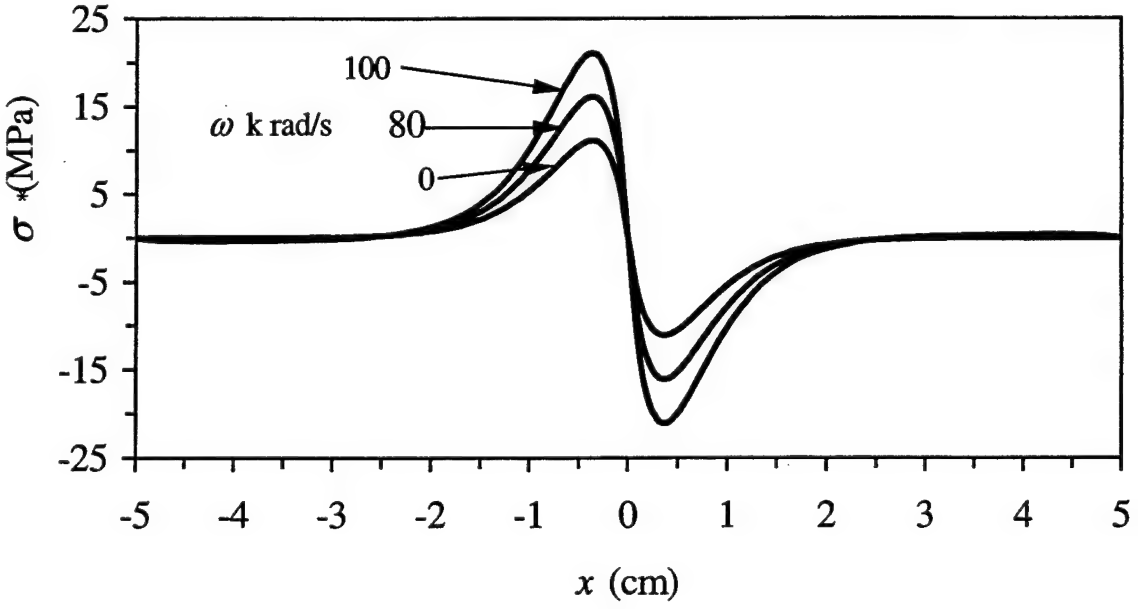

Figure 3.20: Variation of the amplitude of the interfacial shear stress distribution with the loading frequency for the case of a broken fiber at $z = 0$.

3.3.3 Matrix Cracking

For cases involving matrix cracking transverse to the fiber direction, say at $z = 0$, the shear stresses σ_{rz1} and σ_{rz2}, the normal stress $\overline{\sigma}_2$ in the matrix and the fiber normal displacement $\overline{u}_1$ vanish at that location. Within the context of the present modeling, the applicable boundary conditions in the presence of the matrix crack can be summarized as

$$\sigma_{zm}(0) = 0 \ , \qquad u_f(0) = 0 \ , \qquad \sigma^*(0) = 0 \tag{3.14a}$$

$$\sigma_{zf}(L/2) = Pe^{i\omega t} \ , \quad \sigma_{zm}(L/2) = Pe^{i\omega t} \ , \quad \sigma^*(L/2) = 0 \tag{3.14b}$$

Solutions for this case are obtained from Eqs. (3.9) and (3.10), in a manner identical to that of the broken fiber. Therefore no further discussion of this case in necessary. As a byproduct of the analysis, the matrix crack opening can be easily calculated from equation (2.32) by merely setting $\overline{u}_1 = 0$ and $A = 0$, resulting in

$$u_2(0) = -\eta_1 \left.\frac{\partial B}{\partial z}\right|_{z=0} \tag{3.15}$$

The formulation of section 3.3, as well as its application to several situations, is detailed in [26]. There are several ways to compare the results of the dynamic loading formulation with experimental data. One is to compare the phase velocities of propagating waves at different frequencies (dispersion curves). This is done in [27] for the case of a titanium alloy matrix reinforced with three-layer concentric cylindrical SiC fibers. Each fiber is about 140 μm in total diameter and consists of a carbon core and a SiC shell separated from the matrix by another 3-μm-thick carbon layer. The mechanical properties of all the constituents are presented in table 3.1. The effective fiber anisotropic

properties are calculated from these individual isotropic properties by a repetitive application of the procedure outlines in [1], which can handle single material fiber and matrix. The frequency dependence of the fundamental mode is plotted in figure 3.21 and compared with the exact solution and with the experimental data of Huang and Rokhlin. As can be seen, significant improvements are achieved by the improved mixture model when compared with the experimental data as well as with the exact solution.

Table 3.1: Material properties and dimensions for the fiber and matrix materials.

Material	Density kg/m^3	C_{11} GPa	C_{12} GPa	C_{13} GPa	C_{44} GPa	C_{55} GPa	Radius μm
Isotropic carbon	1700	49	17	17	16	49	18
SiC	3200	446	92	92	177	446	68
Interphase carbon	2100	31	21.8	21.8	4.6	31	71
Titanium	5400	193	103	103	45	193	132.3

In this chapter we have shown the versatility of the elasticity-based formulation of the micromechanical behavior of straight fibrous composites. The modeling was found to be applicable to a wide range of important problems, and its validity was established by its ability to reproduce available published results [10]. Its superiority over these previous modelings lies in its ability to solve problems that could not be solved using these models

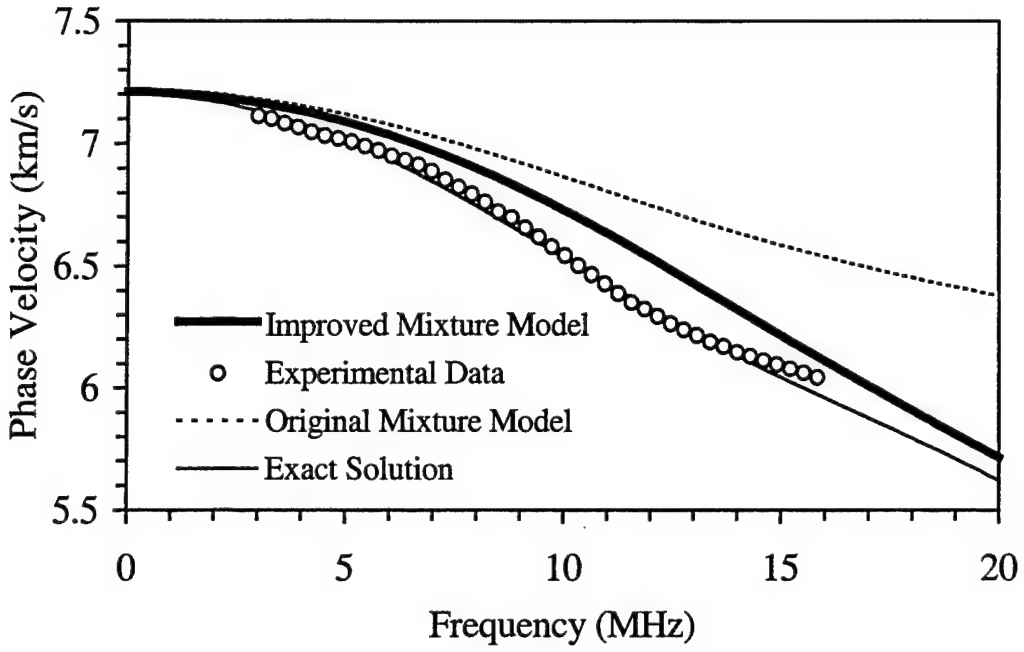

Figure 3.21: Fundamental mode comparisons of the suggested mixture model, the exact solution and experimental data.

in particular problems involving finite length representative cells and transversely isotropic constituents.

CHAPTER 4

DEVELOPMENT OF THE MODEL FOR UNDULATED FIBROUS COMPOSITES

4.1 Introduction

The model developed in chapter 2 for straight fibrous composites will be extended to cases of undulated fiber reinforcement under axial loading. This takes the analysis one step further towards modeling plain woven composites. For simplicity, we assume the undulation to be restricted to a single plane, say the *x-y* plane. The procedure is outlined as follows: First, for a given geometric undulation, we identify and analytically describe local tangents to the fiber. Second, we transform the global coordinates and applied loads to local coordinate systems consisting of the tangent directions and their normals in the plane of undulation. Third, we adapt the results obtained for straight fibers to "straight" segmented fibers along the tangents. The local stresses obtained under this procedure are then supplemented with the stress contributions that inherently rise in any oriented direction with respect to the loading direction. The resulting local stresses are found to compare favorable with finite element calculations.

4.2 Geometric Model

A typical undulated fiber reinforced composite is shown in figure 4.1. The periodicity of the medium allows us to model it as a concentric cylindrical system

subjected at its outer boundary to vanishing shear stress and radial displacement as illustrated in figure 4.2. The fiber centerline is assumed to follow the periodic function

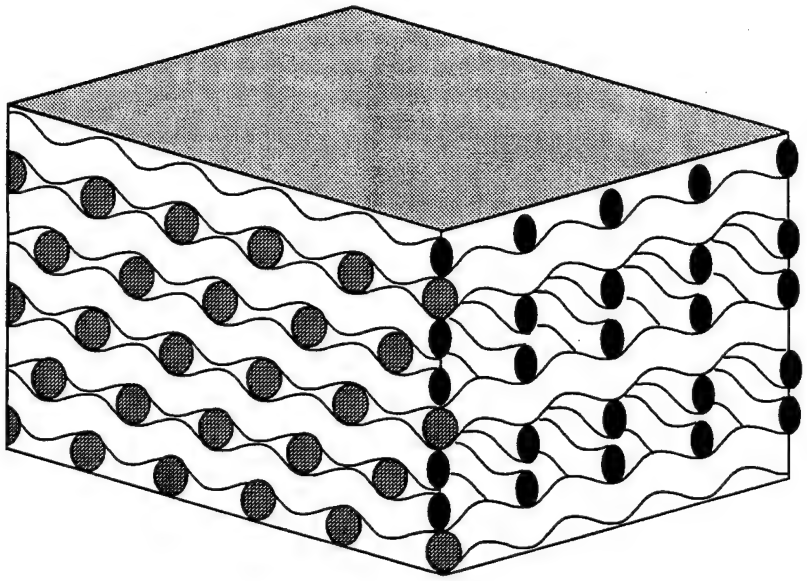

Figure 4.1: Undulated fibrous composite panel.

$$f(x) = A\cos\left(\frac{2\pi n(x-B)}{L_x}\right) \qquad , n = 1, 2, 3,.... \tag{4.1}$$

where L_x is the panel length. At any global location x, the local inclination angle θ is then defined as

$$\theta(x) = \tan^{-1}\left(\frac{df(x)}{dx}\right). \tag{4.2}$$

Along the tangent direction at the angle θ, a "local" coordinate z is chosen which relates geometrically to the global coordinate x as

$$z = x/\cos\theta(x) \tag{4.3}$$

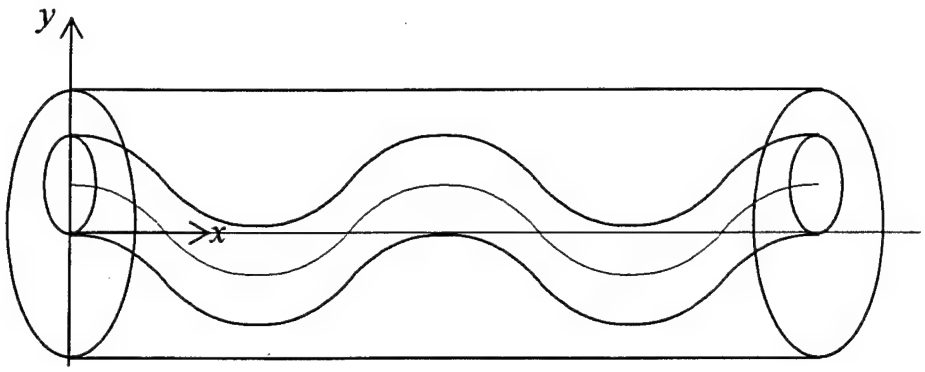

Figure 4.2: Representative unit cell.

4.3 Derivation of the Undulated Case from the Straight Fibrous Case

The representative unit cell of figure 4.2 is assumed to be loaded symmetrically as shown in figure 4.3. The loads consist of axial as well as transverse stress components. The axial boundary stresses are arbitrarily assigned the values P_{x1} and P_{x2}, for the fiber and matrix, respectively. The transverse stress P_y is still an unknown and rises as a consequence of the axially loaded, but laterally constrained, systems. Its value will be approximated and calculated based upon the Lame' type solutions of the system (under axial iso-strain assumptions). Based on the iso-strain analysis, P_y takes the form

$$P_y = \frac{\left(n_1 \nu_1 P_{x1} / E_1 + n_2 \nu_2 P_{x2} / E_2\right)}{\left[n_1(1-\nu_1)/E_1 + n_2(1-\nu_2)/E_2\right]} \tag{4.4}$$

Along the tangent direction, i.e. at the angle of inclination θ, the fiber and matrix boundary stresses transform to

$$\overline{P}_1 = P_{x1}\cos^2\theta + P_y \sin^2\theta \tag{4.5a}$$

$$\overline{P}_2 = P_{x2}\cos^2\theta + P_y \sin^2\theta \tag{4.5b}$$

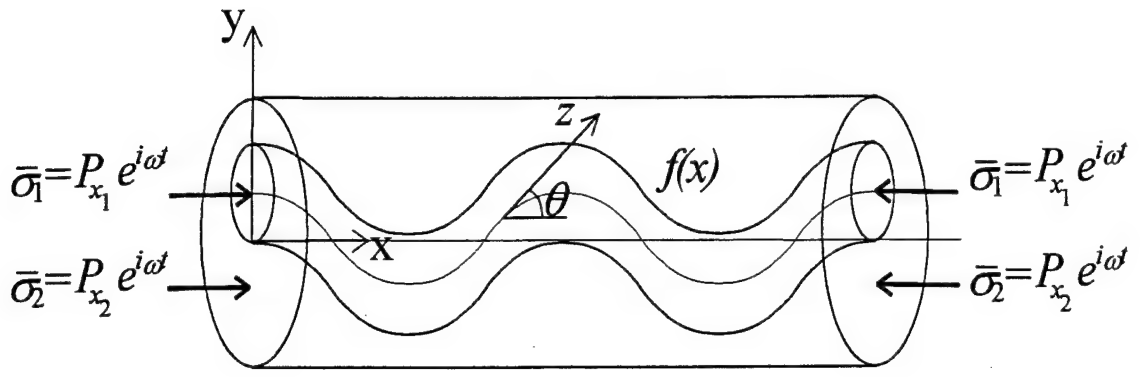

Figure 4.3: Characterization of loads.

The fundamental assumption is that the local stresses, at any location x, constitute a superposition of two components. With reference to figure 4.4, the first is obtained from adapting the solutions of the straight fiber to directions along the tangents and the second is the inherent stresses that rise in the matrix in directions that are inclined to the loading directions. The first component is more difficult to obtain and requires the solution of the field equations for the straight fiber case in cylindrical coordinate system. This, however, was treated in chapter 2.

The equations developed in chapter 2 can be applied to any straight fiber system, having any length and subjected to prescribed axial stresses at its ends. In particular this equation can be updated and used for all segments along the undulated fiber by choosing, for a given $\theta(x)$, the value of P as constructed in Eq.(4.5), and the system length of $L = L_x / \cos\theta(x)$. This constitutes the first part of the stress distribution. The second part is the inherent stress distribution that rises on planes that are inclined at the θ- direction

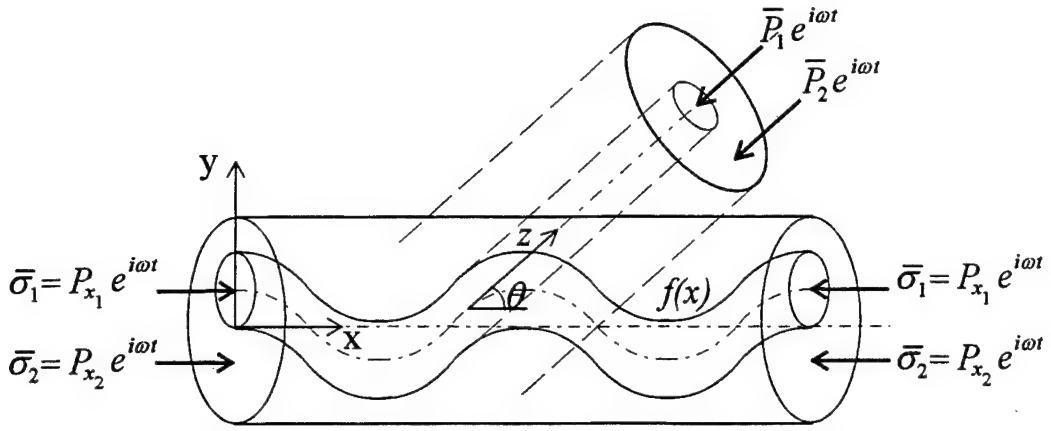

Figure 4.4: Solution Strategy for an undulated segment.

from the loading direction. Thus the final interfacial shear stress distribution takes the form

$$\sigma^*_{un} = \sigma^* - \left(P_x - P_y\right)\sin\theta\cos\theta\sin\varphi \qquad (4.6)$$

where ϕ is the azimuthal angle that runs counter-clock wise along the circumference of the fiber. Thus, it defines the *x-r* plane that is inclined to the plane of undulation. We note that the maximum contribution of the inherent stress components exists at $\phi = \pm 90^o$. These are the directions of the plane of undulation. $\phi = 0^o$ and 180^o define the directions that are normal to the plane of undulation where the inherent stresses vanish. It is obvious that the undulated fiber results reduce to the corresponding case of straight fibers by merely setting the amplitude of undulation to 0.

In the following chapter we provide comparisons of the results of this formulation with those of finite element for a variety of situations. We also discuss the applicability of the formulation to cases involving different types of damage and static as well as dynamic loading.

CHAPTER 5

APPLICATIONS OF THE UNDULATED FIBROUS MODEL

5.1 Application to Cases of Static Loading

The solution strategy described in chapter 2 for the case of straight fibrous composites and extended in chapter 4 for undulated fibrous composites can be applied to cases of static loading. This is done in details in [28]. In that case, the four coupled differential equations (2.28), (2.29), (2.32), (2.40) can be combined into a single equation identical to equation (3.1). The longitudinal coordinate z, however, is now in the local tangent direction for each segment. Loads also have to be transformed into local coordinates as explained in chapter 4. The procedure is demonstrated in this section for two test cases and the results are compared to those of the finite element. The test cases consist of a fiber-matrix composite with eight complete fiber sinosoidal waves. Material properties are the same as those used in [10] and in the examples of Chapter 3. The undulated fiber has a length to amplitude ratio $L_x / a = 8$ and a fiber volume fraction of 0.321.

Finite element results are generated using *ANSYS* package. The FE code source file itself is generated using a modified *MATHEMATICA* program that was originally developed by Al-Huniti [2]. This program requires the fiber and matrix properties, the length/fiber ratio, and the element size. Only half of the problem is solved to make use of the symmetry about the x-y plane. Both tetrahedron and brick elements are used and the problem symmetry about the y-axis is utilized. Overall, 278 higher order tetrahedron elements were used to model the fiber and the matrix volumes. The fiber-matrix

composite displacements are constrained in the lateral direction in order to satisfy the required condition $v_2(z,r_2)=0$, except for the surface $x=L_x/2$, on which the external load is applied. Figure 5.1 shows the finite element model used in the test cases.

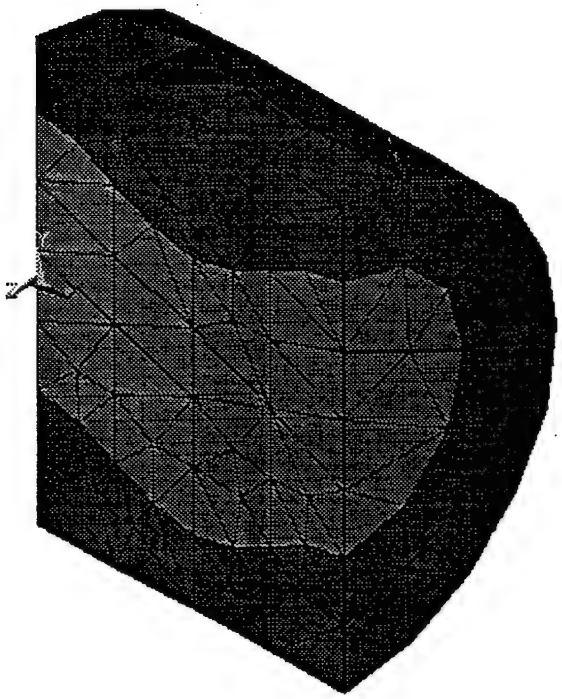

Figure 5.1: Finite element model of a segment of the test case

In the first test case, the undamaged fiber-matrix composite is under condition of fiber pull-out. Therefore, the matrix surface at both ends is stress- free. Results of the fiber normal stress and the interfacial shear stress σ^* are shown in Figs. 5.2 and 5.3. In calculating σ_{zf} from the finite element results at specific cross-sections (results denoted by triangles on the figure), the stress tensor component in the fiber direction was

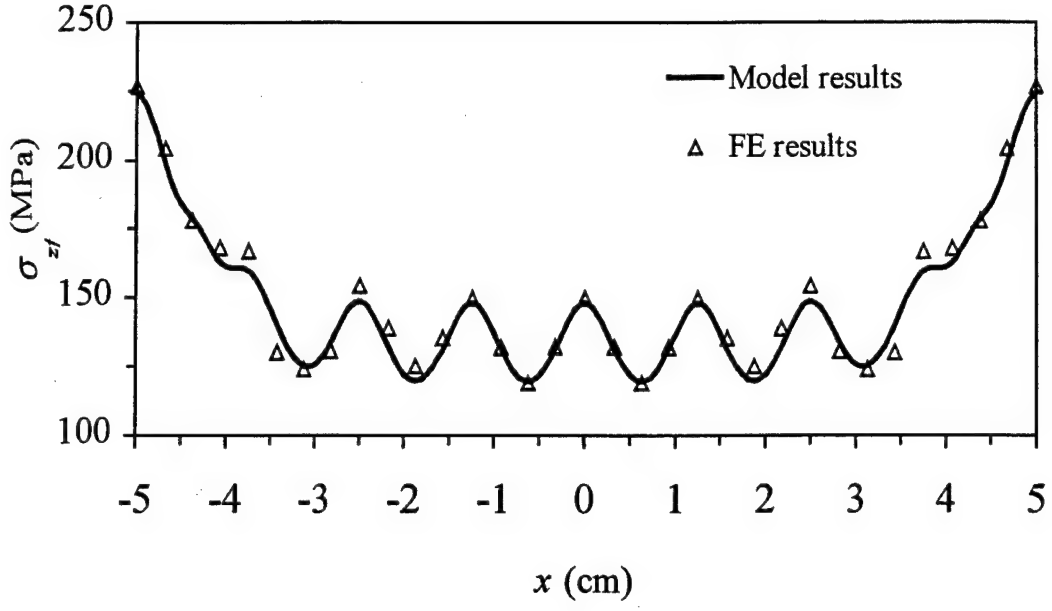

Figure 5.2: Comparison of the fiber normal stress distribution during fiber pull-out in an 8 wave fibrous composite calculated by the proposed model and finite element results.

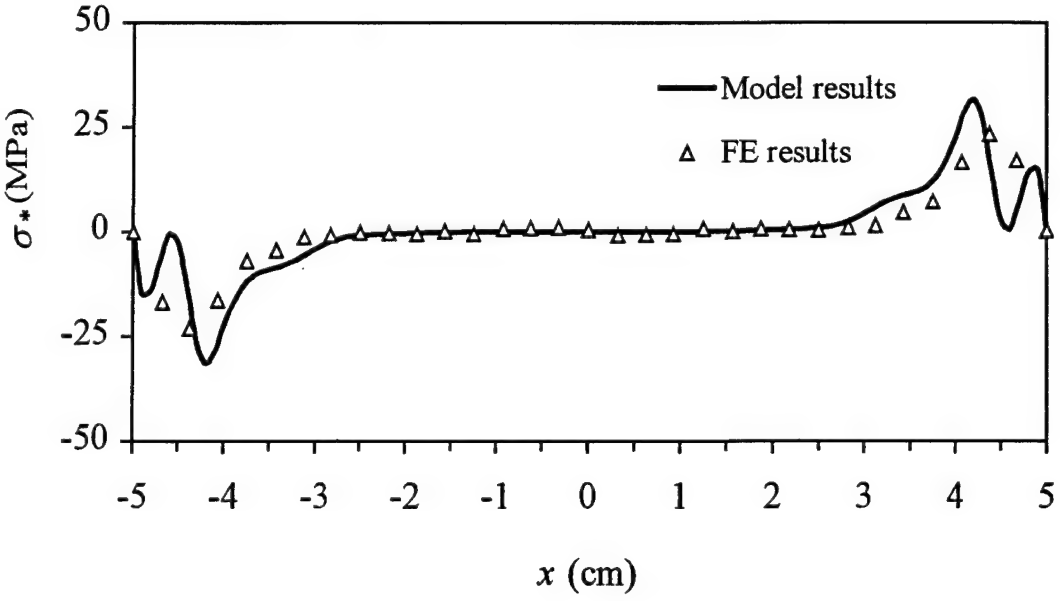

Figure 5.3: Comparison of the interfacial shear stress distribution during fiber pull-out in an 8-wave fibrous composite calculated by the proposed model and finite element results.

averaged over the fiber cross sectional area. A good agreement between the analytically predicted values and the finite element solution can be seen. As expected, the effect of undulation is a maximum at locations of maximum slope θ, and the stress distribution approaches that of the straight fibrous case at locations of zero slope.

In the other test case, damage is introduced in the form of a fiber break at $z = 0$. The composite is subjected to an overall strain of 0.1 % at both ends. As seen from figures 5.4, there exists a very good agreement between the predicted distribution for the

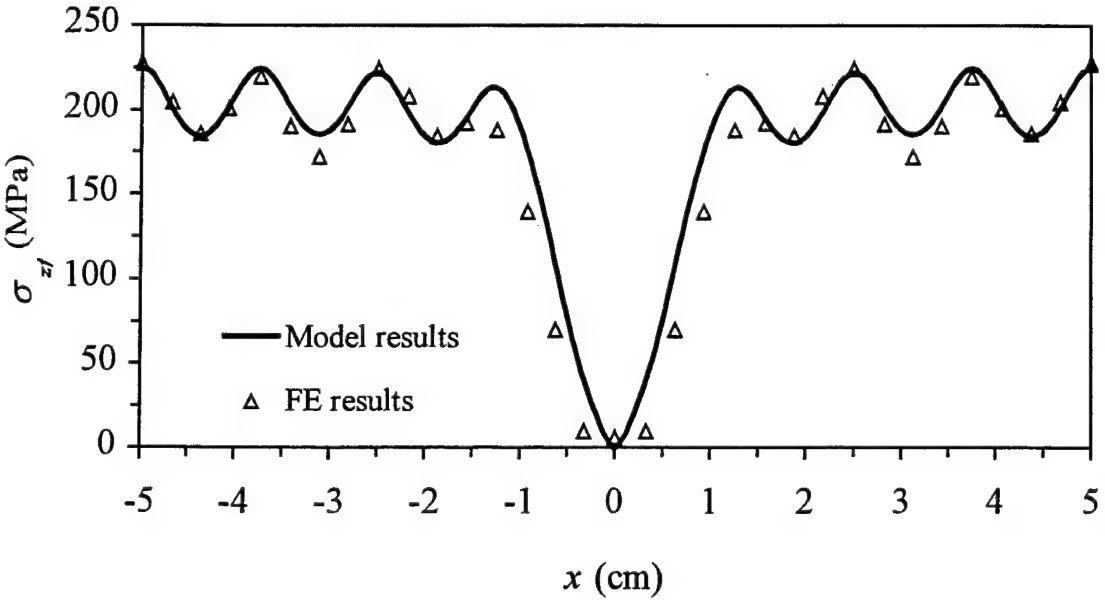

Figure 5.4: Comparison of the fiber normal stress distribution in the presence of a fiber break in an 8 wave fibrous composite under axial loading calculated using the proposed model and finite element results.

fiber normal stress and the finite element results. Results are not so good in the case of interfacial shear stress, as seen in figure 5.5. The reason is that the calculation of σ^*

involves an additional differentiation in both the analytical and the finite element solution. This usually gives rise to some deviation in the results.

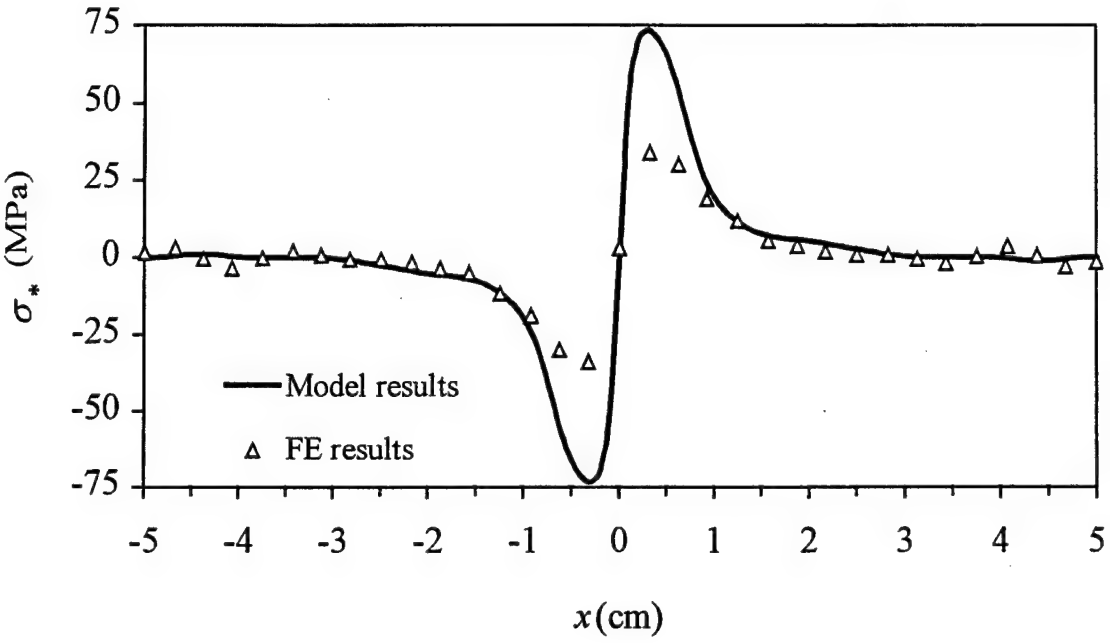

Figure 5.5: Comparison of the interfacial shear stress distribution in the presence of a fiber break in an 8 wave fibrous composite under axial loading calculated using the proposed model and finite element results.

5.2 Cases of Dynamic Loading

As explained in chapter 4, the solution method discussed in chapter 2 can be adopted to cases of undulated reinforcement if the local coordinate as well as the local transformed loads are used. As illustrations of this case, we once more revisit the two test cases of the previous section 5.1. Here, however, we are to investigate the effect of a harmonic type of loading on the stress distributions. Figures 5.6, 5.7 and 5.8 show that effect for the case of fiber pull-out for frequencies below the resonance frequency. Both the fiber and matrix normal stresses increase considerably with the loading frequency,

while the interfacial shear stress distribution is almost independent of it. Figure 5.8 shows therefore, that the progression of delamination, which is caused mainly by the interfacial shear stress σ^*, does not depend on the loading frequency for the case of harmonic loading.

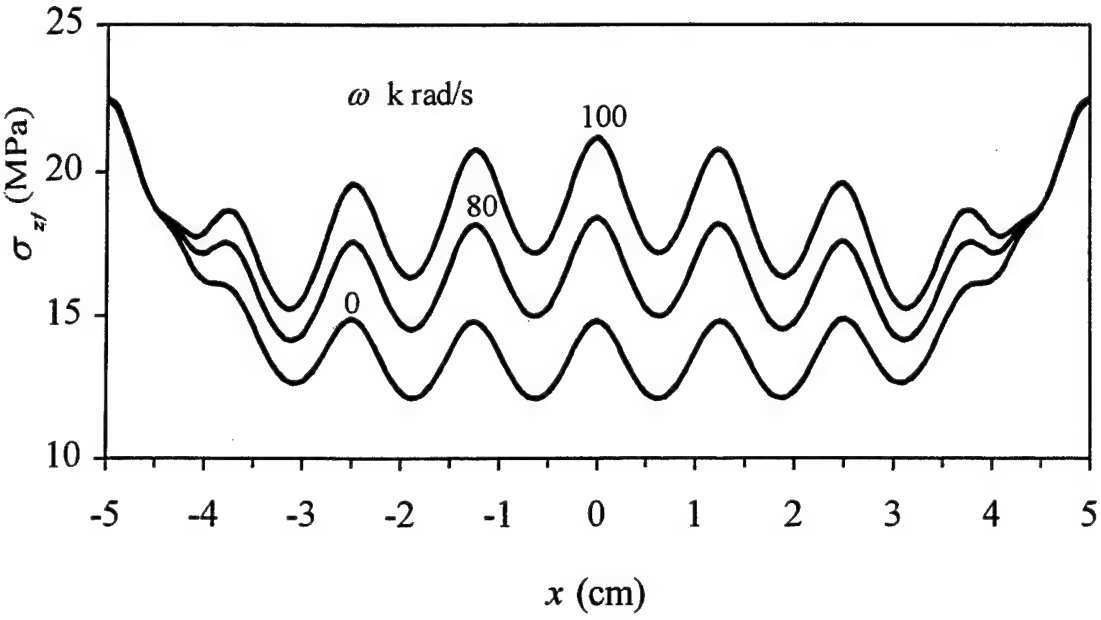

Figure 5.6: Variation of the amplitude of the fiber normal stress distribution with the loading frequency for the case of undulated fiber during fiber pull-out.

Next we consider the other test case of an undulated fibrous composite that include broken fibers under applied harmonic strain of amplitude 0.1%. Figures 5.9, 5.10 and 5.11 show how the amplitudes of the various stress components vary with the loading angular frequency. Figures 5.9 and 5.10 show that the normal stresses exhibit a trend similar to that of the corresponding figures of the fiber pull-out case. The interfacial shear stress near the damage, however, depends considerably on the loading frequency, as seen

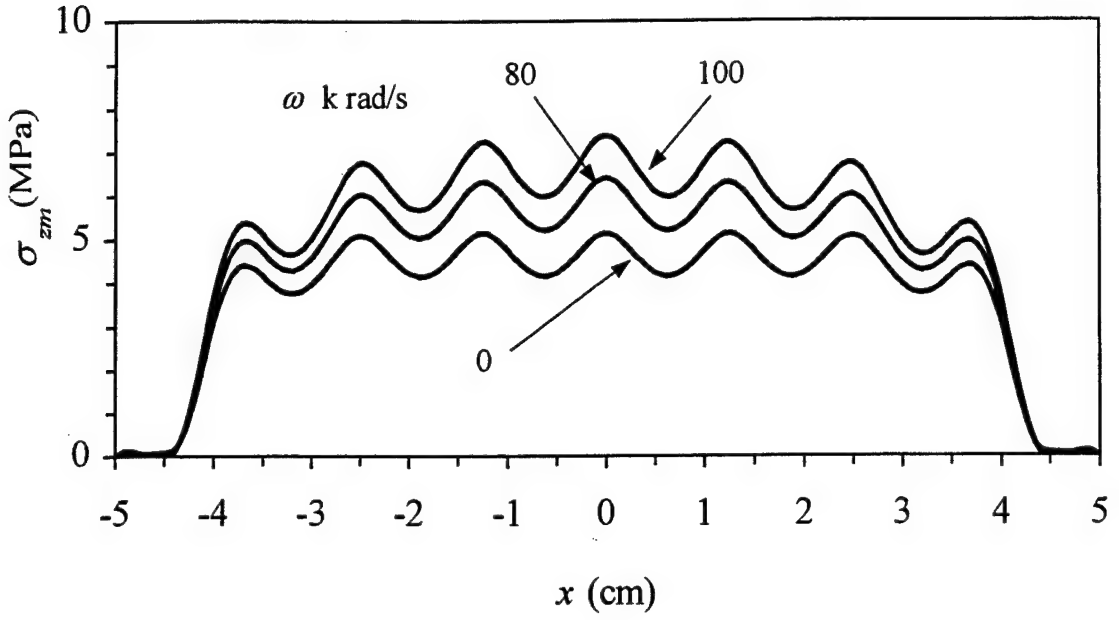

Figure 5.7: Variation of the amplitude of the matrix normal stress distribution with the loading frequency for the case of undulated fiber during fiber pull-out.

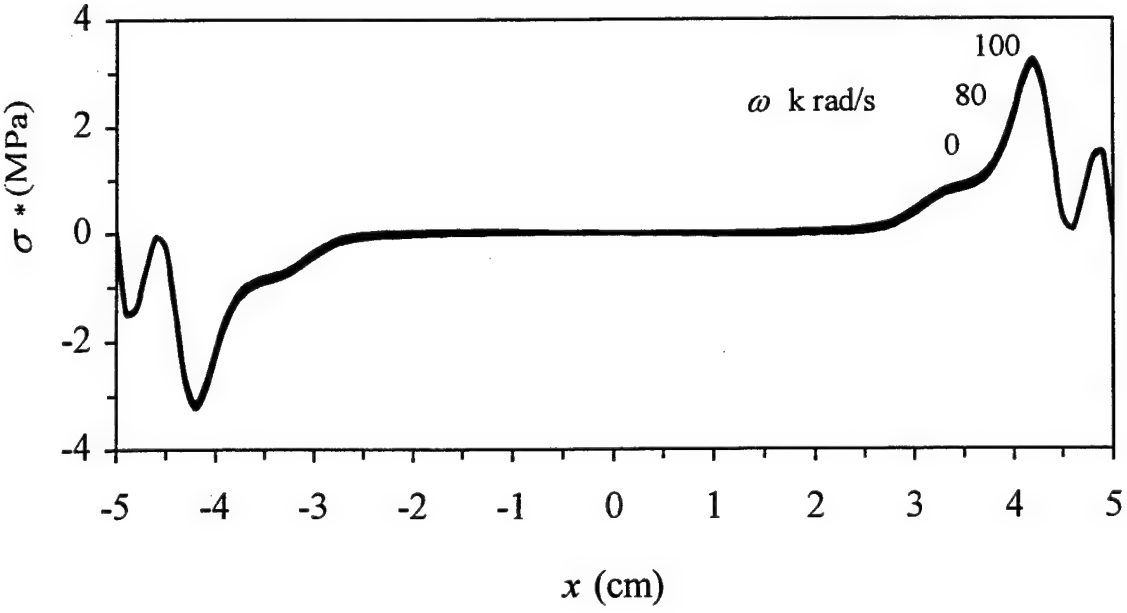

Figure 5.8: Variation of the amplitude of the interfacial shear stress distribution with the loading frequency for the case of undulated fiber during fiber pull-out.

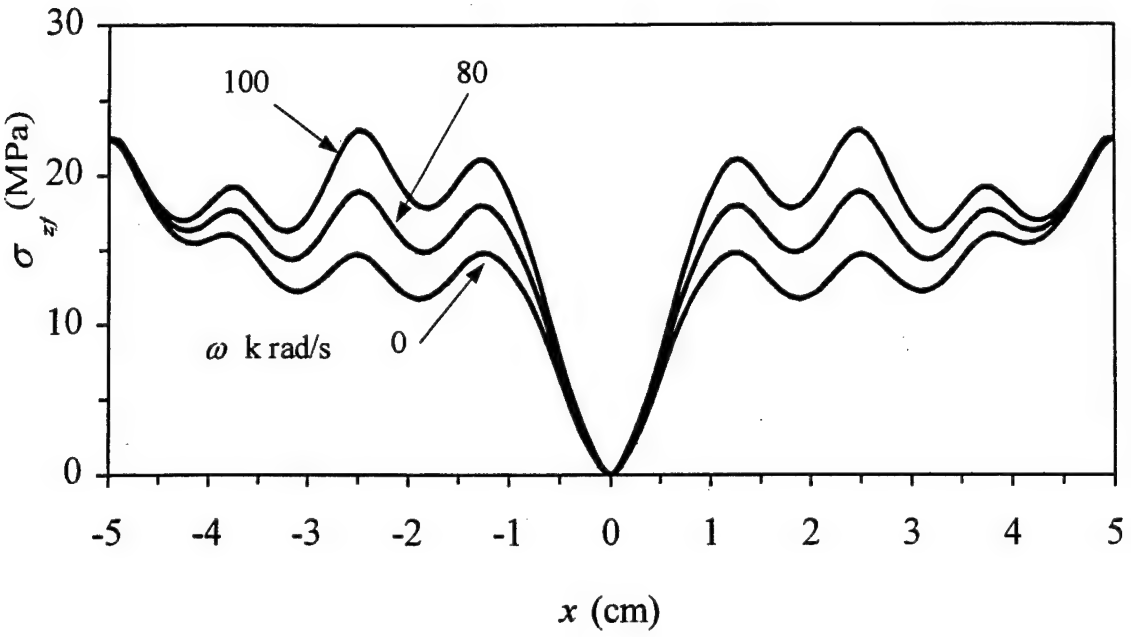

Figure 5.9: Variation of the amplitude of the fiber normal stress distribution with the loading frequency for the case of undulated fiber with a break.

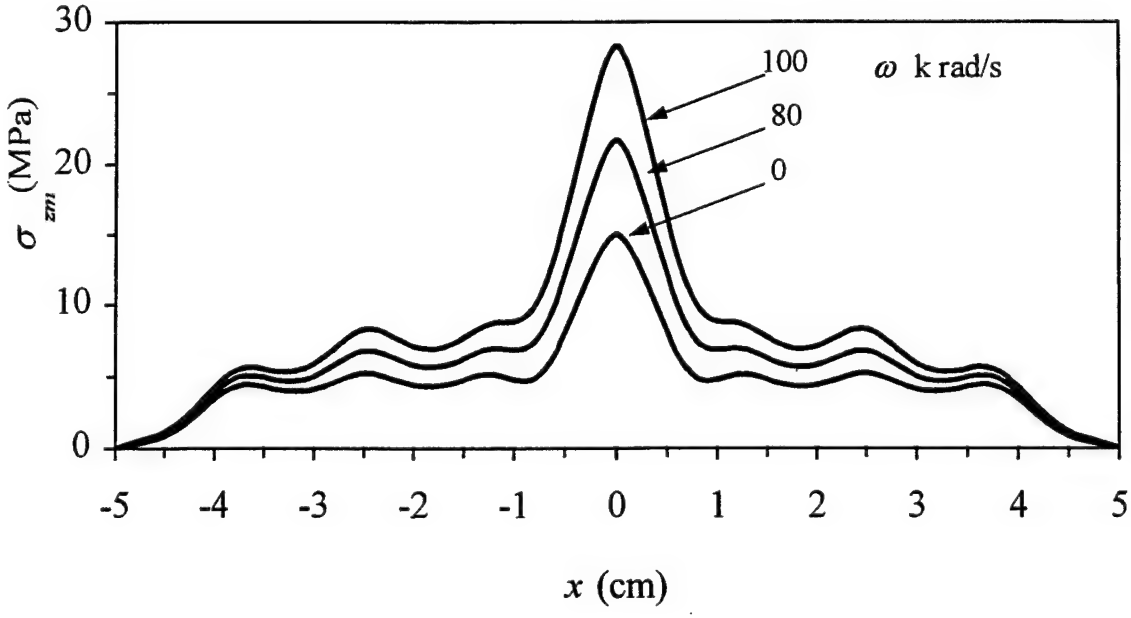

Figure 5.10: Variation of the amplitude of the matrix normal stress distribution with the loading frequency for the case of undulated fiber with a break.

in figure 5.11. Since delamination usually starts at the free surface of a damaged fiber or matrix, this suggests the dependence of the delamination propagation rate in this case on the loading frequency.

Another important variable that can be predicted by the model is the crack opening displacement. The amplitude of the opening $\Delta = u_f(0)$ is calculated as per equation (3.13) and normalized with respect to its value at zero loading frequency (static loading). The variation of this normalized displacement with the loading frequency, up to 1.5 ω_{res}, is shown in figure 5.12. Results of other cases of the behavior of undulated fibrous composites subject to harmonic loading are published in [29].

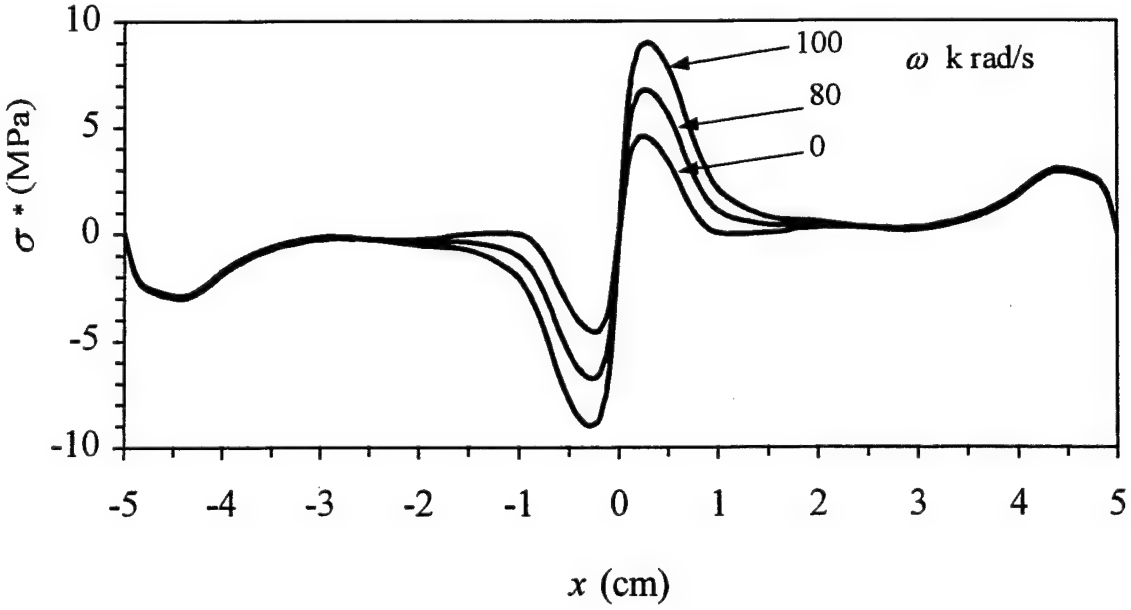

Figure 5.11: Variation of the amplitude of the interfacial shear stress distribution with the loading frequency for the case of undulated fiber with a break.

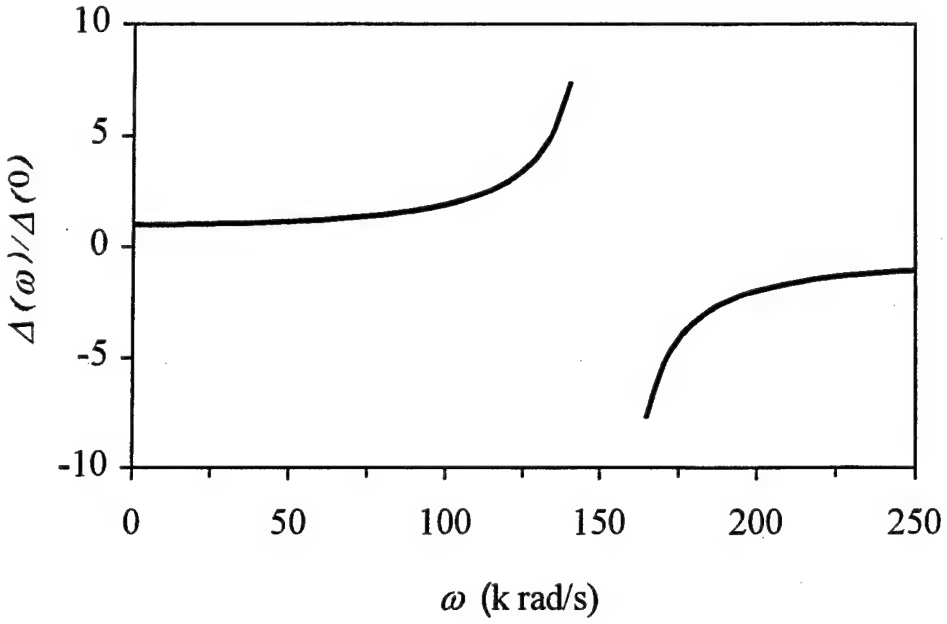

Figure 5.12: Variation of the amplitude of the fiber break opening displacement with the loading frequency for the case of undulated fiber.

With these two test cases, the analysis of the basic element of woven composites, namely the undulated fibrous composite is concluded. The micromechanical model provided accurate predictions for the stresses in both of the composite constituents, which are responsible for constituent failure, as well as for the interfacial shear stress, responsible for the delamination between the fiber and the matrix. These predictions will be used in the next chapter to predict the progression of transverse cracks as well as the extension of regions of delamination. Degradation of the composite properties that takes place will accordingly be quantified.

CHAPTER 6

DAMAGE ANALYSIS IN FIBROUS COMPOSITES

6.1 Introduction

The term damage mechanics is usually used to describe the study of the accumulation of damage from its initiation up to and including rupture. Damage is usually an ill-defined term. By damage here, we mean a local micromechanical failure at the fiber/matrix level. This failure occurs through one of several mechanisms including fiber breaking, matrix cracking, fiber-matrix debonding and fiber pull-out. The existence of a distribution of fiber breaks or matrix transverse cracks significantly degrades the stiffness and residual strength of the composite. It is the purpose of this chapter to study such an effect on straight fibrous composites.

In this chapter we will use our basic model to predict: 1. whether failure takes place in an undamaged composite panel under certain static loading, and 2. how much the successive failure affects the composite stiffness as expressed by Young's modulus. The following two sections explain the procedure to achieve these goals. Our modeling will adopt the maximum stress criterion for the onset of failure.

6.2 Damage Accumulation Prediction

Consider an undamaged straight fibrous composite as shown in figure 2.1. Upon application of external loading P, equation (3.1) can be solved for the fiber normal stress distribution in the representative unit cell. From the equilibrium of the internal stresses at

each section with the external applied load, the normal stress distribution in the matrix is calculated from

$$\sigma_{zm}(x) = (P - n_1\sigma_{zf})/n_2 \tag{6.1}$$

Using the maximum stress criterion, the matrix will fail when

$$X_m - Max[\sigma_{zm}] \leq 0 \tag{6.2}$$

where X_m is the strength of the matrix material. The same is true for the fiber material. When failure takes place in either the fiber or the matrix, the unit cell length should be adjusted accordingly and the process is repeated for increasing load values.

6.3 Evaluation of Young's Modulus

The procedure to calculating the longitudinal stiffness at a general loading step point is described in this section for the case of an existing fiber break in the system. A parallel argument can be made for the case of an existing matrix crack. As mentioned in the previous section, the first generation of results in this modeling is always the fiber normal stress as obtained from solution of (3.1). Next, equation (6.1) is used to determine the matrix normal stress distribution σ_{zm}. Once the normal stresses in the fiber and matrix are known, the integrated constitutive relation (2.27) can be used to evaluate the distribution matrix longitudinal strain, resulting in

$$\frac{\partial u_m}{\partial z} = \frac{1}{m_{11}}(\sigma_m + 2\frac{n_f}{n_m} f_{12}B) \tag{6.3}$$

Integrating this strain over the length of the unit cell, namely from $z = -L_i/2$ to $z = L_i/2$ provides the distribution of longitudinal displacements in the matrix media $u_m(z)$. The total composite Young's modulus is therefore calculated from

$$E_{eff} = \frac{PL_i}{2u_m(L_i/2)} \tag{6.4}$$

The procedures provided in sections 6.2 and 6.3 are better illustrated via a flow chart. This is shown in figure 6.1

Figure 6.2 demonstrates the process of damage propagation, in terms of transverse crack accumulation, in a straight fibrous composite. The external loading is normalized such that failure occurs when the loading has the nominal value of 10 MPa. The fiber and matrix are E-glass and Epoxy, respectively. The mechanical properties of these two materials are obtained from reference [24] as

$E_f = 69$ GPa, $\quad \nu_f = 0.22$, $\quad X_f = 3450$ MPa,

$E_m = 4.6$ GPa, $\quad \nu_m = 0.36$, $\quad X_m = 58.6$ MPa

From the figure, it is clear that in the case of straight fibrous composites the representative unit cell is divided by the cracks into pieces of approximately equal length. This is because the normal stress distribution between two cracks has a maximum value at the mid-point between these cracks. There is experimental evidence that the mean value of the probabilistic distribution of the crack location is close to the middle of the segment. Because of this, we are able to define the crack density for a straight fibrous composite as $c = 1/L_i$, where L_i is the distance between two adjacent cracks at damage step i.

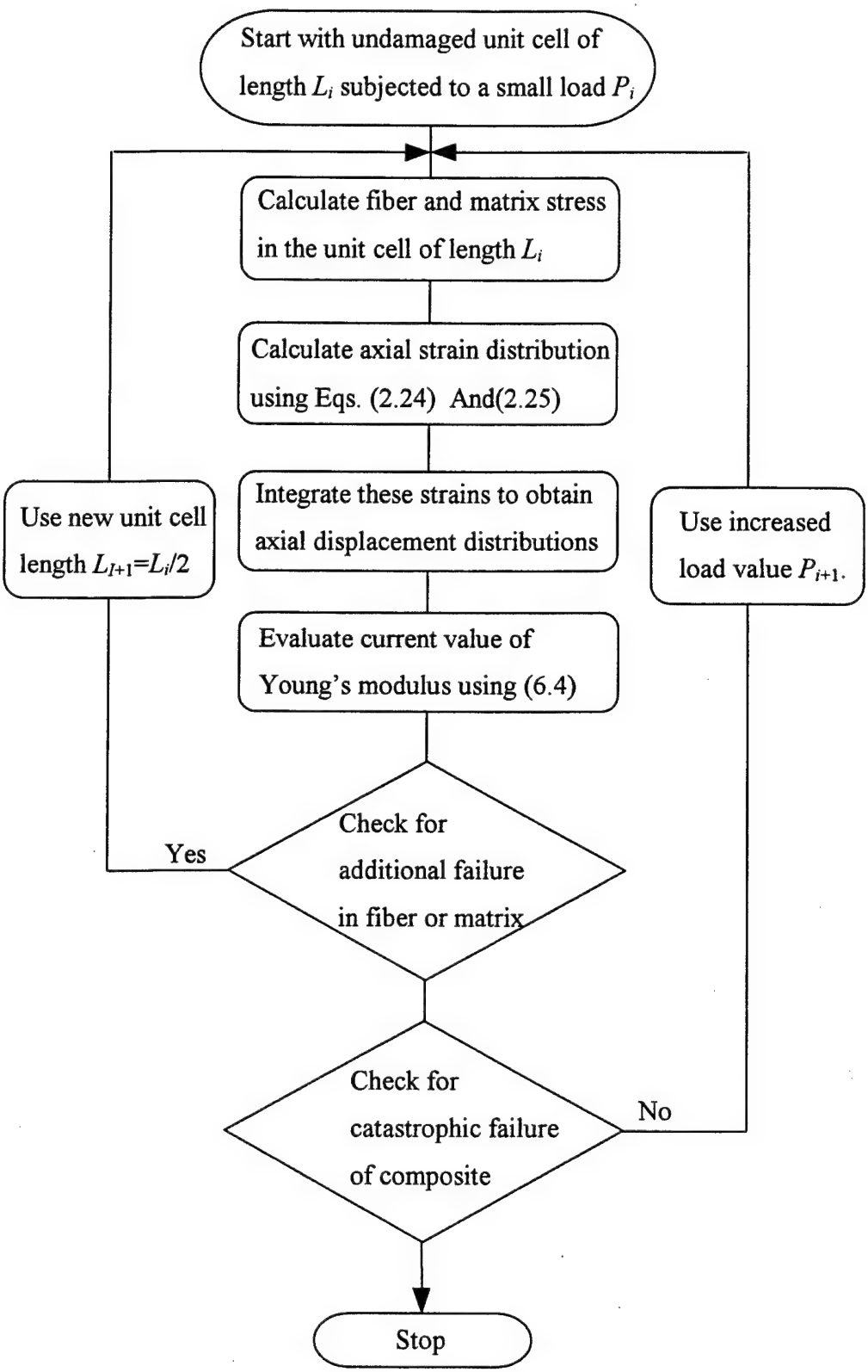

Figure 6.1: Flow chart of calculating the damage accumulation and property degradation.

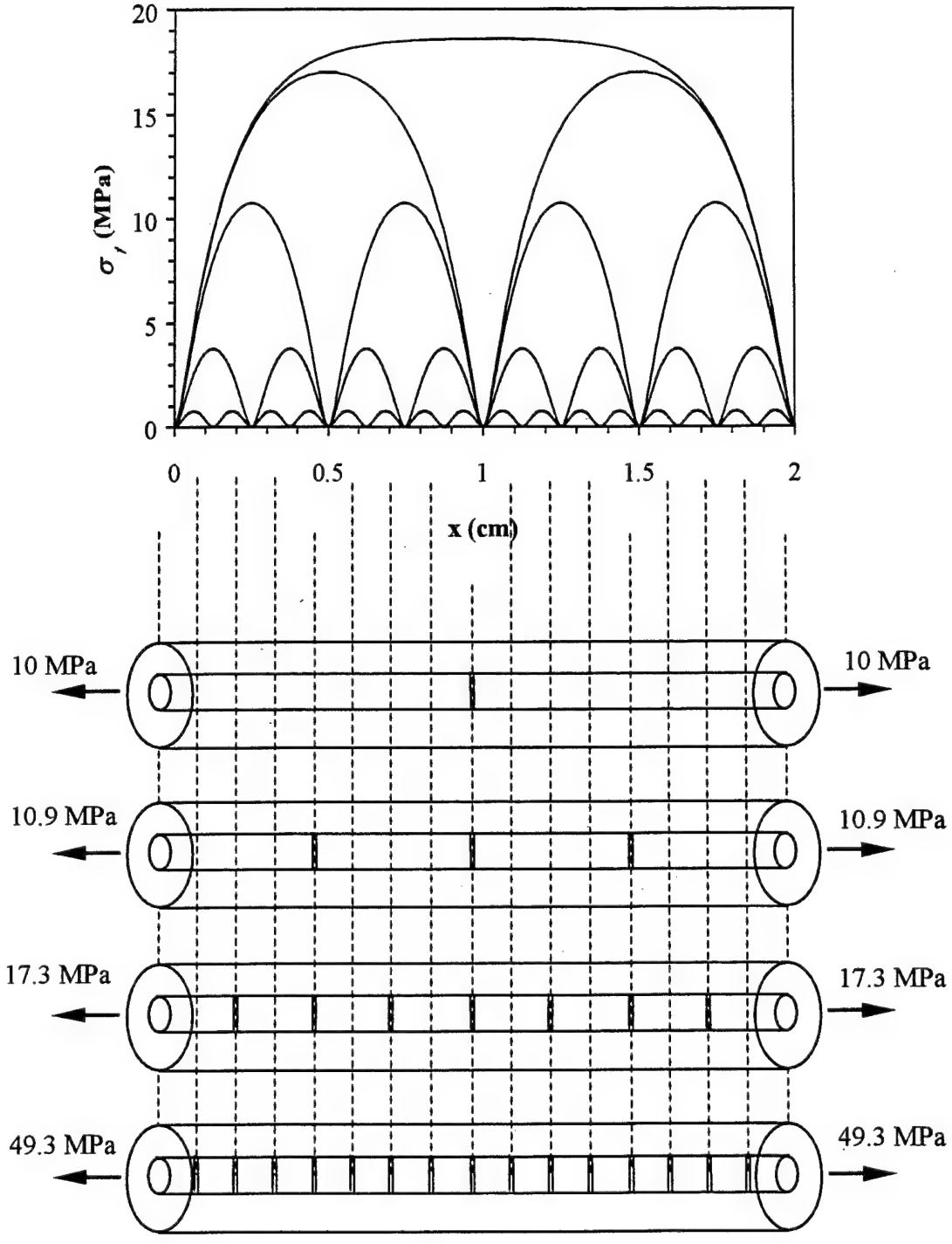

Figure 6.2: Damage accumulation in an E-glass/Epoxy fibrous composite.

The degradation curve of Young's modulus of this composite as calculated from equation 6.4 is shown in figure 6.3 from crack initiation (no damage), to crack saturation (L_i is very small). The value of Young's modulus is normalized with respect to its undamaged value calculated from Lame solution as 73 GPa. At very high crack density, the value of Young's modulus is identical to the case without the fiber.

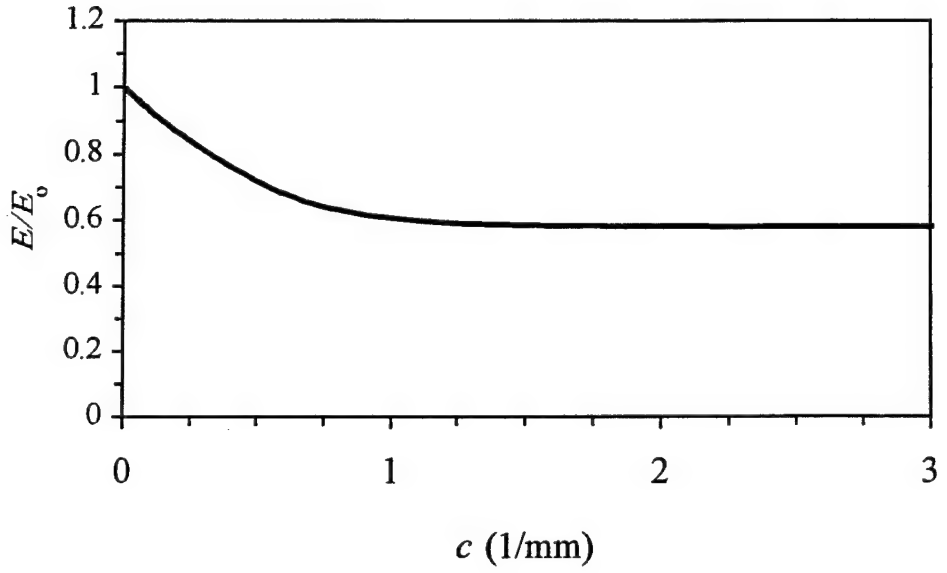

Figure 6.3: Degradation curve for an E-glass/Epoxy Composite from crack initiation to crack saturation.

A modeling similar to that presented in chapter 2 and section 6.3 can be used to study the problem of progressive transverse cracking in symmetric laminated composites. This is useful as most of the experiments are conducted on the commonly used laminated composites. In a recent publication [30] the problem of transverse cracking in the 90° layer of a balanced symmetric [0°/90°] laminate was studied. The E-glass/Epoxy laminate was loaded in the 0° fibers' direction. A comparison of the predicted variation of the

normalized Young's modulus with the experimental measurements showed perfect agreement. For illustration, this comparison is reproduced in figure 6.4. As the figure shows, accuracy of the predicted degradation is maintained all the way from crack initiation (c=0) to the crack saturation case.

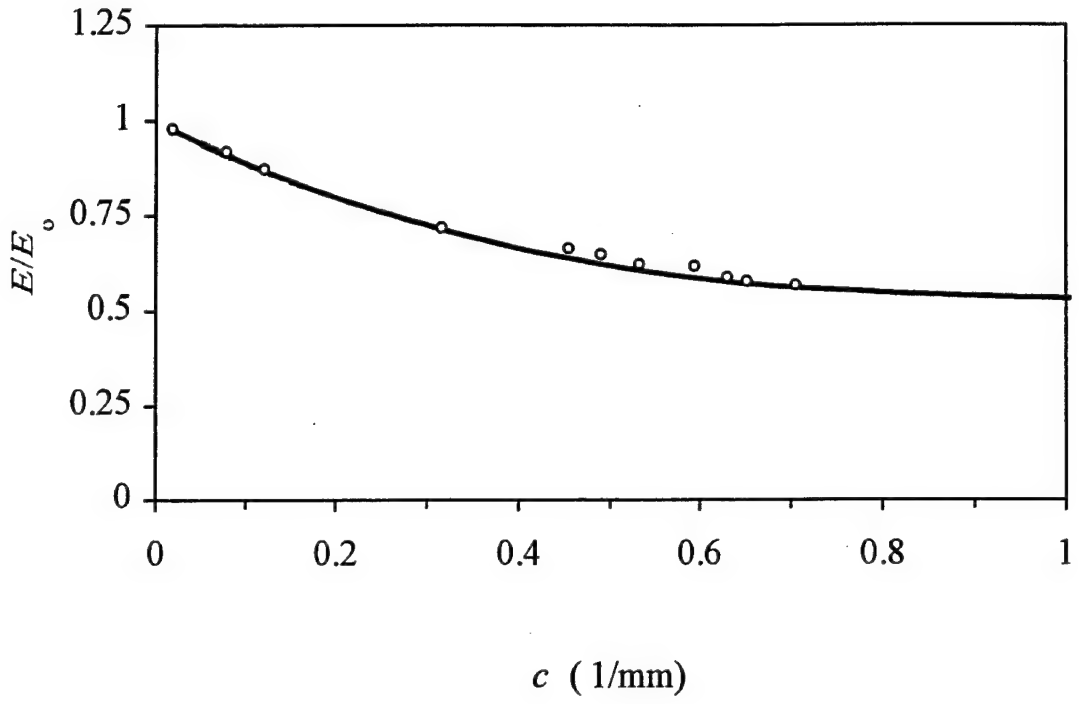

Figure 6.4: Comparison between the predicted distribution of the residual Young's modulus and the experimental measurements.

Having established the procedure of predicting the stiffness degradation caused by the accumulation of cracks in a straight fibrous composite, we proceed in the next section and extend this procedure to the case of undulated fibers.

6.4 Damage Analysis in Undulated Fibrous Composites

The stress distribution in unidirectional undulated fiber reinforced composites was found in chapters 4 and 5 for a variety of situations. In the previous section the procedure for predicting the variation of the composite stiffness with crack accumulation in straight fibrous composites was introduced. In this section this procedure is further extended to investigate the effects of damage evolution due to transverse fiber break or matrix cracking in undulated fibrous composites. Following the same procedure of chapter 4, if we start by an undamaged composite segment having a certain fiber geometric undulation, we identify and analytically describe local tangents to the fiber. Second, for a given applied load we transform the global coordinates and applied loads to local coordinate systems consisting of the tangent directions and their normals in the plane of undulation. Next, we adapt the results obtained for straight fibers to "straight" segmented fibers along the tangents. The local stresses obtained under this procedure are then supplemented with the stress contributions that inherently rise in any oriented direction with respect to the loading direction. Once the state of stress at each point of the two media is found, the maximum stress failure criterion is used to check for failure. Once a failure takes place at some point, the stresses in the new composite unit cell are obtained again under the new boundary conditions (either a free fiber surface or a free matrix surface). These are then used to predict if new fiber breaks/ matrix cracks will develop and the location of these damage surfaces. The process is repeated for an increasing applied load and the break density values are predicted. At every damaged state, the total axial strain in the composite is evaluated from the strain in each segment and the reduction in the longitudinal stiffness, as expressed by Young's modulus, is determined.

6.4.1 Damage Evolution

As the composite is subjected to increasing loads at its ends, damage, in terms of number of fiber breaks, is assumed to propagate at discrete steps. At each step, the stress distribution between adjacent breaks is monitored and the point of possible future break is predicted using the maximum stress criterion, namely

$$X_f - Max[\sigma_{zf}] = 0, \tag{6.5}$$

where X_f is the axial strength of the fiber material.

Assume we start with a damage free composite with its length chosen such that it spans a complete number of fiber waves, say four for example. Because both the geometry and loading are symmetric, the point of maximum stress will be exactly at the middle of the composite. Upon increasing the applied load, a single break occurs at this point, redistributing the stresses everywhere. No further breaks take place until the load increases enough for the failure criterion to be satisfied at the one quarter points of the composite, resulting again in symmetric break pattern. The last mid-span break takes place in each single wave as the load is increased further. Once the composite is divided into half waves, which are not geometrically symmetric with respect to the loading, any further breakage will not necessarily occur at the middle point between already existing breaks. Rather it will depend primarily on the undulation angle, or alternatively on the fiber waviness amplitude.

6.4.2 Illustration and Discussion

To understand how damage, in terms of transverse cracks or fiber breaks accumulates, we consider a generic unit cell made of the same fiber and matrix materials of the examples in chapters 5. The unit cell is initially assumed damage free and subjected to a very small axial loading. Upon increasing of the load, a single crack takes place as shown in figure 6.4. Due to redistribution of loading, no additional cracks occur, until the loading value increases to 14.7 MPa, where 4 cracks are predicted at very small load intervals. This is in contrast to the straight fibrous case where only one crack would occur in a half unit cell. We also notice that due to the shape of the stress distribution, new cracks do not occur close to the middle points between already existing cracks.

As another illustration of the procedure capabilities we consider an undulated fibrous composite with the unit cell having a length to amplitude ratio of 10. The mechanical properties of the E-glass fiber and Epoxy matrix are the same of the illustration of section 6.3.

Figure 6.5 shows the load-damage curve for this composite system. Initially a single transverse crack takes place in the weak epoxy material. Upon increase of loading and monitoring stresses, other cracks at several locations are predicted. It is important to note that due to undulation new cracks do not necessarily occur at the middle point between two already existing cracks as was the case in the straight fibrous case. Results for the straight fibrous case are also plotted on the same figure for comparison. The degradation of the composite as expressed in terms of reduction in Young's modulus is demonstrated in figure 6.6 for both the straight fibrous case as well as for the undulated case. Both values of Young's moduli are normalized in each case with respect to its value

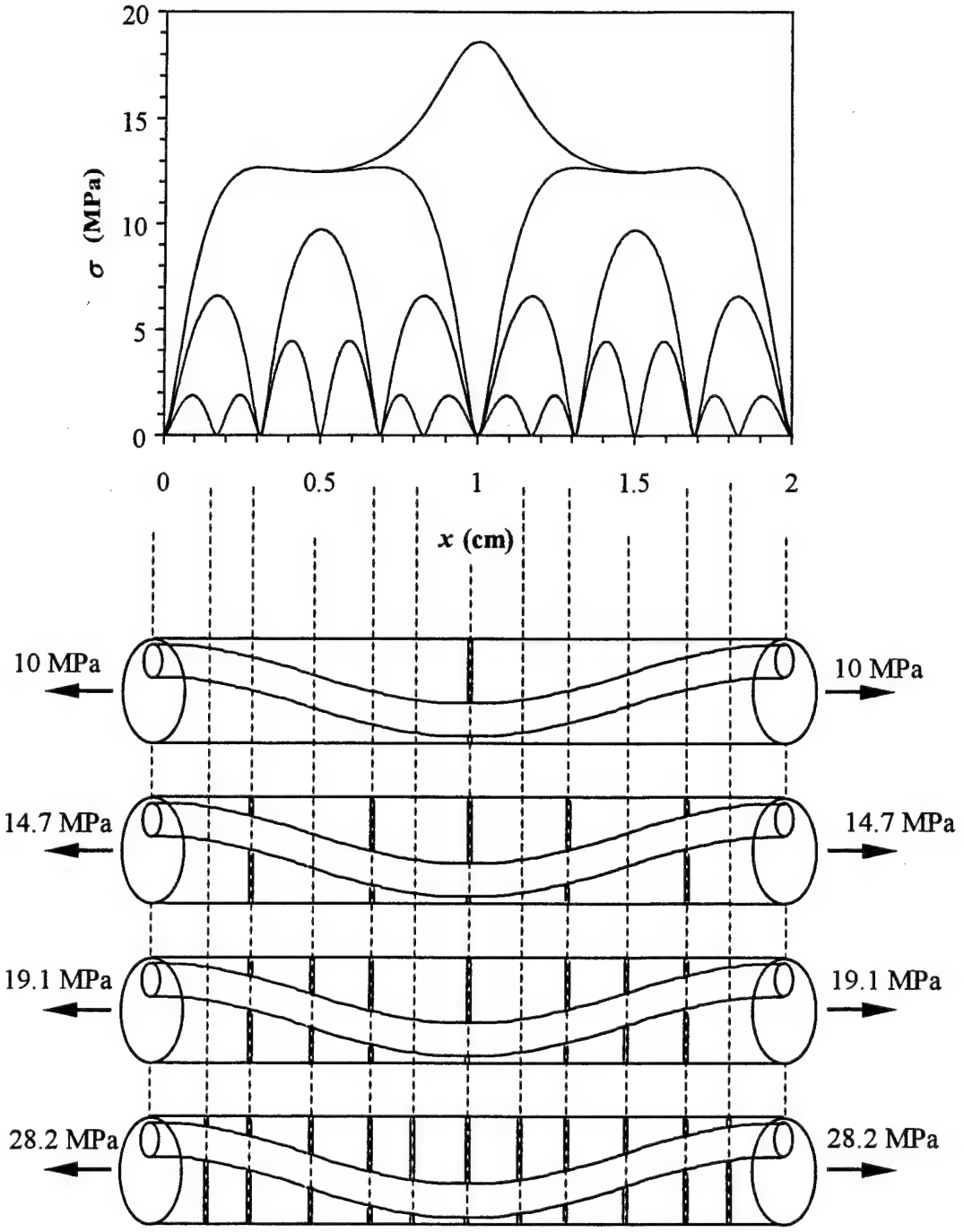

Figure 6.5: Evolution of transverse cracks in a generic unit cell of undulated fibrous composite.

in the absence of damage. The figures are not smooth as they represent the damage accumulation from one discrete loading step to another. Although the value of E_o in undulated fibrous composites is already smaller than that of the straight case, the rate of degradation is not as high. For example at a crack density of 1 mm^{-1}, the undulated fibrous composite retains 30% of its longitudinal stiffness as compared to 20% in the straight fibrous case. Therefore, in applications where both types can be used undulated composites will not deteriorate as drastically upon damage accumulation.

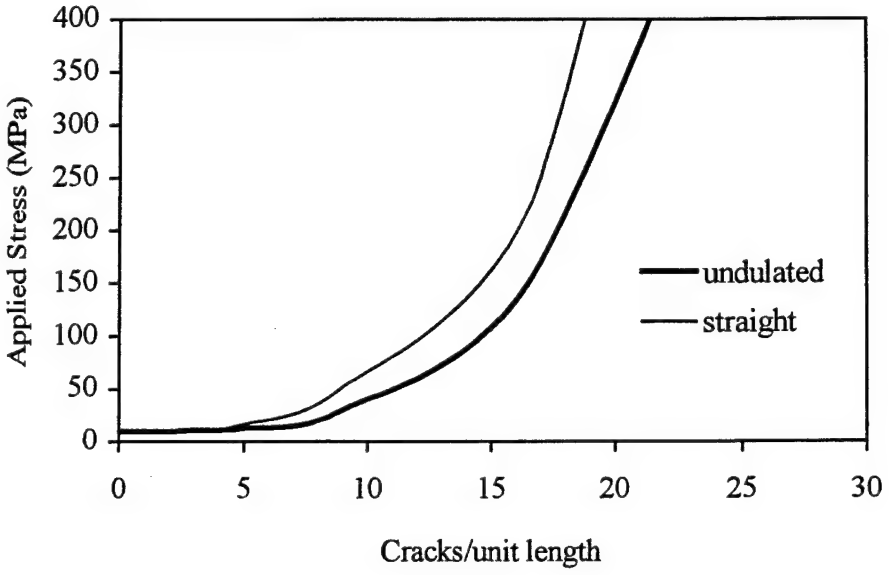

Figure 6.6: Comparison between the load-damage curves for an E-glass/Epoxy composite for both the straight fibrous case and the undulated case.

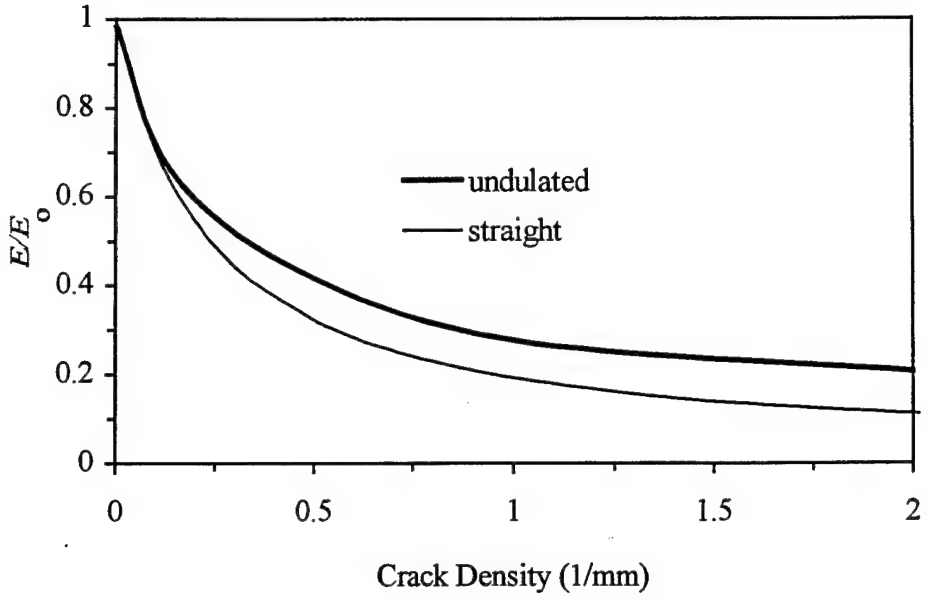

Figure 6.7: Comparison between the degradation curves for an E-glass/Epoxy composite for both the straight fibrous case and the undulated case.

CHAPTER 7

APPLICATION: VIBRATION CHARACTERISTICS OF DAMAGED FIBROUS COMPOSITES

7.1 Introduction

In this chapter, and as a further illustration of the utility of our modeling, procedure, we turn our attention to the study of vibration characteristics of a fibrous composite panel. This modeling, which was developed in chapter 2, is general and can be used in solving many classes of problems, including wave propagation and vibrations. The former problem received a continuous attention in research, see for example Nayfeh [1], Nayfeh and Nagy [31], Simmons et al. [32] and Thurston [33]. In those papers, both approximate and exact formulations were presented for the interaction of fibrous composites with a propagating wave. Much less work is available on the influence of microstructure on the vibration characteristics of fibrous composites, even in the absence of damage. Here, we extend our micromechanical model in order to investigate these characteristics with and without damage. The basic three possible fiber/matrix arrangements are shown in figure 7.1. Damage will be simulated by either a fiber break, a matrix crack or by combinations at selective locations along the fiber direction. Some analytical expressions for the resonance frequency modes will be derived. Numerical results will be presented mostly as comparisons between damaged and undamaged situations.

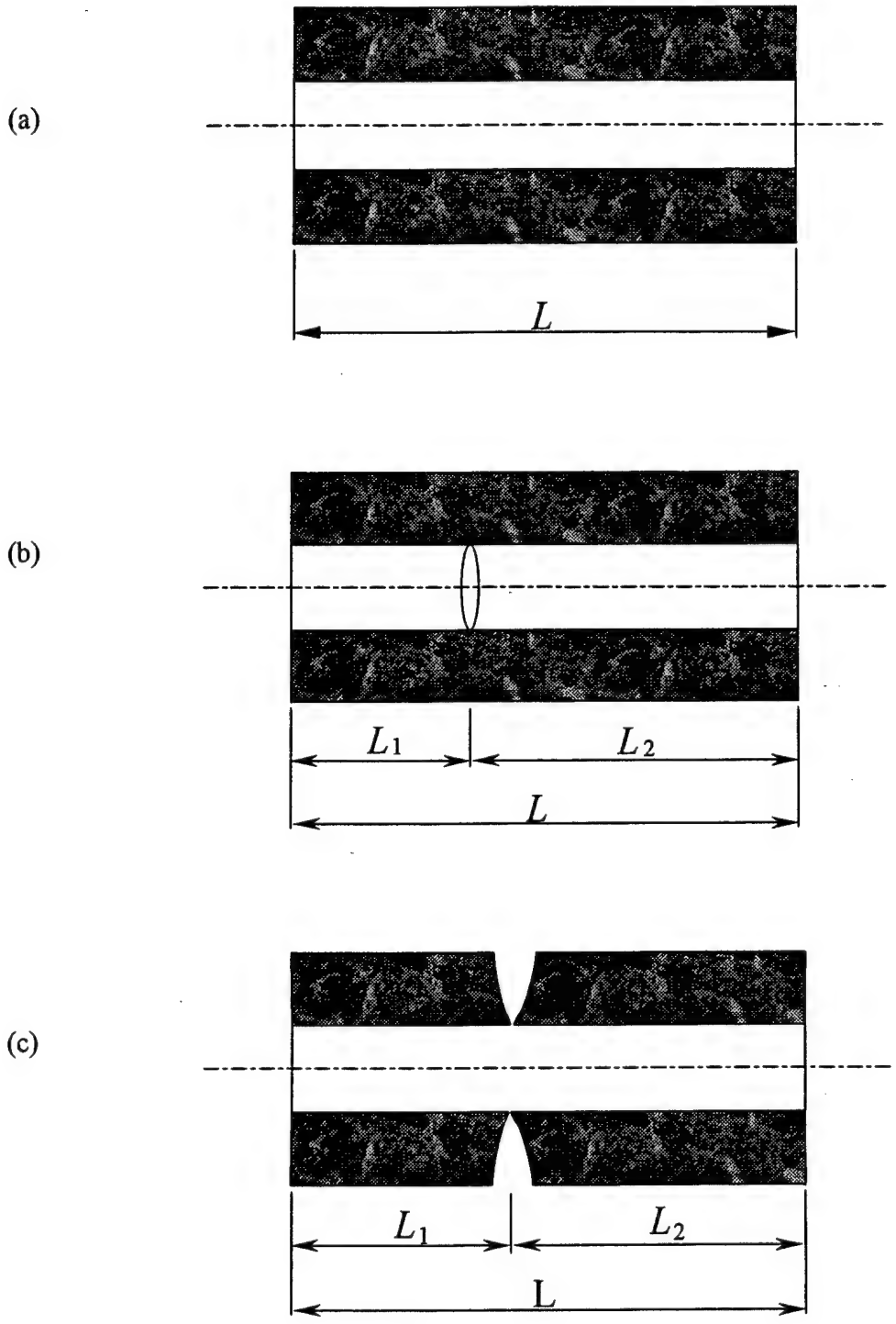

Figure 7.1: Geometry of three applications (a) undamaged case,

(b) case of broken fibers, (c) case of cracked matrix.

7.2 Mathematical Formulation

Since this vibration application is intended only for illustration, and to avoid unnecessary complicated equations, we will make an extra simplifying assumption to the micromechanical model. We will neglect the small effect of the $\partial v / \partial z$ on the shear constitutive relation, Eq. (2.9) for both the fiber and matrix materials, compared to the significant direct effect of $\partial u / \partial r$. This decouples the integrated forms of this equation, namely equations (2.30a) and (2.30,b), into

$$A = \frac{G}{2n_f}\left(\overline{u}_m - \overline{u}_f\right), \tag{7.1}$$

and

$$u^* = \frac{1}{(m_{55} - f_{55}Q)}\left(m_{55}\overline{u}_m - f_{55}Q\overline{u}_f\right), \tag{7.2}$$

where

$$G = \frac{8 f_{55} m_{55}}{r_2^{\,2}(m_{55} - f_{55}Q)}. \tag{7.3}$$

Now, specializing the constitutive relations (2.38a) and (2.38b) to $r = r_1$ and invoking the interface continuity equation (2.10) yields

$$B = \frac{(m_{12} - f_{12})}{2n_f D}\frac{\partial u^*}{\partial z}, \tag{7.4}$$

where

$$D = \frac{1}{2n_f n_m}\left[n_m(f_{22} + f_{12}) + n_f(m_{22} + m_{12}) + 2m_{55}\right]. \tag{7.5}$$

Combining this equation with (7.2), we solve for B in terms of the strain components $\frac{\partial \overline{u}_f}{\partial z}$ and $\frac{\partial \overline{u}_m}{\partial z}$ as

$$B = \frac{F}{2n_f}\left(m_{55}\frac{\partial \overline{u}_m}{\partial z} - f_{55}Q\frac{\partial \overline{u}_f}{\partial z}\right), \tag{7.6}$$

where

$$F = \frac{\left(m_{12} - f_{12}\right)}{D(m_{55} - f_{55}Q)}. \tag{7.7}$$

Finally, substituting from this equation back into the averaged constitutive relations (2.26) and (2.27), combining the resulting equations with equations (2.24) and (2.25) and using equation (7.1) to eliminate A, leads to the two coupled partial differential equations:

$$c_{11}\frac{\partial^2 \overline{u}_f}{\partial z^2} + c_{12}\frac{\partial^2 \overline{u}_m}{\partial z^2} - n_f\rho_f\frac{\partial^2 \overline{u}_f}{\partial t^2} - G(\overline{u}_f - \overline{u}_m) = 0, \tag{7.8}$$

$$c_{22}\frac{\partial^2 \overline{u}_m}{\partial z^2} - c_{21}\frac{\partial^2 \overline{u}_f}{\partial z^2} - n_m\rho_m\frac{\partial^2 \overline{u}_m}{\partial t^2} - G(\overline{u}_m - \overline{u}_f) = 0. \tag{7.9}$$

Here the coefficients c_{11}, c_{12}, c_{21}, c_{22} are given as combinations of the fiber and matrix properties and volume fractions as

$$c_{11} = n_f f_{11} - f_{12}f_{55}FQ, \qquad c_{12} = f_{12}m_{55}F, \tag{7.10a}$$

$$c_{21} = -m_{12}f_{55}FQ, \qquad c_{22} = n_m m_{11} - m_{12}m_{55}F. \tag{7.10b}$$

The behavior of the composite is completely described by equations (7.8) and (7.9). As seen, this system consists of two partial differential equations that couple the two longitudinal averaged displacements. These equations retain the integrity of the distribution of displacements and stresses in the fiber and matrix individually subject to

the influence of the interfacial transfer couplings. Thus, upon loading the composite, the distribution of stresses and displacements in the fiber and matrix components are readily calculable. Furthermore, the form of the coupled equations in our model makes it possible to incorporate damage mechanisms such as fiber break and matrix crack in the composite system. This system is general and can be applied to a variety of physical situations.

7.3 Applications

In the remainder of this chapter we apply the present modeling to the study of the vibration characteristics of fibrous composite systems with or without damage. For damage free composite systems, we choose a generic composite panel that occupies the region $-L/2 \le z \le L/2$ with its center located at z=0. Damage is then simulated as a stress free boundary in either the fiber (for fiber break) or the matrix (for matrix crack) along the panel length.

Depending upon the number of damage zones, the panel is divided into discrete sub-panels connected at the damage locations. Thus, for an arbitrary number N of damage locations, N+1 sub-panel segments are required. Each segment has the individual length L_i, i=1, 2, ...N+1, totaling L. Furthermore, we assign for each segment i the local coordinate z_i with origin located at its center; thus it extends from $-L_i/2$ to $L_i/2$. Since equations (7.8) and (7.9) hold for all segments, formal solutions for each can then be written in terms of two unknown amplitudes. By satisfying the appropriate continuity conditions across segment interfaces and followed by invoking the stress free conditions at the left and right ends of the total panel, we obtain the characteristic equation for the

resonance frequency. Resonance frequencies for situations involving other than stress-free ends of the panel can be just as easily obtained and will not be presented in this paper.

Similar to what we did in all cases involving dynamic loading, a formal solution of equations (7.8) and (7.9) can be assumed in the time harmonic form

$$\bar{u}_f = X_1 e^{\alpha z + i\omega t}, \tag{7.11a}$$

$$\bar{u}_m = X_2 e^{\alpha z + i\omega t}, \tag{7.11b}$$

This results in a coupled system of equations in the amplitudes X_1 and X_2, rearranged in matrix form as

$$\begin{bmatrix} n_f\rho_f\omega^2 + c_{11}\alpha^2 - G & c_{12}\alpha^2 + G \\ -c_{21}\alpha^2 + G & n_m\rho_m\omega^2 + c_{22}\alpha^2 - G \end{bmatrix} \begin{Bmatrix} X_1 \\ X_2 \end{Bmatrix} = \underline{0}. \tag{7.12}$$

For nontrivial solutions, the determinant of equation (7.12) must be zero. For a given frequency, the resulting characteristic equation admits four solutions for α, or more precisely two solutions for α^2. Thus, solutions for α occur in two pairs, each pair having two α's that are negative of each other. We shall label these roots as α_q, q = 1, 2, 3, 4, and further adopt the convention that $\alpha_2 = -\alpha_1$ and $\alpha_4 = -\alpha_3$. For each α_q, equation (7.12) can be used to obtain the amplitude ratio

$$X_{2q} = V_{2q} X_{1q}. \tag{7.13}$$

Using the method of superposition, the formal solutions for the displacements and stresses become

$$\left(\bar{u}_f, \bar{u}_m\right) = \sum_{q=1}^{4} \left(1, V_q\right) X_{1q} e^{\alpha_q z + i\omega t}, \tag{7.14}$$

$$(\bar{\sigma}_{zf}, \bar{\sigma}_{zm}) = \sum_{q=1}^{4} (D_{1q}, D_{2q}) X_{1q} e^{\alpha_q z + i\omega t}, \tag{7.15}$$

where

$$V_q = \frac{G - c_{11}\alpha_q^{\,2} + n_f \rho_f \omega^2}{c_{12}\alpha_q^{\,2} + G}, \tag{7.16a}$$

$$D_{1q} = \left[f_{11} + \frac{2n_m f_{12}(m_{12} - f_{12})(m_{55}V_{2q} - f_{55}Q)}{(m_{55} - f_{55}Q)[n_m(f_{22} + f_{12}) + n_f(m_{22} + m_{12}) + 2m_{55}]} \right] \alpha_q, \tag{7.16b}$$

$$D_{2q} = \left[m_{11}V_{2q} - \frac{2n_f m_{12}(m_{12} - f_{12})(m_{55}V_{2q} - f_{55}Q)}{(m_{55} - f_{55}Q)[n_m(f_{22} + f_{12}) + n_f(m_{22} + m_{12}) + 2m_{55}]} \right] \alpha_q. \tag{7.16c}$$

From the definitions of V_{2q}, D_{1q}, D_{2q}, it is clear that

$$V_{q+1} = V_q, \qquad D_{1\,q+1} = -D_{1q} \quad \text{and} \quad D_{2\,q+1} = -D_{2q}, \qquad q=1,3. \tag{7.17}$$

The formal solutions (7.14) and (7.15) are complete when the four values of X_{1q} are determined. Four displacement and/or stress boundary conditions, depending upon the problem at hand, are therefore required. For free longitudinal vibration of an undamaged panel, for example, we require the vanishing of the normal stresses at both ends $z = L/2$ and $z = -L/2$.

7.3.1 Undamaged Fiber-Matrix Composite

In the absence of damage, figure 7.1a shows that only one segment is necessary to model the composite panel. Imposing the stress free conditions, namely $\bar{\sigma}_{zf} = 0$ and $\bar{\sigma}_{zm} = 0$ at $z = -L/2$ and $z = L/2$, on the formal solution (7.15), leads to the characteristic equation

$$(e^{\alpha_1 L} - e^{-\alpha_1 L})(e^{\alpha_3 L} - e^{-\alpha_3 L}) = 0. \tag{7.18}$$

7.3.2 Case of a Single Fiber Break

For cases involving a single fiber break, say at $z = L_1$, as shown in figure 7.1b, then, according to our convention, the panel is composed of two segments. The formal solutions (7.14) and (7.15) are then adapted for each segment. At $z_1 = L_1/2$ and $z_2 = -L_2/2$, continuity of the longitudinal displacement $\bar{u}_m$ and stress $\bar{\sigma}_{zm}$ are required, whereas the stress $\bar{\sigma}_{zf}$ vanishes for both segments at that location. At the same time, imposing the stress free conditions at the outer ends of the system, namely $\bar{\sigma}_{zf} = 0$ and $\bar{\sigma}_{zm} = 0$ at $z_1 = -L_1/2$ and at $z_2 = L_2/2$, results, after a set of row operations on the resulting determinant of the boundary conditions, in the characteristic equation

$$V_3 D_{11}\left(\frac{S_3^{(1)}}{S_3^{(2)}} e^{-\alpha_3 L_2} + \frac{S_3^{(2)}}{S_3^{(1)}} e^{-\alpha_3 L_1}\right) - V_1 D_{13}\left(\frac{S_1^{(1)}}{S_1^{(2)}} e^{-\alpha_1 L_2} + \frac{S_1^{(2)}}{S_1^{(1)}} e^{-\alpha_1 L_1}\right) = 0 \qquad (7.19)$$

where

$S_i^{(j)} = e^{\alpha_i L_j} - e^{-\alpha_i L_j}$, i=1,3 , j=1,2.

7.3.3 Case of a Single Matrix Crack

If instead of a fiber break we have a matrix crack at the location $z = L_1$, as demonstrated in figure 7.1c, then the interface conditions at $z_1 = L_1/2$ and $z_2 = -L_2/2$ require the continuity of the fiber displacement $\bar{u}_f$ and the fiber stress $\bar{\sigma}_{zf}$ and the vanishing of the matrix stress $\bar{\sigma}_{zm}$ in both segments at the crack location. By inspection, we derive the characteristic equation for the case of matrix crack by simply replacing D_{1i} by D_{2i} and eliminating V_i, i=1,3, in equation (7.19) as

$$D_{21}\left(\frac{S_3^{(1)}}{S_3^{(2)}}e^{-\alpha_3 L_2}+\frac{S_3^{(2)}}{S_3^{(1)}}e^{-\alpha_3 L_1}\right)-D_{23}\left(\frac{S_1^{(1)}}{S_1^{(2)}}e^{-\alpha_1 L_2}+\frac{S_1^{(2)}}{S_1^{(1)}}e^{-\alpha_1 L_1}\right)=0. \tag{7.20}$$

7.3.4 Case of a Damage Combination

The above procedure can be used to obtain solution for the cases involving multiple damage in a composite panel. In a case involving n segments, connected at damage locations, a $4n\times 4n$ determinant need to be manipulated. For n larger than 2, the algebraic manipulation of the determinant becomes increasingly tedious. Hence, we resort to numerical methods to find the zeros of the $4n\times 4n$ determinant reflecting the appropriate interface and boundary conditions.

7.4 Discussion and Numerical Illustrations

Casual inspection of the solution of the undamaged composite, equation (7.18), reveals that two decoupled sets of vibration harmonics are possible to exist in the present panel. This, however, requires both values of α to be pure imaginary. In real situations, this is not always the case. We find that, for sufficiently low resonance frequencies, only one value of α is imaginary, reflecting a vibrating mode, while the other value is real, reflecting an evanescent mode. Whether α is real or imaginary depends on the resonance frequency ranges. Our discussion of this point, and of others to follow, can best be facilitated with the aid of a representative numerical illustration.

In all of our calculations, we shall choose graphite-epoxy as a representative composite panel. This panel has the following necessary geometric and material parameters. The total length and radius of the fiber are arbitrarily chosen as 20 *cm* and 1

cm, respectively with a fiber volume fraction of 0.55. The properties of both the graphite and the epoxy components are quoted from reference [1] and listed for convenience in stiffness matrix format as:

$$f_{ij} = \begin{bmatrix} 235.0 & 3.69 & 3.69 & 0 & 0 & 0 \\ & 26.0 & 3.32 & 0 & 0 & 0 \\ & & 26.0 & 0 & 0 & 0 \\ & & & 5.52 & 0 & 0 \\ & & & & 28.2 & 0 \\ & & & & & 28.2 \end{bmatrix}_{sym} \times 10^{10} \quad \text{dyne/cm}^2$$

for graphite, and

$$m_{ij} = \begin{bmatrix} 7.67 & 3.75 & 3.75 & 0 & 0 & 0 \\ & 7.67 & 3.75 & 0 & 0 & 0 \\ & & 7.67 & 0 & 0 & 0 \\ & & & 1.96 & 0 & 0 \\ & & & & 1.96 & 0 \\ & & & & & 1.96 \end{bmatrix}_{sym} \times 10^{10} \text{dyne/cm}^2$$

for epoxy. Also needed are the material densities $\rho_f = 1.79$ gm/cm^3 for graphite and $\rho_m = 1.26$ gm/cm^3 for epoxy. To further facilitate our discussion, we remind the reader of the trivial solutions for α in a single medium. For single material panels, α is calculated simply from $\alpha = i\omega\sqrt{c_{11}/\rho}$, where c_{11} and ρ are the longitudinal stiffness and density, respectively.

While for the simple case of the single medium α is linear in ω, this is not true in the composite problem and, in fact, equation (7.12) reveals that α has a quadratic dependence on ω; this is illustrated numerically in figure 7.2. Also included for comparison in this figure are the α's of the single graphite, single epoxy and mixture

media and designated as α_f, α_m and α_{mix}, respectively. The mixture value α_{mix} is based upon the effective longitudinal property (along the fiber direction) of the composite. This property is obtained from the original mixture system in the static limit. In this limit, the average displacements in both the fiber and matrix approach each other. By summing both equations subject to $\overline{u}_f = \overline{u}_m = u$, we obtain the single wave equation

$$(c_{11} + c_{12} + c_{21} + c_{22})\frac{\partial^2 u}{\partial z^2} = (n_f \rho_f + n_m \rho_m)\frac{\partial^2 u}{\partial t^2}, \tag{7.21}$$

reflecting the homogenized medium with the effective stiffness and density given respectively as

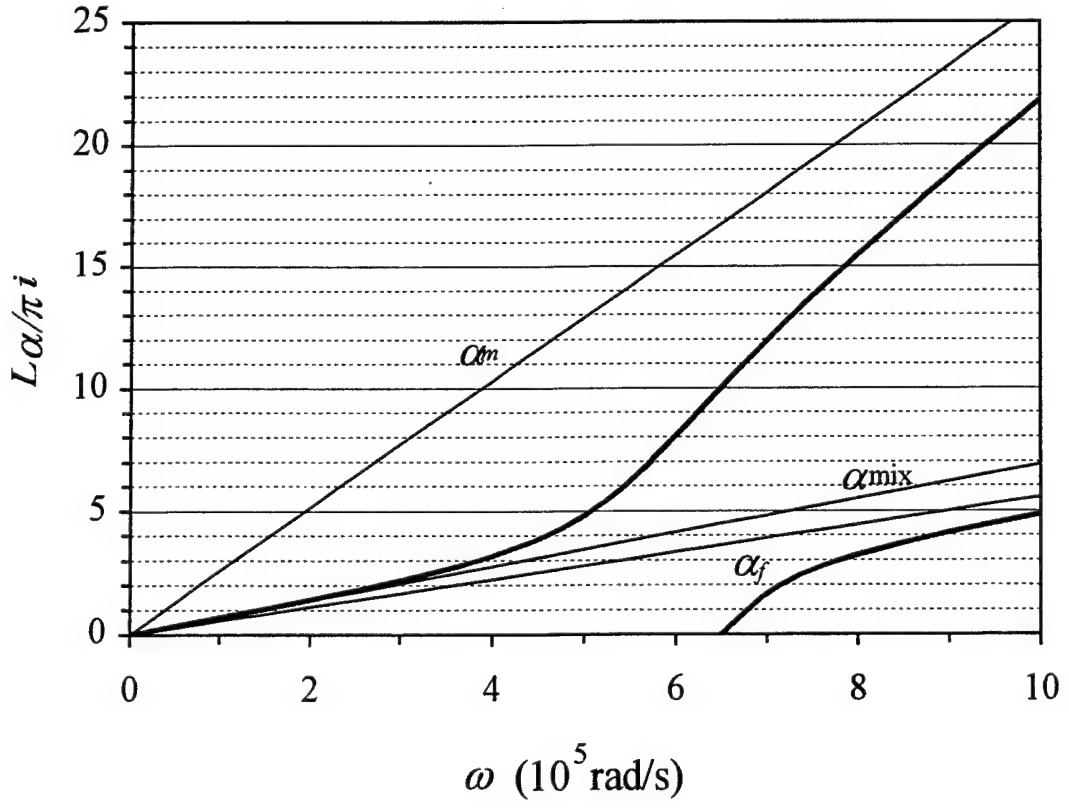

Figure 7.2: Variation of α with the radial frequency ω for undamaged panel.

$$c_{mix} = c_{11} + c_{12} + c_{21} + c_{22}, \tag{7.22a}$$

$$\rho_{mix} = n_f \rho_f + n_m \rho_m . \tag{7.22b}$$

Thus α_{mix} is calculated from

$$\alpha = i\omega\sqrt{c_{mix} / \rho_{mix}} . \tag{7.23}$$

Inspection of figure 7.2 reveals that, at relatively low frequency ranges, only one of the composite α 's is pure imaginary whereas the other is pure real signifying the existence of a single set of vibrating harmonics and that their values are relatively close to that of the effective mixture values. Here, the composite behaves as a single effective (homogenized) material with both of its constituents loose their individual identity and move in concert with each other. As the frequency increases beyond a critical value, both α 's become pure imaginary signifying the existence of two sets of vibrating modes. The analytical expression for this critical frequency is obtained by setting $\alpha = 0$ in the determinant of equation (7.12), and solving for ω, leading to:

$$\omega_{cr} = \sqrt{\frac{G(n_f \rho_f + n_m \rho_m)}{n_f n_m \rho_f \rho_m}} . \tag{7.24}$$

For the present system, this critical frequency is calculated as 6.7274×10^5 rad/s.

The evolution of the two sets of harmonics for increasing frequency is interesting. For moderate frequency ranges beyond the critical frequency, these two modes stay interdependent in that each is dependent on both fiber and matrix properties and the composite geometry. As the frequency increases further, the two sets become more and more distinct and, as the frequency approaches infinity, they become identifiable with

those of the pure fiber and pure matrix panel modes. This can also be seen from figure 7.2 where the two branches asymptotically approach those of α_f and α_m. In the meantime α_{mix} is seen to diverge a little more from the lower branch suggesting that the mixture mode is only valid in the low frequency ranges.

It can be seen that the high frequency limits also have their roots in the original mixture equations (7.8) and (7.9). As the frequency is increased beyond limit, the characteristic equation (7.18) uncouples and leads to two limiting values for α's. Except for a slight coupling from the c_{12} and c_{21} terms, these two limiting values coincide with α_f and α_m.

Having given a qualitative discussion of the behavior of the vibrating modes, we now move to present numerical calculations for cases in which damage is either absent or present. We start with a damage free panel. For stress free outer ends, the resonance frequencies are obtained from satisfying equation (7.18). For this specific situation, these frequencies can also be extracted from figure 7.2. It should be noted that this figure is scaled such that the resonance frequencies are obtained directly by projecting the intersections of the horizontal lines and the α curves on the abscissa. The lowest (fundamental) resonance frequency ω_1 for this undamaged case can either be roughly estimated from the figure or exactly calculated from equation (7.18) as 1.4355×10^5 rad/s. Higher resonance frequencies of this panel can also be easily obtained. Here we list the first fifteen and label them consecutively as $\omega_1, \omega_2, \omega_3, \ldots \omega_{15}$ in Table 7.1. For future reference, we list their normalized values with respect to the fundamental frequency ω_1.

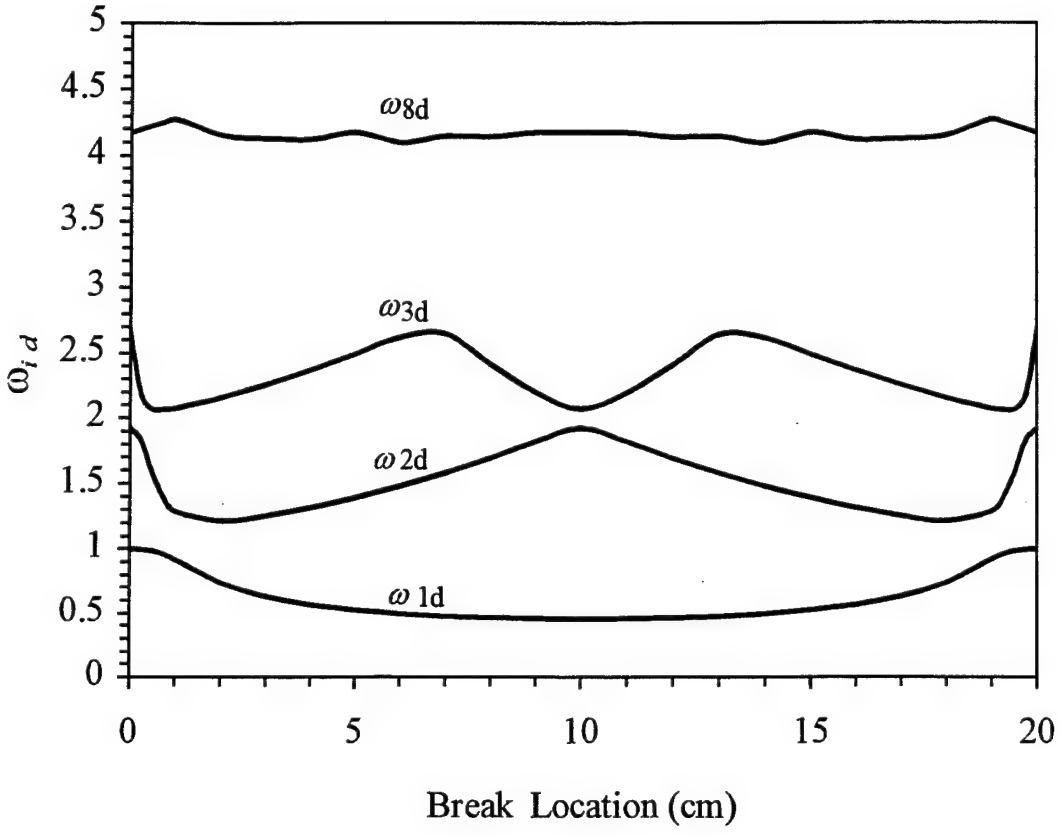

Figure 7.3: Variation of the normalized natural frequencies ω_{1d}, ω_{2d}, ω_{3d} and ω_{4d} with the damage location for the case of broken fiber.

resonance frequencies. This is due to the fact that the graphite fiber is much stiffer than the epoxy and thus little influence can be attributed to the cracked matrix.

As an illustration of the versatility of the present analysis, we finally investigate the sensitivity of the resonance frequencies to the relative volume fractions of the fiber and matrix constituents. The variation of the first three fundamental frequencies of the composite panel with the fiber volume fraction is depicted in figure 7.4 in the presence and absence of damage. For this specific illustration, damage is taken in the form of a fiber break at the center of the 20 *cm* long and 1 *cm* radius fiber composite panel. The

dotted and solid curves belong to damage free and damaged situations. Inspection of figure 7.4 leads to some interesting conclusions. First the two limits of $n_f = 0$ and 1 belong to a panel made up of only matrix or fiber material, respectively. At the limit of zero fiber volume fraction, the fundamental frequencies of the damaged and undamaged panels coincide.

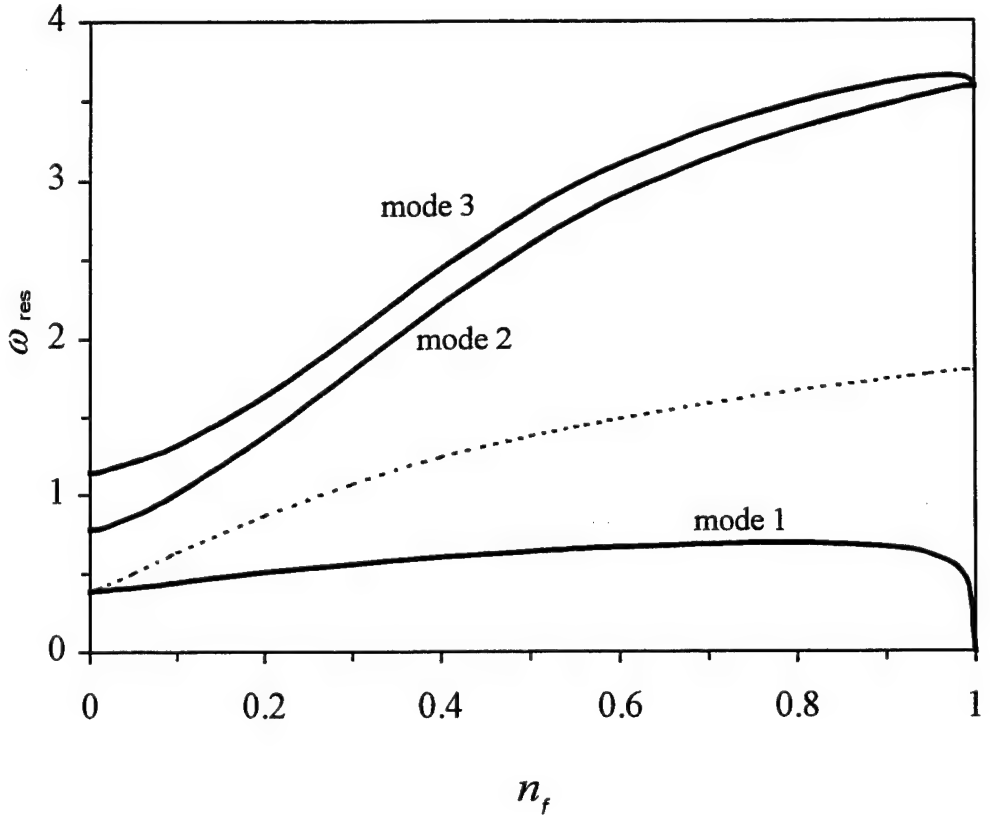

Figure 7.4: Fiber volume fraction dependence of the first three natural frequencies of a composite panel for the undamaged case and for the case of a fiber break at z=0.

As the fiber volume fraction increases, emphasizing thinner matrix cladding, the solutions for the damaged panel depart away from the corresponding undamaged one. In

the limit as the fiber volume fraction approaches unity, the fundamental mode approaches zero, whereas the third mode approaches that of the second. This interesting limit can be easily explained by investigating the behavior of the corresponding mode shapes. For the sake of illustration we investigate the evolution of the σ_{zm} third mode shape with varying fiber volume fraction. As can be seen from figure 7.5, when the fiber volume fraction increases, the two nodal points close to the center approach the crack location at mid-

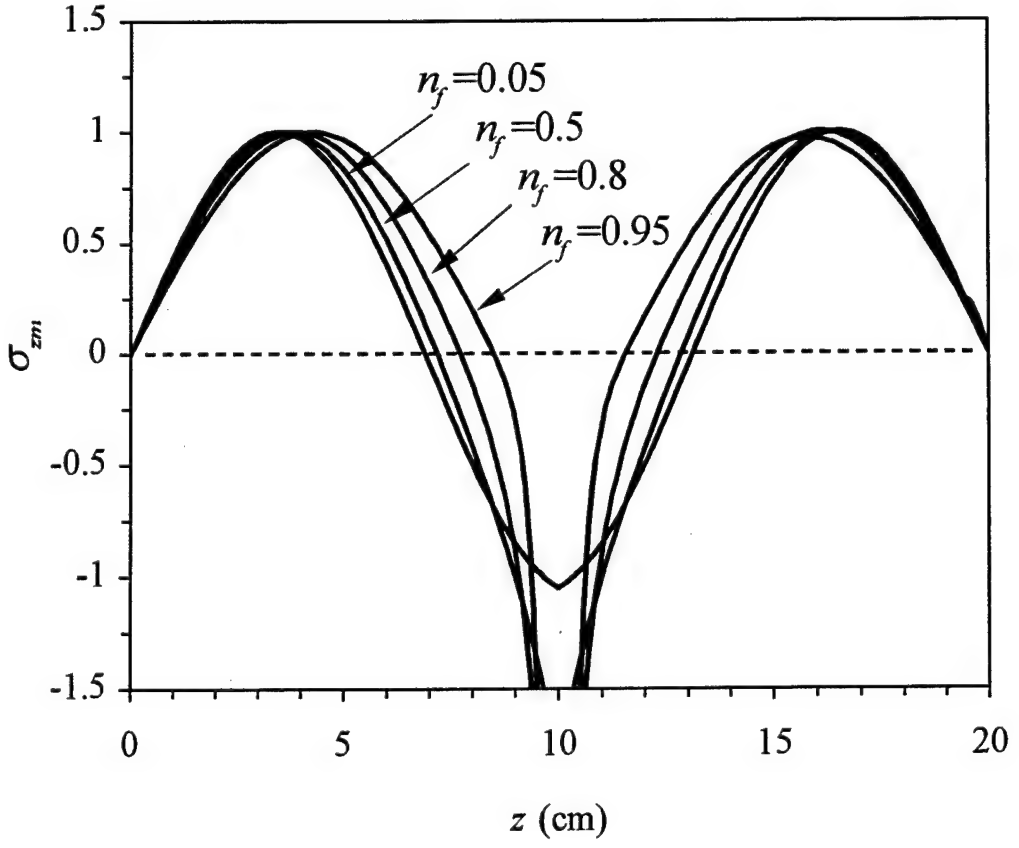

Figure 7.5: Variation of the third matrix stress σ_{zm} mode shape with the fiber volume fraction for the case of a broken fiber at z=10.

span. Meanwhile, the matrix stress peak at the crack location grows, a behavior consistent with the fact that the ever-thinner matrix still has to carry the same load across the crack. At the extreme limit $n_f = 1$, this evolution results in the third mode being coincident with the second mode.

In this chapter, the newly developed micromechanical model is applied to the study the vibration characteristics of fibrous composites with damage. The model proved to be easily adapted for cases involving single fiber break, single matrix crack or multi damage situations. It is used to investigate the dependence of the composite panel resonance frequencies and mode shapes on the damage location and on the fiber volume fraction in the case of a single fiber break. Results, which are also presented in [34], show several interesting characteristics as the fiber volume fraction approaches its limiting values.

CHAPTER 8

CONCLUSION

In this work, a unified micromechanical model for the prediction of the stress distribution in undulated fibrous composites was developed and used to study damage accumulation in this important class of composites. First, the unidirectionally undulated fibrous unit cell is divided into segments each with a local principal direction parallel to the fiber tangent in this segment. Then the interfacial values of some of the stress and displacement components were used together with the averaging technique to reduce the system of resulting equations into a quasi-one-dimensional one. In doing so, certain approximations had to be made regarding the dependence of some of the stress and displacement components on the radial direction. The resulting fourth order differential equation was solved for the stresses in the "local" fiber direction, and the resulting shear stress was then enhanced with the already existing stress between the fiber and the matrix. Damage in the composite in the form of a fiber break or a matrix crack is modeled by the equation through using the right set of boundary conditions. The accuracy of the modeling is verified by several comparisons with both available published results and finite element generated solutions.

Having obtained the stress distribution in both constituents, the maximum stress failure criterion is used to check if additional damage will occur in any of the constituents upon the increase of loading. The process is repeated for as many load steps until catastrophic failure occurs. At each load-step, the integration of the displacements in the global composite axial direction provides a means of estimating the composite stiffness.

Monitoring stiffness and damage density upon loading the composite provides important performance information. This includes the load-damage diagram and the stiffness-damage diagram. These diagrams stress the fact that weakening due to damage accumulation is more significant in composites reinforced with straight fibers than in those with undulated ones

A final application of the model was that in the area of vibrations. The model was easily adapted to study vibrations of damaged straight fibrous composites. The fact that damage location affects the system natural frequencies and mode shapes is of practical significance, since it can be used in the prediction of damage location.

The proposed formulation opens several paths for future studies. From geometry point of view, the analysis can be extended to cover both the warp and weft yarns. Existing models which deals with both yarns tend to neglect the continuity of their undulation, as for example, the mosaic model. Although not discussed here, the effect of undulation on the degradation in transverse properties can also be investigated. Finally, other potential capabilities for the model need to be fully explored. This includes problems of wave propagation and vibrations in textiles.

Bibliography

[1] Nayfeh, A. H., 1995, Wave Propagation in Layered Anisotropic Media with Application to Composites, Elsevier publishing Co., Amsterdam, The Netherlands.

[2] Al-Huniti, N., 1996, Micromechanical Modeling of Woven and Textile Composites, Ph.D. Dissertation, University of Cincinnati.

[3] Smith, G. E. and Spencer, A. J. M., 1970, *Journal of the Mechanics and Physics of Solids*, 18, pp. 81-100.

[4] Nayfeh, A. H., 1977, "Thermomechanically Induced Interfacial Stresses in Fibrous Composites," *Fiber Science and Technology*, 10.

[5] Nayfeh, A. H., 1978, "Dynamically Induced Interfacial Stresses in Fibrous Composites," *Journal of Applied Mechanics*, 45, pp. 442-445.

[6] Steif, P. S., 1984, "Stiffness Reduction Due to Fiber Breakage," *Journal of Composite Materials*, 17, pp. 153-172.

[7] Gao, Y. C., Mai, Y. W. and Cotterrell, B., 1988, *Z. angew. Math. Phys.*, 39, pp. 550-572.

[8] Carapella, E., Hyer, M. W. and Griffin, O. H., 1992, "Micromechanics of Noncircular Fibers," *Proceedings of the American Society for Composites*, Seventh Technical Conference, pp. 827-836.

[9] Kishore, P. V., Lau, A. C., and Wang, A. S. D., 1992, "On Fiber-Matrix Interfacial Stresses during Fiber Pullout with Thermal Stressing," *Proceedings of the American Society for Composites*, Seventh Technical Conference, pp. 827-836.

[10] McCartney, L. N., 1989, "New Theoretical Model of Stress Transfer between Fiber and Matrix in a Uniaxially Fibre-reinforced Composite," *Proceedings of the Royal Society of London*, A 425, pp. 215-244.

[11] Nedele, M. R., Winsom, M. R., 1992, "Micromechanical Modelling of a Unidirectional Carbon Fiber-Epoxy Subjected to Mechanical and Thermal Loading," *Proceedings of the American Society for Composites*, Seventh Technical Conference, pp. 328-336.

[12] Goldberg, R. K. and Hopkins, D. A., 1995, "Application of the Boundary Element Method to the Micromechanical Analysis of Composite Materials," *Computers and Structures*, Vol. 56, No. 5, pp. 721-733.

[13] Tsai, S. W. and Wu, E. M., 1971, "A General Theory of Strength for Anisotropic Materials," *Journal of Composite Materials*, 5, pp. 58-80.

[14] Reifsnider, K. L., Talug, A., 1980, "Analysis of Fatigue Damage in Composite Laminates," *International Journal of Fatigue*, 3.

[15] Highsmith, A. L., Reifsnider, K. L., 1982, "Stiffness-Reduction Mechanisms in Composite Laminates," *Damage in Composite Materials, ASTM STP 115*, pp. 103-117.

[16] Hashin, Z., 1985, "Analysis of Cracked Laminates: A Variational Approach," *Mechanics of Materials*, 4, pp. 121-136.

[17] Talreja, R., 1985, "A Continuum Mechanics Characterization of Damage in Composite Materials," *Proceedings of the Royal Society of London*, 399, pp. 195-216.

[18] Talreja, R., 1985, "Transverse Cracking and Stiffness Reduction in Composite Laminates," *Journal of Composite Materials*, 19, No. 4, pp. 355-375.

[19] Hashin, Z., 1987, "Analysis of Orthogonally Cracked Laminates Under Tension," *Journal of Applied Mechanics*, 54, pp. 872-879.

[20] McCartney, L. N., 1992, "Theory of Stress Transfer in a 0°-90°-0° Cross-Ply Laminate Containing a Parallel Array of Transverse Cracks," *Journal of the Mechanics and Physics of Solids*, 40, No. 1, pp. 27-68.

[21] Akshantala, N. V. and Talreja, R., 1998, "A Mechanistic Model for Fatigue Damage Evolution in Composite Laminates," *Mechanics of Materials*, 29, pp. 123-140.

[22] Allen, D. H., Harris, C. E., Groves, S. E., 1987, "A Thermomechanical Constitutive Theory for Elastic Composites with Distributed Damage-Part I: Theoretical Development," *International Journal of Solids and Structures*, 23, No. 9, pp. 1301-1318.

[23] Pochiraju, K., Chou, T-W, and Shah B. M., 1996, "Modeling Stiffness and Strength of 3-D Textile Structural Composites," 37th AIAA/ASME/ASCE/AHS/ASC Structures, Structural Dynamics and Materials Conference, Salt Lake City, Utah, pp. 2294-2304.

[24] Herakovich, C. T., 1998, Mechanics of Fibrous Composites, John Wiley and Sons, Inc., New York, N.Y.

[25] Nayfeh, A. H. and Abdelrahman, W. G., 1998, "Micromechanical Modeling for Load Transfer in Fibrous Composites," *Mechanics of Materials*, 30, pp. 307-324.

[26] Nayfeh, A. H. and Abdelrahman, W. G., 1999, "Dynamic Stress Transfer in Fibrous Composites with Damage," *Composites Part B: Engineering*, 30, pp. 233-243.

[27] Nayfeh A. H. and Abdelrahman, W. G., 1998, "An Improved Continuum Mixture Model for Wave Propagation in Fibrous Composites," *Journal of the Acoustical Society of America*, 104, 2, pp. 867-873.

[28] Abdelrahman, W. G. and Nayfeh, A. H., 1998, "Micromechanical Modeling of Stress Distribution in Undulated Composites under Axial Loading," *Mechanics of Materials*, 30, pp. 83-90.

[29] Nayfeh, A. H. and Abdelrahman, W. G., 1998, "Dynamically Induced Stress Distribution in Undulated Fibrous Composites," *Review of Progress in Quantitative Nondestructive Evaluation*, 17, pp. 1627-1634.

[30] Abdelrahman, W. G. and Nayfeh, A. H., 1999, "Stress Transfer and Stiffness Reduction in Orthogonally Cracked Laminates," *Mechanics of Materials*, 31, pp. 303-316.

[31] Nayfeh, A. H. and Nagy, P. B., 1996, "General Study of Axisymmetric Waves in Layered Anisotropic Fibers and their Composites," *Journal of the Acoustical Society of America*, 99, 2, pp. 931-941.

[32] Simmons, E., Drescher-Krasicka, J. A., and Wadely, H. N. G., 1992, "Leaky Axisymmetric Modes in Finite Clad Rods," *Journal of the Acoustical Society of America*, 92, 1061.

[33] Thurston, R. N., 1978, "Elastic Waves in Rods and Clad Rods," *Journal of the Acoustical Society of America*, 64, 1.

[34] Nayfeh, A. H. and Abdelrahman, W. G., 1998, "Vibration Characteristics of Fibrous Composites with Damage," accepted for publication in *Journal of Vibration and Control.*